Aalto University
School of Engineering

Muhammad Saad Akram

Optical Fuel Spray characterization of Hydrotreated Vegetable Oil (HVO) and Ethanol

Espoo, 3.9.2018

Supervisor: Professor Martti Larmi
Advisor: Ossi Kaario, D.Sc. (Tech.)

Author Muhammad Saad Akram

Title of thesis Optical fuel spray characterization of Hydrotreated Vegetable Oil (HVO) and Ethanol

Master programme Master's programme in Advanced Energy Solutions – Sustainable Energy Conversion Processes **Code** ENG3069

Thesis supervisor Professor Martti Larmi

Thesis advisor(s) Ossi Kaario, D.Sc. (Tech.)

Date 16.4.2020 **Number of pages** 84 **Language** English

Abstract

The global concern about climate change has remarkably increased because of its tangible environmental effects. Transportation being one of the major contributors to greenhouse gas emissions is taking a substantial part in global warming and climate change. Fortunately, the shift of emerging transportation technology towards electric power sources has proven to be a favorable solution towards sustainable and cleaner transportation addressing global climate change. However, some constraints related to battery technologies and charging infrastructure created a necessity of research towards alternative cleaner fuels for internal combustion engines. Ethanol is one of the alternative fuel that has caught much attention because of its remarkably low emissions.

The experimental study in this thesis investigated the comparison of HVO and ethanol with EN590 diesel fuel sprays in terms of overall spray geometry and droplet size measurements by analyzing the monochrome spray images. The fuel sprays were injected using two different fuel injectors with different nozzle orifice diameters into a constant volume chamber at varying conditions of injection pressure and gas density.

In terms of overall spray geometry and droplet size measurements, HVO and EN590 diesel sprays showed quite similar trends, however, significant differences could be observed for ethanol sprays. Ethanol sprays were characterized with lower penetration, larger opening angles and smaller droplet sizes than HVO and EN590 sprays. A Significant decrease in mean diameters and droplet size distributions could be identified by increasing the injection pressures. Furthermore, the results for the injector with increased nozzle orifice diameter compared with the reference nozzle suggested decrement in spray penetration and increased opening angles for EN590 fuel sprays.

Keywords Fuel, ethanol, diesel, Hydrotreated Vegetable Oil (HVO), compression ignition, fuel spray, spray geometry, spray penetration, spray opening angle, droplet size, shadow imaging, image analysis

Preface

This thesis, focusing on the fuel spray characterization of high-pressure Hydrotreated Vegetable Oil (HVO), Diesel EN590 and Ethanol fuels, has been conducted in the internal combustion engine laboratory of Aalto University. The experiments were performed according to the requirements and test matrix provided by AGCO Power, who was collaborating in this thesis. The provided funding for this project is highly acknowledged.

I want to express my deepest gratitude to the whole staff of the internal combustion engine laboratory. Their guidance and assistance were significant milestones in the successful completion of the experiments. I would especially like to thank Olli Ranta, Otto Blomstedt, Qiang Cheng and Zeeshan Ahmad for providing their expertise and kind opinions whenever needed. I would also like to recognize the extraordinary assistance that I received from Ari Ainsalo, particularly during the experiments. Furthermore, I want to extend my sincere gratitude to Professor Martti Larmi and Ossi Kaario, D.Sc. (Tech), for supervising my thesis and guiding me throughout. In the end, I express my special thanks to Professor Martti Larmi and AGCO Power for giving me an opportunity to explore the field of my interest in the form of this thesis topic.

16.4.2020

Muhammad Saad Akram

Table of Contents

1 Introduction

1.1 Background

In the engines market, internal combustion engines have been in the highlights because of their better efficiencies, reliabilities and lower manufacturing costs. With the existence of other engine technologies that compete with IC engines, the need for development and research started to increase in the past. However, due to phenomenal research from the last decade, internal combustion engines are nowadays, considered amongst better efficiencies engines with lower emissions. Compression ignition engines are indeed taking a lead from other ignition engines due to their better efficiencies. However, the development in emission reduction technologies in SI engines has improved the emission treatment system, thus reducing the emissions in SI engines. This lead the research to focus more on advanced emission control technologies alongside the improvement in the fuel injection system of compression ignition internal combustion engines.

Combustion of fuel sprays plays a vital role in understanding the emission formation in compression ignition engines. CI engines are based on mixing controlled combustion, therefore particulate emissions relate with the formation of fuel spay that mixes with the surrounding gas. Improving the spray formation for better evaporation in the surrounding leads towards improved air-fuel mixing, thus reducing the particulate emissions. Therefore, proper research and development in spray combustion may lead to an improvement in emission reductions.

With the consciousness towards the environmental effects related to exhaust gas emissions and the strategic developments for climate change, the emission legislations have become stringent towards cleaner energy sources. The hybridization and the introduction of electrically driven vehicles are well serving the purpose for shorter travel vehicles. However, more clean energy sources solutions are still required for heavy-duty vehicles for long-distance travelling. This gives rise to the research needed in investigating newer and cleaner liquid fuels.

Alternative fuels like Ethanol and Methanol that are produced from biomass have recently been into a remarkable consideration as an alternative fuels. This is because of the high oxygen content in ethanol, which reduces carbon emissions. Despite the ongoing research on ethanol fuel, there is still a huge margin for investigating the high-speed ethanol sprays. It would be interesting to see how ethanol spray geometry and droplet sizes differ from typical diesel fuel sprays. Furthermore, the research in finding better fuels also resulted in the production of Hydrotreated Vegetable Oil (HVO), which is renewable diesel fuel, produced from oils and fats. Investigating the HVO sprays further with typical diesel sprays would help in getting rid of existing emissions rich fuels.

1.2 Aims and Objectives

This thesis aims to investigate high-pressure fuel sprays of Hydrotreated Vegetable Oil (HVO), ethanol and diesel EN590 fuels injected into a constant volume pressurized test chamber. The experiments are performed in two phases with different imaging arrangement to determine different spray characteristics. However, the common aim is to study fuel spray characteristics that are related to air-fuel mixing, thus affecting the emissions and combustion efficiency. At the first stage, the spray geometry of fuel sprays is determined by investigating the spray penetration and opening angles. This is followed by the analysis of droplet sizes and their distributions at the edge of sprays. The experimental setup for this thesis is based on backlight imaging system with a high-speed monochrome camera in order to get the greyscale images for sprays to be investigated. Furthermore, the objectives of this thesis also include the investigation of EN590 Diesel spray behavior by changing the nozzle orifice size.

The theoretical part of the thesis provides a comprehensive introduction of spray formation theory along with the explanation of essential fuel spray parameters and the optical measurement techniques for investigating fuel sprays. This is followed by a detailed discussion about the experimental setup and analysis techniques. Furthermore, the explanation regarding uncertainties and sources of errors has also been discussed in the later stage of the thesis.

2 Diesel Injection system

The name “Diesel engine” comes from the inventor of the compression ignition (CI) engine, Rudolf Diesel. CI engines generally have better fuel efficiency than SI (Spark Ignition) engines, but particularly in the past, they were much noisier than SI (gasoline) engines. CI and SI engines produce slightly different emissions, and some emission components are treated by different exhaust treatment systems.

Diesel engines are categorized as compression ignition engines rated as the most efficient combustion engines due to their reduced emissions, fuel consumption and noise. In order to supply fuel to the engine, the fuel injection system is installed in diesel engines that work firstly by achieving the required fuel injection pressure with the help of the injection pump. Passing through the injector tubing, high-pressure fuel is forced to the injector nozzle that injects the fuel into the chamber through nozzle hole/holes. The whole injection system comprises a fuel tank, fuel filter, fuel injection pump and the injectors with nozzles for injection. (Robert Bosch, 1994)

Most of the diesel engines work on the 4-stroke working cycle defined generally by the piston movement. The cycle begins with the intake of air in the first stroke by a downward moving piston, followed by compression stroke (i.e. upward piston motion) where the temperature of the air is increased, and fuel is injected at high pressure through injector nozzle at the end of this compression stroke. The third stroke holds the ignition of fuel that ensures downward motion of piston because of the increased pressure of the cylinder. The upward motion of piston finally pushes out the exhaust gasses entrapped inside the cylinder in the fourth stroke to provide new ground for an incoming charge of fresh air for the next cycle. (Robert Bosch, 1994)

2.1 Common rail Injection system

Diesel engines working on common rail (CR) injection systems have adapted to the growing demands of faster switching times, high pressures and variable rates of discharge to stand amongst the most economical and clean engines category. By separating pressure generation from the fuel injection system, the CR injection system took over the conventional system of fuel injection (Dietsche and Reif, 2011). This can be seen in Figure 1, taken from Reif and Dietsche’s work. With this promising feature, injection pressure and timing can be varied largely, hence increasing the power output with reduced fuel consumption, reduced noise levels, fewer emissions, and increased efficiency. This is the reason why most of the commercial and passenger car diesel engines use common rail system (Dietsche and Reif, 2011).

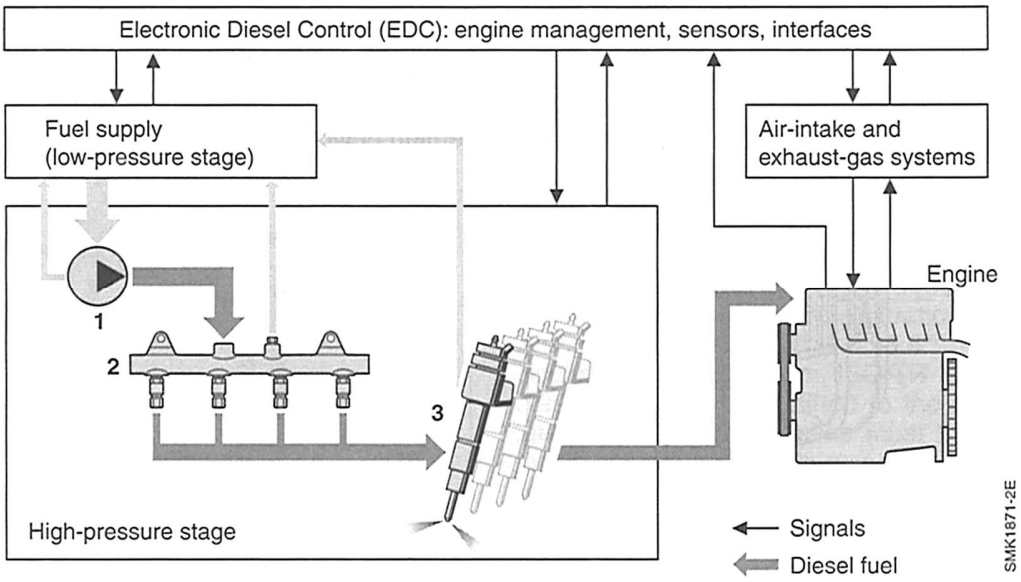

Figure 1 System control areas in common rail injection system for engine management focusing on 1) High-pressure pump, 2) Common rail and 3) Fuel injectors. (Reif and Dietsche, 2011)

It can be seen from the above figure that common rail system consists of low and high-pressure stages. The low-pressure system includes a fuel supply system while the high-pressure stage comprises a high-pressure pump, common rail, injectors and high-pressure fuel lines along with Electronic Diesel Control (EDC). Injectors connected to the common rail system is the key design feature of the CR system because this helps in regulating the injection pressure for individual cylinders (Dietsche and Reif, 2011).

2.2 Fuel Injection

In diesel engines, the fuel injection system governs the supply of fuel to the engine. Fuel injection must be carried out in an accurately measured quantity (taking load of the engine into account), at the correct time, for the precise duration and in a manner that suits the combustion process (Robert Bosch, 1994). The fuel injection process occurs in different steps, starting from generating required pressure by using the fuel injection pump. Pressurized fuel passing through high-pressure fuel injection tubing, reaches up to the injector nozzle that sprays the fuel directly into the combustion chamber. The solenoid-actuated valve connected with the injector helps to control the opening and closing of the injector nozzle by using the control system of the engine. Fuel injection system comprises of following components: fuel tank and fuel filter, fuel supply pump, injector nozzles, and high-pressure injection tubing. Quantity of fuel and its method of injection into the chamber largely affects the process of combustion in diesel engines. Quantity of fuel injected can be determined by system pressure and the opening time of injector. Independent of the engine and pump speed, the quantity of fuel is proportional to the solenoid valve switching time at constant pressure. (Robert Bosch, 1994; Dietsche and Reif, 2011)

2.3 Solenoid-valve diesel injector

In common rail engine systems, injection is carried out by using solenoid valve injectors controlled by the control system. The internal structure of the solenoid-valve diesel injector is shown in Figure 2. The actuator, present in the solenoid valve injector (or piezo injector) controls the electrical voltage, temperature, and vibrations, according to the automotive requirement and also controls the rapid opening and closing of servo valve (Van Basshuysen, Richard, 2004). High common rail pressure refers to increased injection pressure that enhances the air-fuel mixing in the chamber by improving the spray formation thus resulting in efficient combustion with reduced emissions. Constant pressure in common rail during the injection helps in maintaining controlled fuel injection. Injection nozzle at the end of the injector acts as an interface allowing the annexation between the combustion chamber and the fuel injection system. Injector nozzle strongly affects the injection properties and the mixing of fuel inside the chamber. Injection parameters such as injection pressure, injection duration, injection timings, and possible pre injections before the main injection are controlled electronically by the control system. (Mollenhauer and Tschoeke, 2010; Hillamo, 2011)

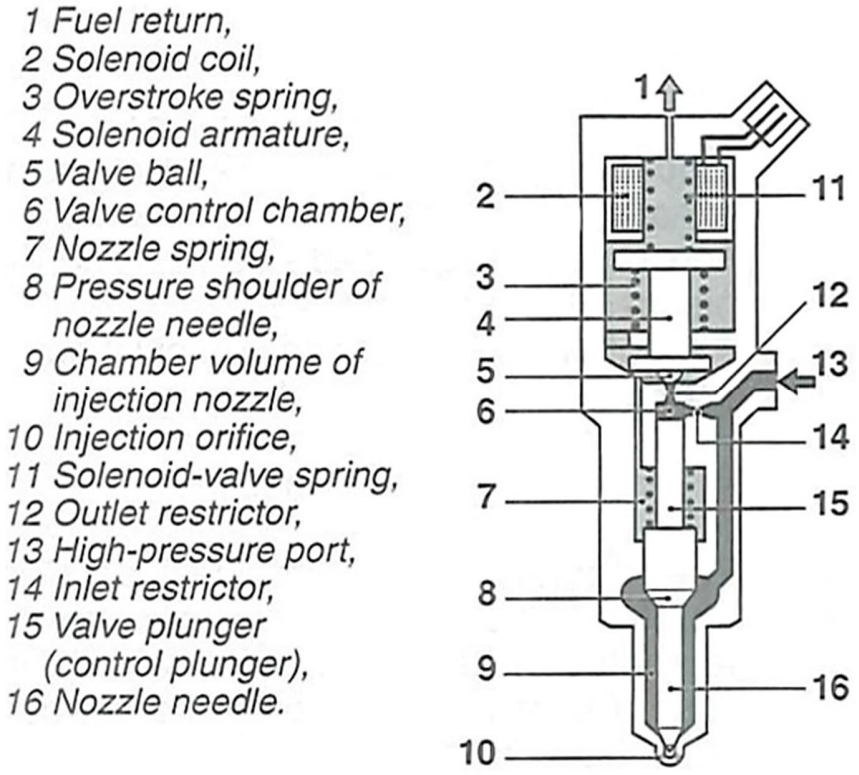

Figure 2 Schematic of Solenoid-valve Injector (Dietsche and Reif, 2011)

3 Fuel spray

3.1 Formation of Fuel spray

3.1.1 Occurring phenomenon in combustion chamber

The combustion chamber includes various physical and chemical phenomena even before the ignition process starts. The disintegration of fuel spray into droplets, evaporation of fuel, and the formation of the air-fuel mixture (due to the fuel diffusion into the chamber air) are characterized as physical phenomena. On the other hand, there exist some chemical processes like atomization of hydrocarbons into smaller ones and the pre-ignition process due to this disintegration (Karimi, 1989). However, because of their protruding amongst each other, there exists no specific boundary, which differentiates these occurring chemical and physical processes (Karimi, 1989).

For optimization of the engine's efficiency and operation, it is always required to have complete information about the processes such as mixture formation, combustion, etc. occurring inside the chamber and how these processes can be affected by different parameters like temperature, pressure, density, velocity, and fuel, etc. One of the critical processes is the formation of the air-fuel mixture inside the combustion chamber before combustion occurs. This air-fuel mixing is generally affected by many factors such as the composition of fuel and the ambient conditions of the chamber. Optimization of fuel injection inside the chamber can assist in improving the mixture formation. (Itani, 2016)

3.1.2 Pressure Atomizers

In IC engines, efficient combustion relates to the proper mixing of evaporated fuel with air that acts as an oxidizer. The mixing is followed by efficient evaporation of liquid fuel when injected into the chamber. The high evaporation rate is one of the main features that is always taken into consideration while selecting the fuel for combustion. Atomizers that convert pressure into kinetic energy are generally used to serve this purpose as they inject liquid fuel at a relatively higher velocity than the ambient air velocity in the chamber, resulting in the fuel to be evaporated suitably for mixing. Generally, some pressure atomizers or rotary atomizers ensure this by injecting liquid fuel at high velocity into the stream of air or any gas in the chamber moving relatively slower. Alternatively, by injection of liquid fuel jet to the high-velocity stream of air, which is commonly called as air blast atomization. (Lefebvre, 1989; Ainsalo, 2018)

Surface tension force tends to keep the liquid fuel spray from disintegrating into droplets unless external forces overcome the surface tension and viscosity. However, as a result of the domination of some aerodynamic forces over surface tension and viscosity, liquid fuel is forced to disrupt into droplets. The initial disintegration of liquid jet due to the turbulence created by the disruptive forces is termed as primary atomization, which is followed by secondary atomization where the droplets having greater sizes than critical further atomize into smaller ones (Lefebvre, 1989). Mostly, pressure atomizers are of plain-orifice and simplex nozzles type, but there are various other designs with variable geometry, duplex and dual-orifice injectors. To avoid or reduce the pressure losses, nozzle orifice length is usually kept short (Lefebvre, 1989).

Flow properties and the initial turbulence in the flow are strongly affected by the nozzle, its orifice size, and geometry. It has experimented that in-nozzle flow experience cavitation when subjected to high injection pressure (Ning et al. 2008). Figure 3 presented by Heisler, explains the nozzle tip, hydraulically operated needle (fuel) valve, fuel gallery, sac volume, and nozzle orifices.

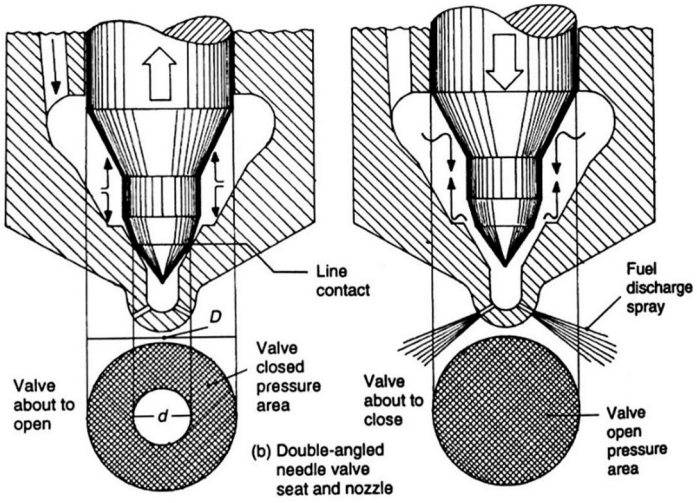

Figure 3 Cross section of injector nozzle showing opening and closing (Heisler, 1995; Hillamo, 2011)

3.1.3 Fuel spray progress and atomization

Fuel injector injects the liquid fuel jet from small orifice/orifices usually of size around 0.3mm (Lefebvre, 1989). Orifice size has a profound impact on the atomization or disintegration of fuel jet as the atomization will get more efficient with smaller orifice diameters. Along with orifice diameters, atomization can be affected by certain other factors such as the geometry of atomizer, fuel properties and the gaseous medium of the chamber. (Lefebvre, 1989)

Liquid fuel follows the path by first pumped from the fuel storage tank to the injection pump while passing through the fuel filter. Then from the injection pump, it is pushed to the injector nozzles at high pressure, returning the excess fuel, back towards the fuel storage tank. The pressure difference method is utilized in order to introduce fuel into the chamber depending upon the engine characteristics. Usually, high pressure difference is applied in order to give a maximum thrust of velocity to the fuel jet at the time of injection, allowing the fuel jet to disintegrate at a maximum level for efficient evaporation. (John B. Heywood, 1988)

Liquid fuel jet enters the combustion chamber filled with air causing atomization and the first thing that the liquid jet must encounter is the air resistance inside the chamber. This reduces the velocity of colliding fluid due to the viscosity effect, thus disintegrating it into droplets. As the fuel is injected with high velocity, this increases the turbulence in the fuel jet and along with higher aerodynamic resistance, fuel spray comes across breakdown. While moving away from the nozzle after injection, the air mass starts to increase in liquid fuel jet leading to a decrement in its velocity by increasing the width. The velocity of the liquid jet is relatively very low on the

outer edges as compared to the center axis of the jet, so the spray starts to disintegrate from outer edges that act as a boundary layer between the liquid fuel spray and air inside the chamber. The leading spray jet encounters greater air resistance and is considered as lower velocity portion of the jet whilst the fuel jet following the leading jet faces relatively lower resistance that makes it to be characterized as higher velocity portion, which forces the leading jet towards the outer edge of the spray for disintegration. The following fuel jet with relatively higher velocity then forces the later coming fuel and lower air resistance towards the boundary layer and this continues until the full penetration of the fuel spray is achieved. In other words, the factors that are mainly involved in the disintegration of fuel in the chamber are listed as the high velocity of jet, aerodynamic forces on jet, turbulence, and cavitation. (John B. Heywood, 1988; Lefebvre, 1989) Stiesch presented certain droplet breakup modes as atomization, Rayleigh and wind-induced droplet breakup regime. In the atomization mode of droplet breakup, the droplet sizes are smaller than the nozzle exit diameter. These modes are explained in Figure 4 (Stiesch, 2003)

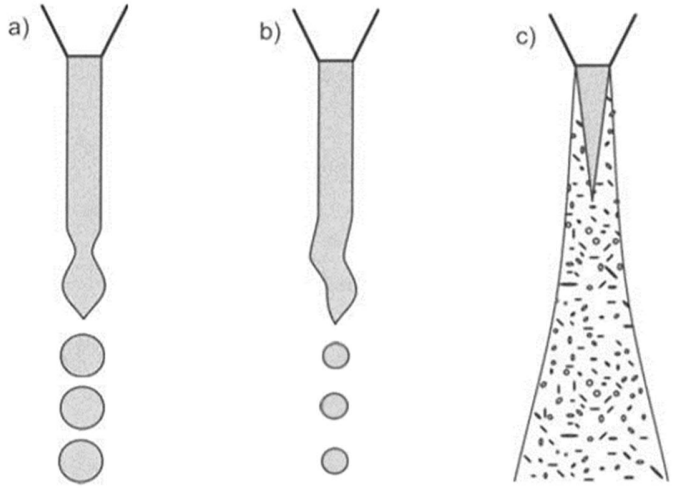

Figure 4 Schematic representation of spray breakup modes. a) Rayleigh breakup b) Wind induced breakup c) Atomization (Stiesch, 2003)

Fuel spray after being injected into the chamber constitutes some parameters that define its characteristics. The liquid column of fuel disintegrates into droplets within the combustion chamber over a finite length, after leaving from the injector nozzle. This finite length of the liquid fuel column is termed as breakup length. (John B. Heywood, 1988) Spray then continues to penetrate inside the chamber as the injection process proceeds and reaches to the maximum point of penetration. The distance, which the fuel spray travels from the tip of the nozzle till the maximum penetration is termed as spray tip penetration. A relatively denser region of spray includes an un-breakup portion of the liquid fuel and is termed as the core of spray (Arai, 2012) Fuel spray parameters can be seen quite effectively in Figure 5.

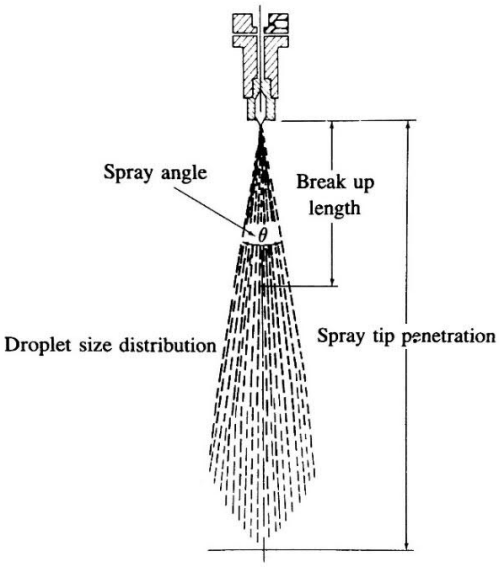

Figure 5 Schematic illustration of diesel spray parameters (John B. Heywood, 1988)

3.1.4 Spray and droplet break-up

Research on fuel spray is still not able to come up with a defined and authentic breakup model for the spray breakup phenomenon because of high jet velocities and some other factors like density etc. However, some models have been presented for fuel spray breakup, and are mostly divided into spray and droplet breakups that are also studied as primary and secondary breakups. (Hillamo, 2011; Arai, 2012) Stiesch presented a two-phase flow ejected from the atomizer to show different spray fuel regimes. The spray regime starts from a thick flow of spray at the nozzle exit which begins to disintegrate into ligaments and then to droplets. (Stiesch, 2003) For numerical purposes, the basic breakup model of diesel fuel jet was presented by Arai and can be seen in Figure 6 (Arai, 2012).

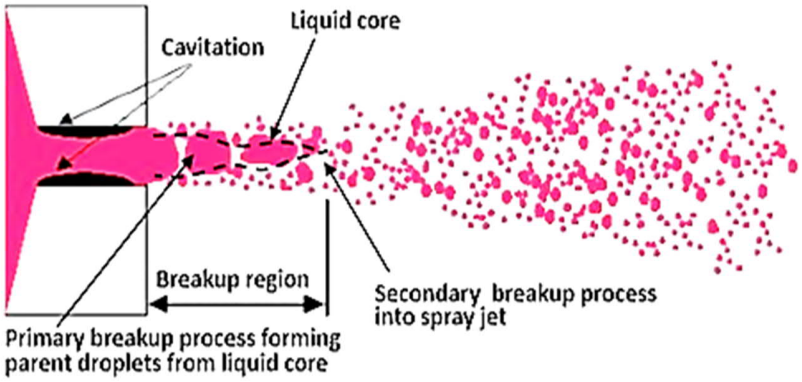

Figure 6 Diesel fuel jet breakup model (Arai, 2012)

Primary or Spray break-up

Liquid jet, when injected from the injector nozzle, disintegrates first into ligaments and droplets of relatively larger sizes. This initial breakup of the liquid jet is referred to as primary breakup. Primary spray breakup can be affected by the flows inside the nozzle orifice e.g. turbulence and cavitation mostly. Aerodynamic forces created due to the velocities difference between the surrounding air and liquid jet also affect somehow the spray breakup process. The primary breakup model presented by Stiesch can be seen in Figure 7 where the flow from nozzle orifice is studied into zone 1 and 2. The region where there is high momentum liquid jet is zone 1 and zone 2 contains cavitation bubbles and ligaments having lower momentum. (Stiesch, 2003)

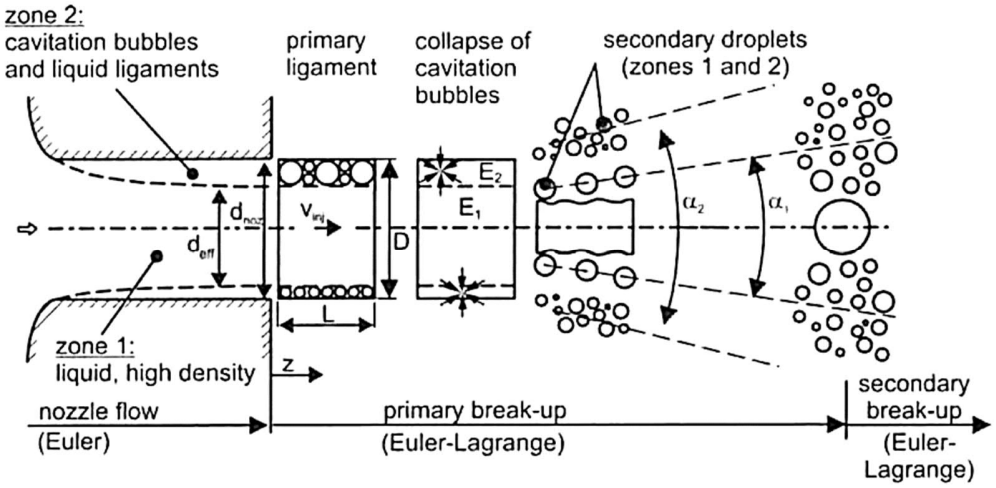

Figure 7 Schematic presentation of primary breakup model (Stiesch, 2003)

Secondary or Droplet breakup

Fuel spray followed by primary breakup proceeds with the disintegration of ligaments and relatively larger droplets into smaller fine droplets. This is referred to as the secondary or droplet breakup of the fuel spray. Droplet breakup is due to the effect of aerodynamic forces on fuel spray, which causes turbulence in the parent spherical droplet and leads to its breakup. Nevertheless, in doing so, these forces have to overcome the surface tension force which prevents the droplet from the breakup or any other distortion. (Stiesch, 2003) The secondary breakup also depends somehow on the dynamics of initial parent droplets and the surrounding gas that interacts with the droplets. (Arai, 2012) Stiesch presented a dimensionless property called Weber number (We) which relates the aerodynamic forces to the surface tension and can be used to measure the droplet breakup behavior as:

$$We = \frac{\rho_g r_d v_{rel}{}^2}{\sigma}$$

where ρ_g is the density of the gas, r_d is the droplet radius, v_{rel} is the relative velocity between the droplet and surrounding gas, and σ is the surface tension of the droplet fluid. (Stiesch, 2003; Hillamo, 2011) Weber number is used to find out the relation between the surface tension (which keeps the droplet from disintegration) and aerodynamic forces (which tends to break the droplets). It can be seen from the above relation that with the increased values of Weber number, the effect of surface tension forces will be lesser and thus increase in the aerodynamic forces that tend to break the droplets: This is is termed as atomization. (Sirignano, and Tryggvason, 2000) Droplet breakup depends relates with the critical Weber number value in such a way that in the droplets having the Weber number values higher than the critical Weber number, the aerodynamic forces subjugate the surface-tension forces and tend to cause breakup of the droplets. On the other hand, surface-tension forces overshadow the aerodynamic forces in the droplets having Weber number values below the critical value, thus maintaining the shape of the droplet stream. The critical Weber number depends upon the relative liquid-gas velocity (Sirignano, and Tryggvason, 2000)

The experimental research has shown that droplet breakup has various breakup mechanisms depending upon the Weber number. Following five breakup regimes typically shows the different breakup mechanisms:

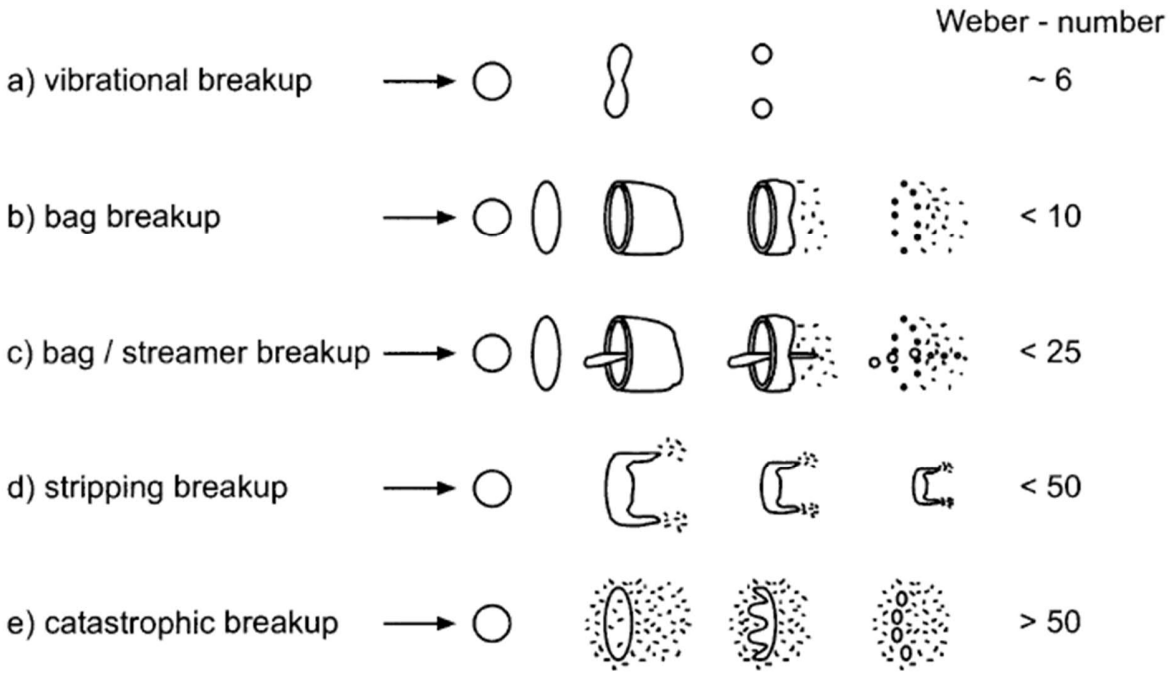

Figure 8 Different droplet breakup regimes (Wierzba [1990], in Stiesch, 2003, p.154)

The oscillations created in the droplet for a Weber number near the critical value of six generally breaks down into two identical size droplets. Further increase in Weber number causes the

droplet to adapt a bag-like shape. For Weber number range between 10 and 25, an appended streamer-shaped interior structure of droplet develops inside the bag. Moreover, Weber number range between 25 and 50 gives rise to stripping breakup in which small droplets strip off from the primary bigger droplets. Lastly, a catastrophic breakup occurs when the Weber number is above 50. However, there are uncertainties between the defining Weber numbers, mostly among the higher Weber numbers after which the catastrophic breakup occurs. (Arai, 2012, Stiesch, 2003)

High-pressure diesel or gasoline fuel sprays possesses all the above-mentioned breakup mechanisms. The Weber number and the relative velocity between droplet and gas influence the droplet breakup regime in such a way, that the areas having larger relative velocities between the droplet and ambient air, such as close to the injector nozzle, experience catastrophic breakup because of the increased Weber number values. On the other hand, the relative droplet velocities are lower far from the nozzle, thus different droplet breakup mechanism exists. (Stiesch, 2003)

3.1.5 Fuel Jet exit

Injectors can be of different types with varying nozzle designs and the number of holes, but the working principle of nozzles is almost the same as plain nozzle orifice as presented by Hillamo (2011) in Figure 9. High velocities are usually attained before the nozzle exit because of the high-pressure difference created due to the increased fuel pressure in the injector and the lower pressure of air in the cylinder. Taking Bernoulli's equation into consideration, the value of flow velocities in diesel injector nozzles ranges from 400 to 700m/s. (Hillamo, 2011). High-velocity fuel ejects from the nozzle and starts to disintegrate because the orifice walls can no more keep the fuel jet in compact form, thus fuel jet has to face turbulence and other external forces like air resistance for atomization. (John B. Heywood, 1988; Hillamo, 2011)

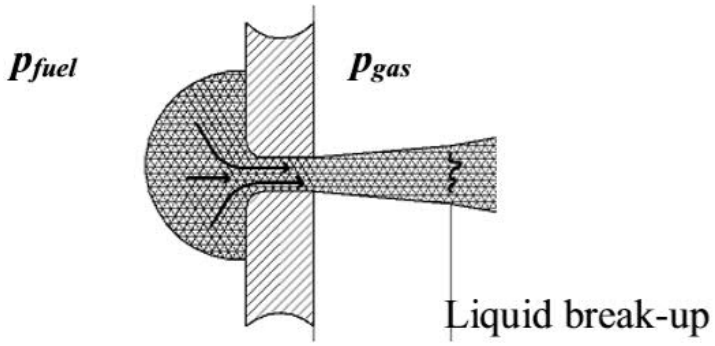

Figure 9 Flow from plain orifice driven by pressure difference. (Hillamo, 2011)

3.1.6 Fuel Jet Exit Velocity

The exit velocity of fuel jet along with the turbulence effects can affect the spray properties majorly, as increased jet velocity relates to increased momentum and increased slip velocity amongst the air and liquid fuel, resulting in increased atomization. Bernoulli's equation can be

used to assess the maximum jet exit velocity for diesel injectors and the equation is: (Naber and Siebers, 1996; Hillamo, 2011)

$$U_{fuel,max} = C_v \times \sqrt{2 \times \frac{(p_{fuel} - p_{gas})}{\rho_{fuel}}}$$

Where:

'$p_{fuel} - p_{gas}$ [Pa]' is termed as pressure difference between the fuel and the gas (air) in the chamber, '$\rho_{fuel}[kg/m^3]$' is the density of fuel and 'C_v' is the coefficient of nozzle velocity and can be approximated for calculations. For instance, it can be defined as unity for the assessment of theoretical maximum velocity. (Naber and Siebers, 1996)

3.1.7 Effect of Jet velocity on Spray distribution regions

Lefebvre suggested in his work that there comes a stage in fuel spray penetration where the flow changes its regime from laminar to turbulent by going through a short period of transition or semi-turbulent flow where the fluid is accelerating slowly. This effect can be observed with the help of Reynold's number (Re), as Re>2300 suggests turbulence of the flow. (Lefebvre, 1989)

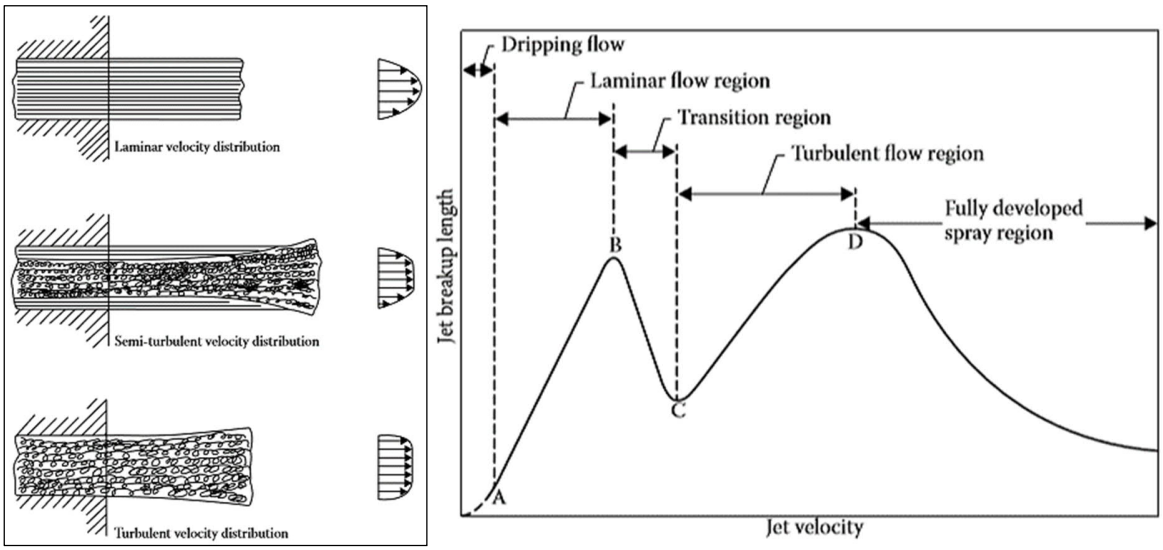

Figure 10 Change of flow from laminar to transition and then to turbulent with change in relative flow velocity. (Lefebvre, 1989)

3.1.8 Fuel Flow rate

The behavior of fuel in the fuel injection system is not easy to assess, but estimations exist about the flow rates through the injector nozzles. It was presented by (John B. Heywood, 1988) that if the upstream fuel pressure of injector nozzle can be estimated, keeping in mind certain considerations that the flow is quasi-steady from every nozzle, unidimensional, and incompressible, then the mass flow rate of the fuel-injected through the nozzle can be calculated as:

$$\dot{m}_f = C_D A_n \sqrt{2\rho_f \Delta p}$$

Where:

A_n is the minimum area of nozzle, C_D as the discharge coefficient, ρ_f the fuel density and Δp is for the pressure drop across the nozzle. (John B. Heywood, 1988)

3.1.9 Cavitation

As explained earlier about the factors involved in the primary breakup of the fuel spray, cavitation is one of them. It is indeed a useful phenomenon as it enhances the breakup process of spray with the help of bubble formation and their explosion while ejecting from the injector nozzle. It is very challenging to analyze the internal flows of injectors because the real size injector and nozzles are of quite small dimensions and work at high injection pressures. Therefore, most of the studies are being performed on large scale models. (F. payri, V. Bermúdez, R. Payri, 2003)

The pressure difference between the fuel in the injector nozzle and the gas in the chamber accelerates the fuel when it is in the nozzle, resulting in immense turbulence in the flow while exiting from the nozzle orifice. This results in the reduction of the effective cross-section area of the nozzle due to the contraction of streamlines, hence the velocity of the flow further increases. Because of this, Bernoulli's Law suggests decrement in static pressure to almost equal to the vapor pressure of fuel and thus cavitation bubbles start to generate inside of the nozzle. It can be seen in Figure 11. These bubbles eject out of the nozzle into the chamber, explode and help in the disintegration of the fuel spray. (Stiesch, 2003)

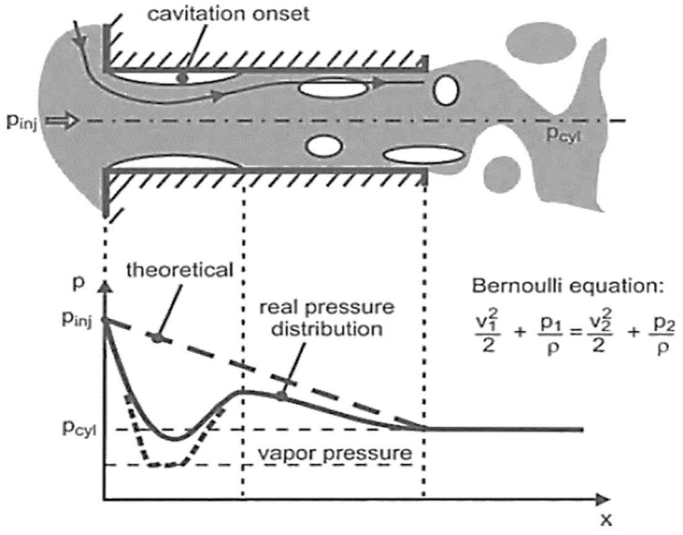

Figure 11 Schematic of cavitation formation inside the injector nozzle (Stiesch, 2003)

Despite cavitation helps in disintegration, there is a detriment associated with it regarding the injector nozzle. Chaves in his experimental work mentioned the damage caused by cavitation as it might corrode the surfaces of the nozzle while opening and closing during various injections. Therefore, finely rounded and smooth nozzles can get deformity after some injections, when cavitation occurs inside the nozzles. (H. Chaves, M. Knapp, 1995)

3.1.10 Shockwave Generation

High-pressure difference at the nozzle orifice results in high velocities of spray in diesel injectors, which allow the generation of shockwaves in diesel fuel sprays. The bending of these shockwaves at certain angles helps in the estimation of fuel spray velocity at the exit giving the local Mach number values. The edge of fuel spray progresses with high velocity (supersonic) within the surrounding having stationary gas and the shockwaves travel with a local speed of light. This makes the shockwaves to lag behind the fuel spray (Hillamo *et al.*, 2010).

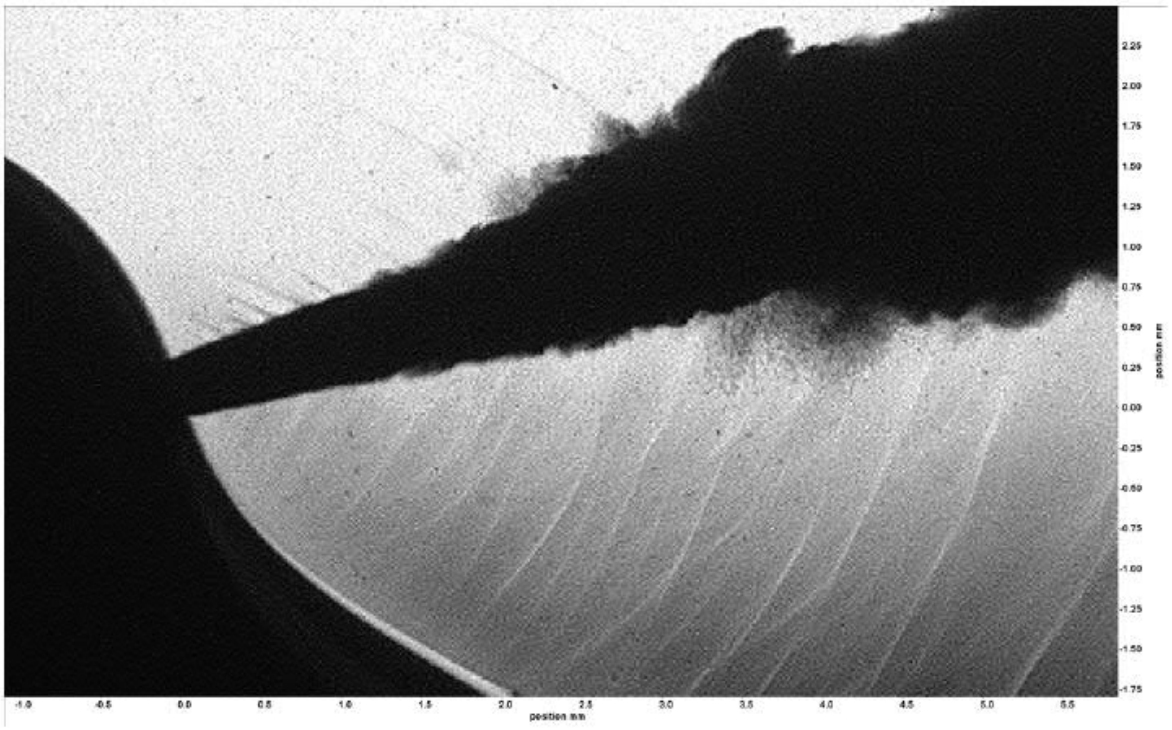

Figure 12 Shockwaves generation at the nozzle exit with the hole diameter of 0.36 mm. (Hillamo et al., 2010)

3.2 Fuel spray parameters

3.2.1 Overview

Fuel sprays are characterized by following parameters presented by (Arai, 2012)

- Spray angle
- Breakup length
- Core of spray
- Spray penetration
- Size distribution of spray
- Spatial distribution of spray
- Mean diameter of spray
- Turbulence

Most of the fuel spray characteristics can be seen in Figure 13. The parameters illustrated in the figure were known as macroscopic parameters of the fuel sprays. In this thesis, the focus is on three of these parameters: spray penetration, opening angle and droplet size distributions. A further detailed explanation of these parameters will be discussed in the later chapters of this thesis.

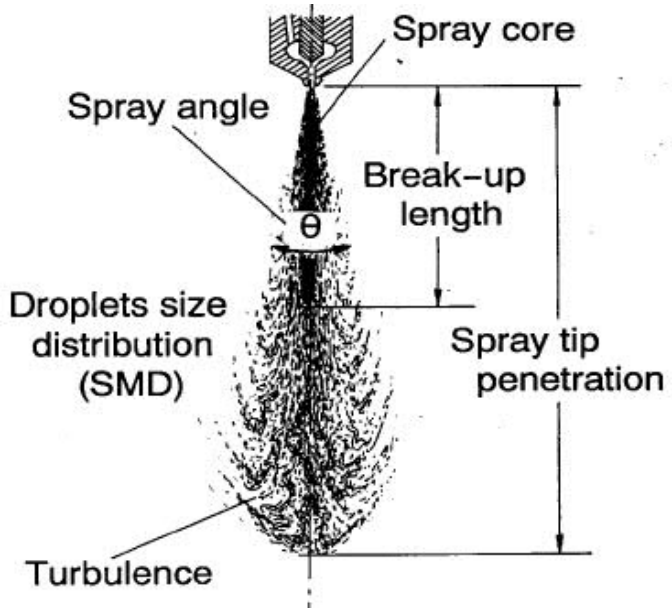

Figure 13 Characteristic parameters of diesel spray (Arai, 2012)

3.2.2 Spray angle

One of the most interesting spray characteristic parameters is the spray angle. Spray angle sometimes can be hard to define in a simple way. However, it can be explained by many different definitions because of the variation in the spray angles during the injection (Hillamo, 2011; Arai, 2016). The variation of spray angle occurs in a way that the spray angle, in the

beginning is somehow transient and followed by relatively constant angle as the spray propagates (Naber and Siebers, 1996). Furthermore, the side eddies can also change the spray angle readings at varying distances from the injector nozzle (Hillamo, 2011). Therefore, the definition is typically modified according to the spray angle measurement technique.

Spray angle was defined as the angle between two lines drawn from the nozzle tip to the outer edge of the spray at a distance of 60 nozzle hole diameter downstream the nozzle (Lefebvre, 1989; Hillamo, 2011) It can be seen in Figure 14.

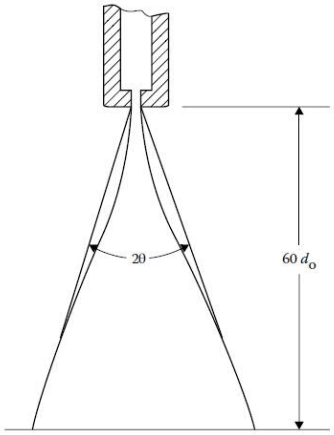

Figure 14 Definition of spray angle based on the measurement from a certain distance from the injector nozzle. (Lefebvre, 1989; Hillamo, 2011)

Spray angle is considered a very important property of fuel sprays because increased spray angle results in efficient air-fuel mixing which in the end effects on soot formation and combustion temperatures. Moreover, minor increment in the spray angle can result in a promising improvement of the air-fuel mixing (Hillamo, 2011)

Spray dispersion can be explained by characterizing the spray angle in two different cases with two separate definitions by (Arai, 2016). In the first case, the spray angle is defined as the maximum angle between the edges that can be measured throughout the whole penetration (Case 1 in Figure 15). The other case is to define the spray angle at a fixed distance from the nozzle tip. (Case 2 in Figure 15). Moreover, the spray angles are defined differently for the beginning of fuel injection (A), constant injection at the later stage of injection (B) and at the end of injection (C) in Figure 15.

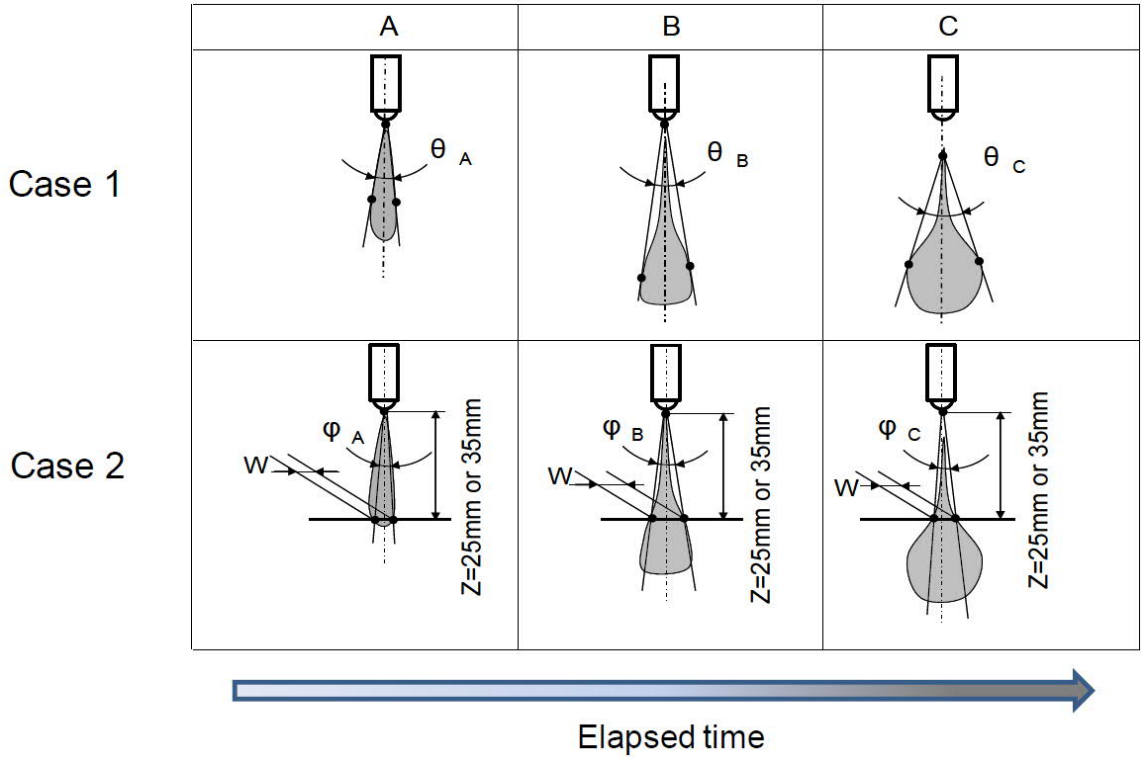

Figure 15 Spray angle definition of a transient diesel fuel spray (Zama et al. [2011], in Arai, 2016)

Generally, the spray angle increases when the gas density and the injection pressure increases (Hillamo, 2011). However, some other factors are also involved in increasing the opening angle. The spray angle increases when:

- Injection pressure is increased. This effect was observed with the pressure values under 1000 bar (Hillamo, 2011). Moreover, similar trends were observed by (Hiroyasu and Arai, 1990) with lower injection pressures
- Ambient gas density is increased (John B. Heywood, 1988; Naber and Siebers, 1996).
- Nozzle orifice size is decreased (Hillamo, 2011).
- Nozzle length to diameter ratio is decreased (John B. Heywood, 1988).

3.2.3 Spray penetration

Just like opening angle, spray penetration is also an importing fuel spray property. In larger diesel engines, over-penetration can result in the collision of fuel with cold combustion chamber

walls having very low air swirl. This leads to the wastage of fuel during the combustion and causes hydrocarbon (HC) emissions to increase. Contrarily, under-penetration results in inefficient air-fuel mixing, because the air/gas present far away from the injector nozzle might not be able to mix with the fuel droplets. Therefore, spray penetration should be matched with the combustion chamber's size and geometry, in order to have efficient engine performance. (John B. Heywood, 1988; Lefebvre, 1989)

Defining the spray penetration is pretty much easier than spray angles. Spray penetration can simply be described as the distance from the origin of spray at the nozzle tip to the tip of spray penetrating inside the chamber. The spray tip is determined using the backlight intensity, during the imaging. Moreover, image quality, contrast, and brightness of the images also affect the intensity threshold. Good spray penetration results can be achieved from good quality and high contrast images. However, the results are majorly affected by the spray-to-spray variations during multiple injections. Nevertheless, these variations can be minimized by averaging the results taken from a series of measurements. (Hillamo, 2011; Ainsalo, 2018

There are two phases of spray tip penetration in the spray penetration curve plotted as a function of time. Initially, the penetration progress is very fast because when jet exists in the liquid form and experience less aerodynamic resistance against the flow. However, the progress of penetration gets slower at the later stage, because the jet loses its velocity and disintegrates into smaller droplets due to the increasing air resistance. (Arai, 2016)

Various correlation of spray penetration have been presented by Dent (eq. 2) and Hiroyasu (eq. 3,4 and 5) in (John B. Heywood, 1988) as a function of time based on the data collected through experiments and turbulent gas jet theory.

$$S = 3.07\left(\frac{\Delta p}{\rho_g}\right)^{\frac{1}{4}}(td_n)^{1/2}\left(\frac{294}{T_g}\right)^{\frac{1}{4}} \tag{2}$$

And,

$$t < t_{break}: S = 0.39\left(\frac{2\Delta p}{\rho_l}\right)^{\frac{1}{2}} t \tag{3}$$

$$t > t_{break}: S = 2.95\left(\frac{\Delta p}{\rho_g}\right)^{\frac{1}{4}}(td_n)^{1/2} \tag{4}$$

$$t_{break} = \frac{29\rho_l d_n}{(\rho_g \Delta p)^{1/2}}. \tag{5}$$

Where,

Δp: Pressure drop across the nozzle (Pa)
ρ_g : Gas density (kg/m^3)
ρ_l : Liquid density (kg/m^3)
ρ_l : Liquid density (kg/m^3)
d_n : Nozzle orifice diameter (m)
T_g : Gas temperature (K)

The effect of injection pressure and ambient gas pressure/density has been presented in (Naber and Siebers, 1996; Arai, 2016) as the spray penetration decreases with increasing ambient gas pressure. However, the effect of injection pressure seems not to be very significant. Moreover, fuel spray is the source for most of the turbulences created during the combustion even. Slight changes in penetration can have a major impact on combustion, as increased penetration causes the increased cone volume, which can affect the mixing of air and fuel in the chamber. Therefore, spray penetration measurement is handled very carefully. (Hillamo, 2011)

3.2.4 Droplet size distributions

In internal combustion engines, it is essential to have the evaporation effective enough to support efficient combustion. Evaporation of fuel sprays gets more efficient with an increased surface area of droplets. Therefore, liquid fuels are subjected to atomization with an aim to achieve an increased surface area of the droplets. The surface is area is higher where the droplet sizes are smaller and thus results in better evaporation. The knowledge and thorough understanding of droplet sizes are necessary while designing the modern Internal combustion engines (Stiesch, 2003; Hillamo, 2011). In general practice, all fuel sprays possess a range of varying droplet sizes and are characterized by droplet size distributions. (Hillamo, 2011) The droplet size distribution of diesel spray is shown in Figure 16 by comparing it with other types of droplets.

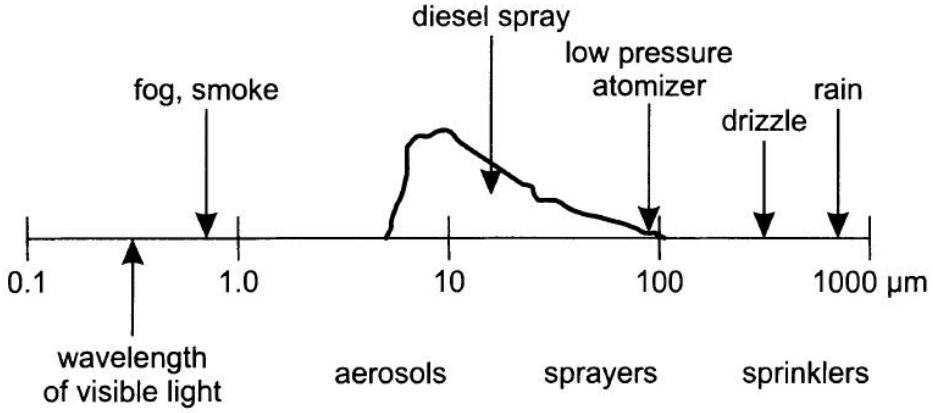

Figure 16 Droplet size distribution comparison of a typical diesel fuel spray with other fuel spray types. (R.D. Reitz, in Stiesch, 2003, p. 119)

In the literature, different definitions for droplet size distribution are available along with various diameter calculation relations. However, the most common mean diameter amongst them is the Sauter Mean Diameter (SMD or D32) used to explain the droplets mean diameters in the fuel spray analysis. Sauter Mean Diameter can be defined based on droplet numbers (eq. 1) or droplet mass (eq. 2) as:

$$D_{SM} = D_{32} = \frac{\sum n_i {D_i}^3}{\sum n_i {D_i}^2} \qquad \text{eq. 1}$$

$$D_{SM} = D_{32} = \frac{\sum m_i}{\sum m_i / {D_i}^2} \qquad \text{eq. 2}$$

The SMD helps to relate with the volume-to-surface area ratio of droplets and the whole spray. The droplet possessing the diameter value of SMD shows that it has a similar volume-to-surface area ratio as that of the complete spray. Volume-to-surface area ratio is an important factor to be considered because it affects fuel combustion practically. Moreover, processes like heat and mass transfer, evaporation and fuel mixing significantly get affected by the surface area of droplets. (John B. Heywood, 1988; Lefebvre, 1989; Arai, 2016; Ainsalo, 2018)

Measurement of the droplet size distribution of diesel spray shows the droplet size variation with the location in spray and is presented by (John B. Heywood, 1988) At the spray edges, the droplet size distribution seemed to show smaller diameters (John B. Heywood, 1988). However, other studies also show the opposite trend of increased diameters by going away from the center axis towards the spray edge (Larmi et al., 2002). The contradictions in the results of different studies give rise to the discussion that experimental setup, technique, and parameters might have a strong effect on the results. Furthermore, studies have shown the variation of droplet sizes with changing injection stages. The results of (Ueki, Ishida and Sakaguchi, 2005) show that during the transient injection stage, the droplets with larger diameter appeared to increase in number.

Various techniques have been adapted to overcome the glitches in measuring the droplet sizes of very small droplets. Moreover, some other constraints also appear while performing droplet size measurement techniques. Measurement of very large and high-velocity droplets, a wide range of droplet sizes, the variation in droplet sizes with evaporation and coalescence are some of the factors that can sometimes make size determination analysis problematic. However, the measurement accuracy depends on the sample size. This relates to the fact that some very large-sized droplets may affect the mean droplet diameter of the sample. If the sample size is smaller (i.e. 1000 droplets) the effect of few odd droplets on the mean droplet diameter will be higher. However, if the sample size is kept relatively bigger (i.e. at least 5000 droplets), the measurement accuracy of droplet size distribution can be increased. (Lefebvre, 1989)

4 Optical measurement techniques

4.1 Overview

The optical research on Diesel engines focuses mainly on pollutant emissions and its possible causes, combustion properties, fuel injection, fuel spray characterization, ignition, etc. This research aims for analyzing the effects of engine operating parameters (e.g. injection pressures, mechanical design, fuel properties, etc.) on engine performance and emissions. This leads to the necessary modifications required for the engine design and the operating factors (Ainsalo, 2018).

Various optical measurement techniques are being in use for optical research in diesel engines, especially the fuel spray characteristics. The most common optical measurement technique used for basic spray characteristics such as spray tip penetration and spray opening angles is using the simple backlight imaging system consisting of a backlight and high-speed camera (Zhao, 2012). Research on fuel sprays also includes droplet size measurements, which is typically done with various methods that include electrical, mechanical and optical techniques. However, due to certain constraints mechanical and electrical techniques are typically considered meddlesome techniques. Mechanical techniques indeed are cost-effective, however, the abstraction and assortment of the spray sample data is the main issue (Lefebvre, 1989; Greenhalgh and Jermy, 2002; Ainsalo, 2018).

Recently, two general categories divide the optical measurement techniques for spray patternation and are termed as imaging and non-imaging methods for optical measurements. The imaging techniques have been modified and improved quite well by overcoming the incident light attenuation issues. Moreover, the imaging methods provide the opportunity to see the sprays and their behavior. Imaging techniques typically include photography and holography. On the other hand, non-imaging techniques are further explained into two categories, where one group of techniques analyzes every droplet of the spray individually, whilst the other one characterizes a large bunch of droplets (Lefebvre, 1989; Ainsalo, 2018).

Lequien (2015) presented another classification of optical measurement techniques as active and passive methods of optical measurements. Active technique refers to the method of optical measurement in which, an external light source is used to illuminate the spray. However, in passive optical techniques, the spray is illuminated by the actual photon emitting from the spray itself. In this thesis, the fuel spray used were non-reactive, therefore, only active techniques were considered for the optical measurement of spray characteristics. Furthermore, Greenhalgh and Jermy (2002) presented three different optical methods Phase Doppler anemometry, Fraunhofer diffraction and laser sheet imaging. These techniques are commonly used for the measurements of droplet sizes. However, high-speed photography is also used for optical measurements of droplet size distributions (Lefebvre, 1989; Zhao, 2012).

4.2 Photography

Photography is the most commonly used optical technique used for global fuel spray characteristics (i.e. spray penetration and opening angles). Photography for optical fuel spray characterization includes single shot and high-speed modes (Zhao, 2012; Ainsalo, 2018). Basic setup for photography consists of a backlight source and a high-speed camera can be seen in Figure 17. Sometimes, milk glass is used in the same axis between the camera and backlight. This helps in getting homogenous light intensity in the image background, thus smoothing the background of images.

The fuel sprays typically are considered as high-speed flows, therefore, to freeze the high-speed and transient spray motion, high-intensity backlight with high illumination is required for a very short interval of time. For this purpose, a pulsed light source is typically used that is equipped with a xenon arc lamp and has the pulse width range in one microsecond. In most of the cases, this kind of light source with microsecond pulse width works fine, however, sometimes the

spray motion is very fast that it requires the use of lasers having pulse widths range of tens of nanoseconds. (Zhao, 2012)

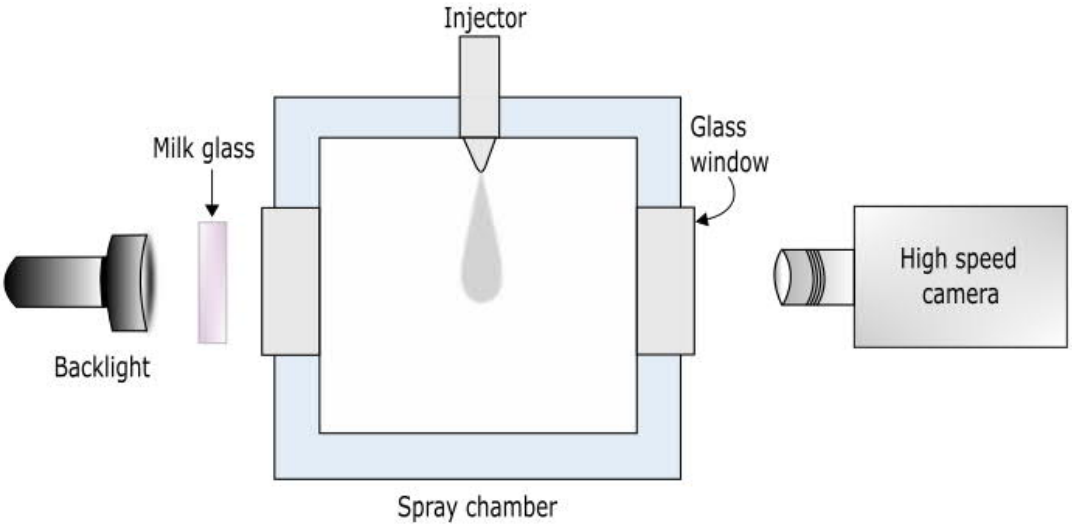

Figure 17 Basic arrangement of backlight photography

Regarding the droplet size imaging, area of interest and the droplet sizes should have to be compromised with each other. This means that if the area of investigation is small, the droplets with smaller sizes have good chances to be detected properly at the expense of accuracy regarding the larger droplets incidence. However, an increased image area restricts the detection of smaller droplets (Zhao, 2012). Moreover, the fuel spray droplets are detected individually based on their sizes. Therefore, the denser sprays possess lower accuracy with regards to the droplet detection. This is because, in denser sprays, some droplets are very close to each other that they even seem to be overlapping with each other. This makes the individual droplet detection very hard and requires enhanced magnification. Increasing the magnification of image area helps in separating those droplets for individual detecting but at the cost of depth of field (Lefebvre, 1989; Zhao, 2012)

Furthermore, the droplets are observed as dark spots on the images and by setting a specific intensity threshold, they are recognized from the background. Generally, the droplets are detected within one pixel distance by their sharp edges in such a way that the intensity of the background area possessing the droplet drops to almost zero. However, by using the intensity threshold gradient within the distance of several pixels, the droplets are characterized by their sizes on the basis of their respective intensity threshold. This means that the droplets with blur and sharp edges possess different intensity threshold value. The droplets that are away from the depth of field generally appear with blurred edges and they can be excluded from the analysis by applying the certain minimum filter for the intensity gradient (Rantanen et al. 1993)

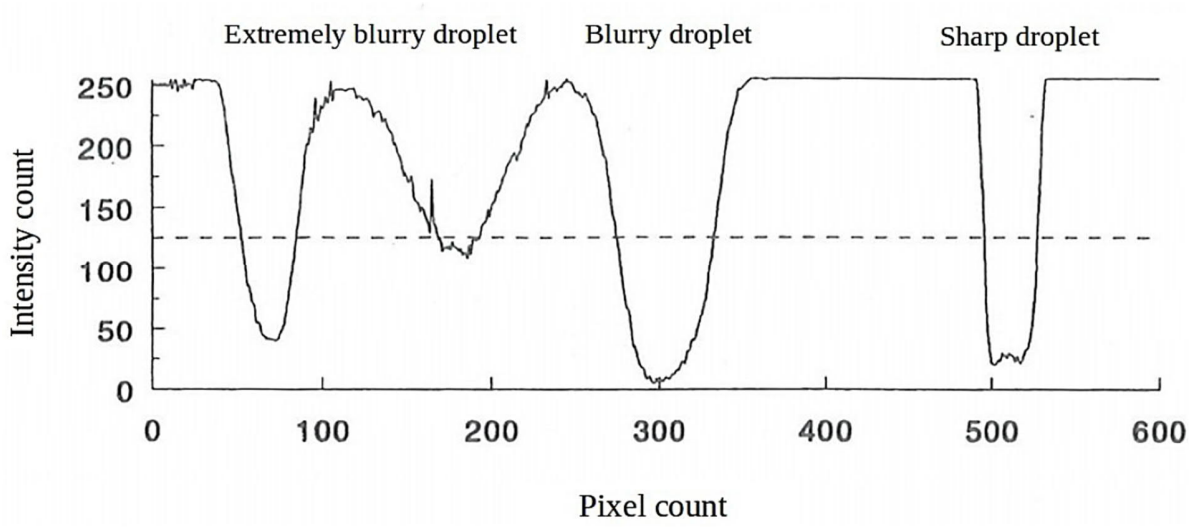

Figure 18 Intensity levels at image cross section. Taken from (Rantanen et al. 1993)

4.3 Other optical techniques

Some other optical measurement techniques that are used for optical measurement of fuel spray characterization are listed as:

- Ballistic imaging
- Fraunhofer diffraction method
- Phase Doppler anemometry
- Laser sheet droplet sizing
- SLIPI

All these methods have different optical measurement techniques but with a common aim of spray characterization including the droplet sizes, spray penetration and the opening angles. Ballistic imaging and SLIPI are very different optical measurement techniques with a common idea to improve the image quality while dealing optically denser sprays by rejecting the multiplied scatter photons. In order to do so, the ballistic imaging technique requires a separate optical arrangement by adding a mechanical shutter in the system before the camera. However, in SLIPI, the scattered photons are discarded by taking three images and perform post-processing with spatial intensity modulations (Linne, 2013).

These methods have their own pros and cons regarding the measurements. Greenhalgh and Jermy, (2002) presented some basic features of some of Phase Doppler anemometry (PDA), Fraunhofer diffraction method and Laser sheet droplet sizing (LSD) techniques. (See Table 1)

Technique	Advantages	Disadvantages
MPS	Simple Easy to calibrate Low cost	Line-of-sight Low spatial resolution Difficulties in dense sprays
PDV	High spatial resolution Easy to calibrate Real-time data Simultaneous dropsize and velocity Most comprehensive method for detailed measurements	Point specific Requires a specific off-axis forward scatter geometry Cannot cope with dense sprays Very expensive Full spray mapping requires a long measurement time
LSD	Simple Modest cost Images the full spray Works in dense sprays Also measures liquid volume fraction	Requires a separate calibration Only *proven* for temporally averaged SMD measurements

Table 1 Advantages and disadvantages of MPS (Malvern particle sizer/ Fraunhofer diffraction method), PDV/PDA (phase Doppler velocimetry/ anemometry), and LSD (laser sheet droplet sizing) summarized by Greenhalgh and Jermy, (2002)

Greenhalgh and Jermy, (2002) also proposed that all these methods face challenges while working on denser sprays that sometimes leads to false and misleading measurement results. When the spray density is very high, the measurement results from the PDA technique come up with a remarkable contradiction with the Faunhofer diffraction method. However, with the fuel sprays possessing lesser densities, the measurement results for PDA and Faunhofer diffraction method show quite reasonable agreement with each other (Greenhalgh and Jermy, 2002).

Along with these presented optical techniques, there are other optical measurement techniques that exist and being tested. Although, all of these techniques are not presented here in this thesis work, the literature of (Coghe and Cossali, 2012), (Greenhalgh and Jermy, 2002),(Lefebvre, 1989), (Zhao, 2012) and (Linne, 2013) gives a detailed explanation regarding the optical measurement techniques.

5 Fuels

The fuels used in the engines have been revolutionized from the last decade. Comparing the quality of fuels now a days with that of the fuels ten years or more ago, it can be satisfactorily said that the availability of fuels having high quality, lower or zero Sulphur content, ash-free and possess no heavy fractions is more frequent in the developed countries. This has also improved the quality of engines remarkably by increasing their lifetimes and reduced maintenance (Aatola *et al.*, 2009). Diesel engines have been considered as one of the best possible efficient and emission-free engine technologies due to their increased thermal efficiency as compared with gasoline engines. However, the performance proved a strong need for emission reductions in diesel engines. This has pushed the research to focus more on finding better and cleaner fuels for diesel engines (Sugiyama *et al.*, 2012).

Lapuerta *et al.*, (2011) suggested three alternative fuel options that are considered viable to use in the diesel engines amongst all proposed conventional fuel alternatives. These alternatives are termed as biodiesel fuels, hydrotreated oils, and Fischer-Tropsch (FT) diesel fuels. The use of biodiesel in compression ignition engines as direct or a blending component does not require certain modifications in the engine design and is considered also as carbon-neutral fuel (Bezergianni and Dimitriadis, 2013).

Hydrotreated Vegetable Oil (HVO) and Ethanol fuel are used in this thesis to analyze the fuel sprays and compare with normal diesel EN590 fuel sprays.

5.1 Hydrotreated Vegetable Oil (HVO)

5.1.1 Manufacturing

Hydrotreated Vegetable Oil (HVO) is a very high quality bio-based diesel fuel that is generally termed as 'renewable diesel fuels'. Aatola *et al.*, (2009) proposed HVO to be a mixture of paraffinic hydrocarbons. The highly available feedstocks such as animal fats or vegetable oils along with the waste oils are used to produce Hydrotreated Vegetable Oil (HVO) from a process called hydrotreating of oils and fats. Isomerization process is also used to overcome the cold properties of HVO and making the HVO meet the local requirements (Aatola *et al.*, 2009; Hartikka et al., 2012)

HVO is considered as highly paraffinic fuel having a high cetane number with no aromatics, olefins or naphthenes. Hartikka et al., (2012) proposed a simplified manufacturing process of HVO that is divided into three main processes i.e. pre-treatment of feedstock, hydrotreatment, and isomerization. The impurities in the form of metals, phosphorus, nitrogen, etc. are removed in the pre-treatment phase. The catalyst used in the later stages of hydrotreatment and isomerization handles the leftover impurities that sustained the pre-treatment phase. The next phase is the hydrotreatment of pre-treated feedstock, in which the high temperature and high-pressure hydrogen are utilized to remove the oxygen leaving behind straight chain paraffins of the fuel. The final stage of the manufacturing process includes the isomerization of hydrotreated

fuel, which includes the adjustment of cold properties of fuel according to the requirement by isomerizing the paraffins. The isomerization does not generally affect any other fuel property (e.g. cetane number etc.) instead of improving the cloud point (Hartikka et al., 2012). Figure 19 presented by (Hartikka et al., (2012) shows the schematic description of the HVO manufacturing process.

Furthermore, along with waste animal fats, various types of vegetable oil feedstocks such as rapeseed, soybean, sunflower and palm oil can be used to manufacture HVO. The very first HVO manufacturing plant was built in Finland at Neste Oil's Porvoo oil refinery and the fuel was branded as 'NExBTL' (Aatola *et al.*, 2009)

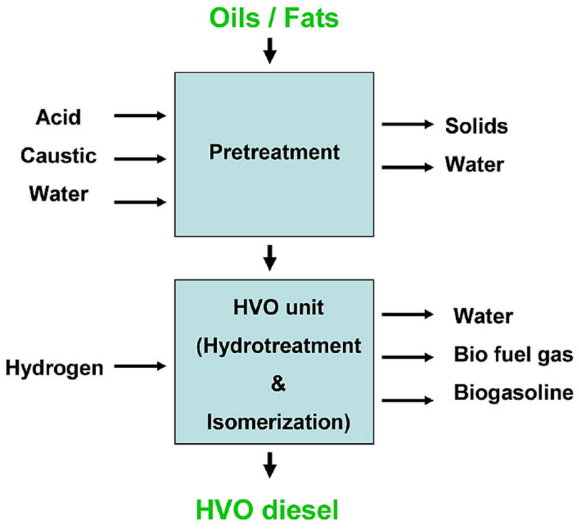

Figure 19 Process description of HVO (Hartikka et al., 2012)

5.1.2 Properties

HVO is sulfur and aromatic free fuel, produced as a result of hydrotreating vegetable oils and animal fats and no specific engine modifications are required to use HVO directly in the engines. HVO being hydrocarbon has comparable properties with diesel EN590 fuel. The properties of hydrotreated Vegetable Oil (HVO) are provided by the manufacturer in Appendix 3.

HVO possesses better combustion related properties than crude oil based fuels, which result in developing more advanced strategies to improve the combustion process that also leads to emission reduction. In general, HVO has a higher cetane number, lower boiling, and adiabatic flame temperature, no aromatic hydrocarbon or oxygen content. Density and viscosity of fuels are the main properties that affect the fuel spray behavior. HVO has lower density and viscosity values compared to EN590 diesel fuel (Hulkkonen *et al.*, 2011). Higher cetane number for HVO plays an important role in reduced hydrocarbon and CO emissions (Sugiyama *et al.*, 2012)

Aromatic content in the fuels typically has significant effects on the diesel combustion process. Aromatic content plays its part in soot formation during the combustion. HVO possesses very low (or zero) aromatic content, thus soot formation due to aromatics is very low for HVO. Furthermore, HVO possesses lower boiling components that affect the fuel spray, resulting in bad quality evaporation, hence inefficient combustion mostly when the engines are to be started in lower temperatures (Sugiyama *et al.*, 2012). Cetane number is generally used to measure the ignition quality of fuels and is related to the ignition delay in a way that higher cetane number refers to lower ignition delay. Higher cetane number for HVO due to its n- and iso-paraffinic nature makes HVO beneficial for cod starting of vehicles, noise and emission reduction (Hartikka *et al.* 2012). Sugiyama *et al.* (2012) investigated the effect of high cetane number of HVO on ignition delay and observed that ignition delay with HVO was shorter than diesel fuel, which reduced the combustion noise as well as the NOx and Hydrocarbon (HC) emissions.

During the manufacturing of HVO, cold properties are adjusted by isomerization. HVO is produced typically with a cloud point of approximately -40 or even lower. Hydrotreatment process at high temperature and hydrogen pressure makes the manufactured HVO free from impurities such as sterol glucosides or saturate monoglycerides that can possibly clog the fuel filters by being precipitated above cloud point (Hartikka *et al.*, 2012).

Table 2 gives main properties for HVO and EN590 diesel fuel used in this thesis, provided by the manufacturer.

Properties	**HVO**	**EN590 Diesel**
Density at 15°C (kg/m^3)	779.8	839.2
Viscosity at 40°C (mm^2/s)	2.919	3.545
Aromatics (wt-%)	<0.2	18.9
Cetane Number by IQT analyser	78.9	54.6

Table 2 Comparison of fuel properties

5.1.3 Engine modification and material compatibility

Hydrotreated Vegetable Oil (HVO) contains only normal and iso-paraffins and has no sulfur and aromatic content. Generally, using HVO in the engines does not require special modification in the engine and the design of its components. However, certain small changes must be done in order to get better output from the engines.

The swelling of rubber seals is related to the aromatic content present in the fuel. Therefore, in order to use HVO (with zero aromatic content) in an engine that was designed for other fuels (containing the aromatic content) requires some changes in the rubber seals. However, some real field issues have not been reported regarding this change of rubber seals. Furthermore, HVO is non-polar and paraffinic in nature, due to which water separation is better than other fossil fuels and even with FAME (Fatty Acid Methyl Ether). The absence of double bonds gives non-reactivity characteristics to HVO, resulting in better oxidation stability. HVO also behaves significantly well with long term storage, even in extreme winters (Hartikka *et al.*, 2012).

5.1.4 Effects on engine performance

HVO holds a very high cetane number and relatively low density, affecting significantly the combustion behavior in diesel engines. Considering the lower heating value per mass of HVO, which is slightly higher than that of EN590 diesel fuel. This difference in lower heating value per mass between HVO and EN590 diesel fuel is due to the presence of high hydrogen content in HVO. However, the lower heating value per volume of HVO is 5% lower than the heating value that EN590 diesel possesses, because of the lower density of HVO. This creates an energy difference for both fuels. To overcome this, more fuel in volume needs to be injected while using HVO. The increased fuel volume that is injected into the engine affects the Electronic Control Unit (ECU) parameters such as EGR rate and injection timing. Comparing the injection quantity of HVO and EN590 fossil-based diesel fuel, HVO requires more injection quantity (Hartikka *et al.,* 2012). The advantageous higher cetane number of HVO helps in lowering down the ignition delay, which results in the efficient start of combustion in extreme load conditions and shortening the premixed combustion that affects engine noise and emissions (Hartikka *et al.,* 2012).

Advanced research on fuel spray characterization (including spray penetration, opening angles, and droplet sizes) in modern common rail injection systems have shown that fuel spray behaviors for HVO and fossil-based EN590 diesel fuel are quite similar to each other (Hartikka *et al.*, 2012). However, investigating the comparison of injection quantity for both fuels, Sugiyama *et al.* (2012) presented that for the injection pressure range from 40 MPa to 200 MPa, HVO has more (3-5%) injection quantity than EN590 for the same injection duration. One explanation to this was presented by Crepeau *et al.* (2009) which relates this behavior with Bernoulli's equation. The equation says that the volumetric flow rate is inversely proportional to the square root of density, and since HVO possesses a lower density than EN590, therefore it has a higher volumetric flow rate (approx. 4%) than EN590.

Emission reduction in the engines is caused due to certain characteristic behavior of fuel. For instance, CO and hydrocarbon emissions are reduced with the fuels having no aromatic content and high cetane number. Moreover, the fuels having higher hydrogen to carbon ratio and no aromatic contents helps to reduce the particulate matter and NOx emissions. Since HVO is aromatic and sulfur-free fuel composed of only paraffinic hydrocarbons, therefore it causes lower emission as compared with aromatic EN590 fossil-based diesel fuel (Hartikka *et al.*, 2012).

5.2 Ethanol

5.2.1 Manufacturing

Rapidly growing concern about environmental pollution and GHG emissions due to diesel and other fossil-based conventional fuels turned the researchers and developments to focus more on testing other oxygenated fuels like methanol, ethanol, etc. Ethanol or methanol generally considered as alcohols have the potential to replace the conventional fuel in the internal combustion engines by blending them with the existing fuels or using them as pure individual

fuels (Sayin, 2010). Ethanol is basically isomeric with DME (Di-Methyl-Ether), having the same chemical formula (for both (Agarwal, 2007).

Ethanol is a type of alcohol that is manufactured typically by fermentation of various biomass sources such as corn, sugar beet, sugarcane, molasses, etc. and some other cellulose wastes. The manufacturing of ethanol is a complicated process that involves the pretreatment of biological sources such as crops etc. and other processes from the fermentation to denaturing of ethanol. The process typically starts with the fermentation of sugars, however, sometimes there is a need to perform hydrolysis of carbohydrates into sugars. This conversion of carbohydrates to sugars is also termed as Saccharification of cellulose and the resulting sugars are then subjected for fermentation. This is followed by distillation, dehydration and finally the denaturing of ethanol. (Mofijur *et al.*, 2016)

Ethanol can be manufactured from the feedstocks having multiple sources that can sometimes be very expensive to be used for ethanol production. In practice, many of the feedstocks have proven to be an expensive source, however, the case is different from lignocellulosic feedstocks. The cost of using lignocellulosic feedstocks is least among other available sources, and the availability of lignocellulosic feedstocks is considered to be quite enough for the production of neat ethanol (Wyman and Hinman, 1990) Using lignocellulosic biomass for ethanol production is the most promising production method, which is performed mainly in five steps. The process starts with the pre-treatment of biomass and followed by cellulose hydrolysis, fermentation (of hexoses) separation and effluent treatment (Cardona and Sánchez, 2007).

5.2.2 Properties

The main advantage of using alcohols as fuels is their low viscosity, which helps in efficient atomization, thus better air-fuel mixing leading towards efficient combustion. The high fuel-air ratio, high hydrogen to carbon ratio along with high oxygen and low sulfur content of alcohols make them considered as efficient fuels in regards to the low emissions (Sayin, 2010) The content of oxygen present in ethanol is about half of the oxygen content that methanol possesses. However, hydrogen in ethanol and methanol is present in almost the same amount. (Bechtold, 1997)

The specific gravity of ethanol is almost the same as methanol but higher than gasoline. The freezing point is however very low than typical gasoline, but it starts to increase rapidly with an increase in water content in ethanol (Bechtold, 1997). Considering the boiling point of ethanol (i.e.), it is higher than the boiling point of methanol (i.e.). This boiling point of ethanol is very high, as compared to the initial boiling point of gasoline (Bechtold, 1997). Ethanol sometimes can show problems with storage and handling due to its complete solubility in water. The interaction of water and the impurities coming with water can dilute the value of ethanol to be used as fuel (Bechtold, 1997). The viscosity of ethanol is less than diesel fuel but greater than gasoline (Bechtold, 1997).

The autoignition temperature of ethanol is higher than diesel duel quite significantly. This property of ethanol gives the advantage of lowering down the chances of ignition if ethanol fuel

spills on the engine's hot surfaces (Bechtold, 1997). The performance of the engine can also be affected by the volatility of fuel. Ethanol has a single boiling point unlike the wide boiling range of gasoline that is composed of a mixture of different components. This property of ethanol makes ethanol an effective fuel when cold starting of engines is required in cold weather conditions (Wyman and Hinman, 1990). Another factor that affects the engine's performance is the pre-ignition of fuel which is determined by the fuel properties. Pre-ignition is actually the burning of fuel earlier than actual ignition and is determined by the octane number of fuels. Generally, fuels having a higher octane number possesses a lower tendency to be pre-ignited, and anhydrous ethanol is amongst those having an octane number of 98. This higher octane number of ethanol is significantly better than the typical gasoline fuel (Wyman and Hinman, 1990). Agarwal (2007) presented the comparison of physical properties of alcohols with CNG, DME and petroleum fuels in Table 3.

	Methane	Methanol	Dimethyl ether	Ethanol	Gasoline	Diesel
Formula	CH_4	CH_3OH	CH_3OCH_3	CH_3CH_2OH	C_7H_{16}	$C_{14}H_{30}$
Molecular weight (g/mol)	16.04	32.04	46.07	46.07	100.2	198.4
Density (g/cm^3)	0.00072[a]	0.792	0.661[b]	0.785	0.737	0.856
Normal boiling point (°C) [30]	–162	64	–24.9	78	38–204	125–400
LHV (kJ/cm^3) [31]	0.0346[a]	15.82	18.92	21.09	32.05	35.66
LHV (kJ/g)	47.79	19.99	28.62	26.87	43.47	41.66
Exergy (MJ/l) [30]	0.037	17.8	20.63	23.1	32.84	33.32
Exergy (MJ/kg) [30]	51.76	22.36	30.75	29.4	47.46	46.94
Carbon Content (wt%) [30]	74	37.5	52.2	52.2	85.5	87
Sulfur content (ppm) [32]	~7–25	0	0	0	~200	~250

Table 3 Properties of primary alcohols compared with gasoline, diesel and DME (Agarwal, 2007)

Summing up the properties of ethanol compared with the gasoline fuels, it can be concluded that ethanol indeed possesses much better properties required for the engine's efficient performance. Compared with ethanol, gasoline fuels are much more toxic in nature, have low octane numbers than ethanol, emits more harmful emissions, much unsafe to be stored because of the gum deposition on the storage surfaces of gasoline and have more chances to burn or even explode (Agarwal, 2007). Moreover, the lower octane rating of gasoline than ethanol required larger cooling systems for compression ignition engines. These disadvantages of typical gasoline fuels turned the research to focus more on alternative fuels like ethanol, which can be one of the best possible fuels for CI engines as a replacement for diesel fuels.

Note: Ethomeen (O/12, ~ 1 m-%) was added as a lubrication additive in Ethanol fuel while performing the tests with ethanol in this thesis.

5.2.3 Engine modification and material compatibility

Ethanol and other alcohols (i.e. methanol) are used mostly in the form of blends with other fuels such as diesel etc. Ethanol-based blends of fuels are used in the same engines that are designed for gasoline, however, due to the properties difference between gasoline and ethanol (see Table 3), certain engine modifications are generally required to operate efficiently.

Agarwal (2007) listed some engine modifications required to use ethanol as a fuel or ethanol-based blends. He proposed that the recalibration of the carburetor is typically needed because of the lower stoichiometric air-fuel ratio and high heat of vaporization. In order to improve the evaporation of ethanol, the intake manifold is modified to provide more heat for evaporation. Some material modifications such as pure tin coating of the fuel tank and cadmium brass made fuel lines can also improve the engine's performance with alcohols. Re-dimensioning of fuel filtering systems is also required to increase the fuel flow rates and the compression ratio of the engine is generally increased to about 12:1, because of the high octane rating of ethanol (Agarwal, 2007).

The use of ethanol also has some serious effects on the materials of engines. Corrosion is one of the main effects that is considered regarding the use of ethanol. Brink *et al.*, (1986) presented the effects of alcohol with gasoline blends in the form of corrosion in the carburetor. He divided the corrosion caused by ethanol into general dry and wet corrosion. Some non-metallic components (such as seals and O-rings present in the fuel injection systems) can also be affected by ethanol by getting stiffed or swelled (Agarwal, 2007). It is to be noted that during the experimental phase of this thesis, it was expected that using ethanol might cause some problems in the fuel injection system. However, the experiments with ethanol went with complete success without any damage to the injector or to the injection system.

5.2.4 Effects on engine performance

Adding ethanol improves the engine performance and exhaust emissions by improving the volumetric efficiency, fuel consumption, brake power, brake thermal efficiency, cold and hot engine starting and remarkable CO and NOx emissions. (Agarwal, 2007). Studies to analyze the effects of using alcohols (especially ethanol) have shown great environmental benefits. Ethanol proved to be one of the cleaner, environment friendly and lowest GHG emitting alternative fuel.

The emission of CO in the engines typically happens due to the incomplete combustion caused mostly by non-oxygenated fuels. However, the presence of oxygen in the molecular structure of ethanol reduces the chances of incomplete combustion, thus CO emissions are substantially reduced (Agarwal, 2007). The emission of hydrocarbons (such as benzene etc.) is also reduced significantly because of the higher octane rating of ethanol (Taylor *et al.*, 1996). One of the important components of particulate matter is the dry soot emissions, which are indicated by the smoke opacity. The smoke opacity is reduced by increasing oxygenated alternatives such as alcohols in the fuel. Thus, by adding ethanol, dry soot emissions are reduced (Sayin, 2010).

Higher octane number and latent heat of evaporation of ethanol give a better anti-knocking capability (Nakata *et al.*, 2006; Stein *et al.*, 2013). These properties of ethanol enable to reduce the compressed gas temperature in the compression stroke of the piston, thus reduces the chances of knocking. As a consequence, ethanol substantially increases the thermal efficiency and the engine's torque (Nakata *et al.*, 2006). Along with the high knock resisting property of ethanol, it also allows using a high compression ratio, which results in increased thermal efficiency.

6 Experimental setup and analysis methods

6.1 Spray Chamber

The experiments were conducted by using the spray chamber that is designed particularly to perform spray measurements. The chamber has two circular borosilicate glass windows equipped opposite to each other in order to set up the camera and backlight for imaging, thus providing optical access to the fuel sprays. The glass windows have an effective diameter of 100mm with a thickness of 55mm (Ainsalo, 2018). There were two other hollow spaces in the chamber design, one of which was used to install the calibration plate in order to calculate the pixel to mm ratio and the other was closed by using a metal plate. The injector is installed vertically downward from the top of the chamber. The fuel spray ejects from the injector nozzle at a certain angle with horizontal and is presented in Figure 23 below. The maximum allowed gas pressure for the chamber is 35 bar. Along with the opening for the injector, the chamber has two inlets for nitrogen gas inlet and outlet. The chamber was equipped with temperature and pressure sensors in order to log the pressure and temperature values to calculate the chamber density.

The detailed and dimensional explanation regarding the constant volume chamber is provided in Figure 21 taken from the chamber design data created by Teemu Sarjovaara in 2005. Furthermore, the location/orientation of the injector inside the chamber is further explained in detail from Figure 23.

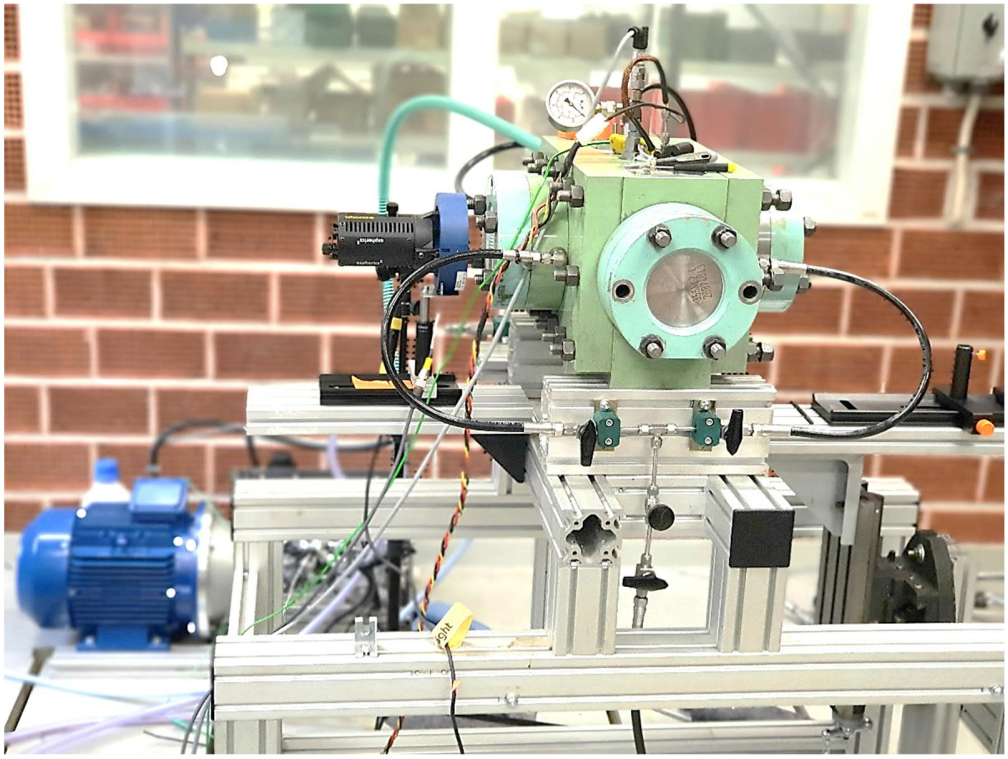

Figure 20 Spray chamber for fuel spray measurement

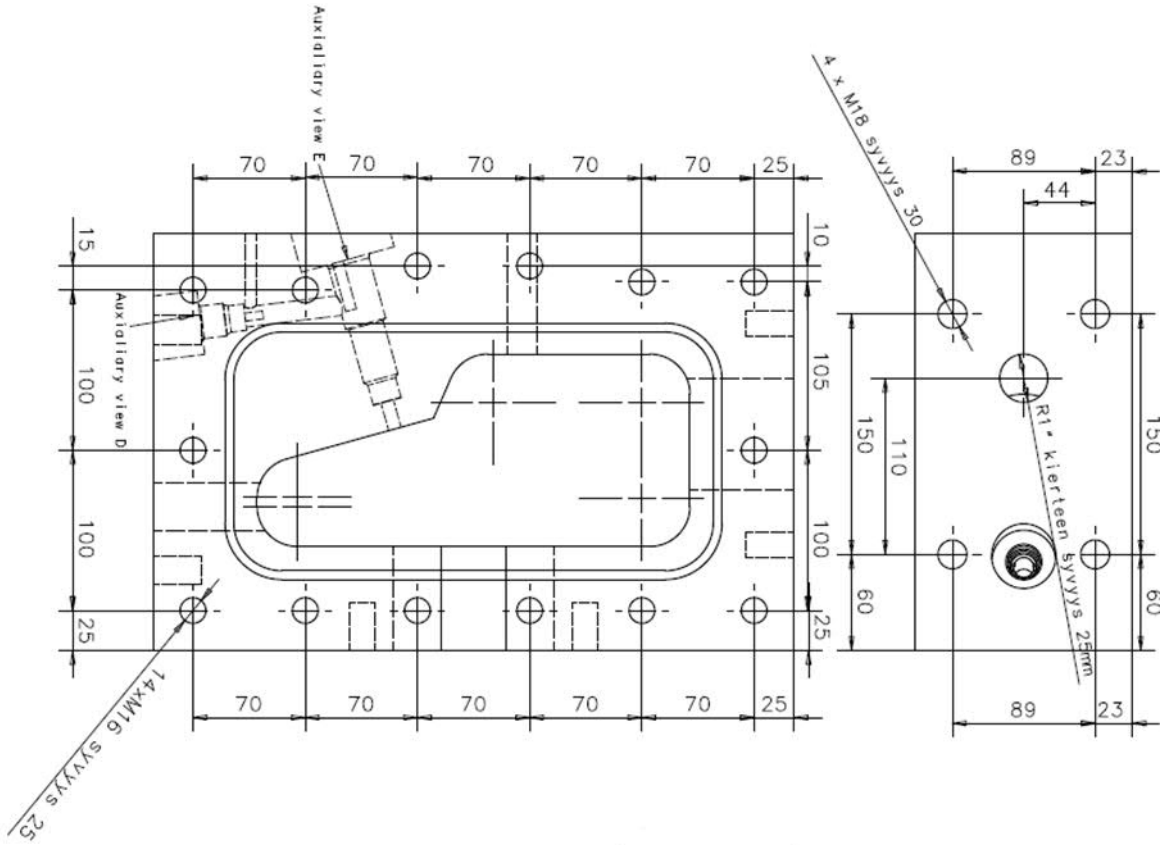

Figure 21 Dimensional diagram of constant volume chamber (Taken from chamber design data by Teemu Sarjovaara, 2005)

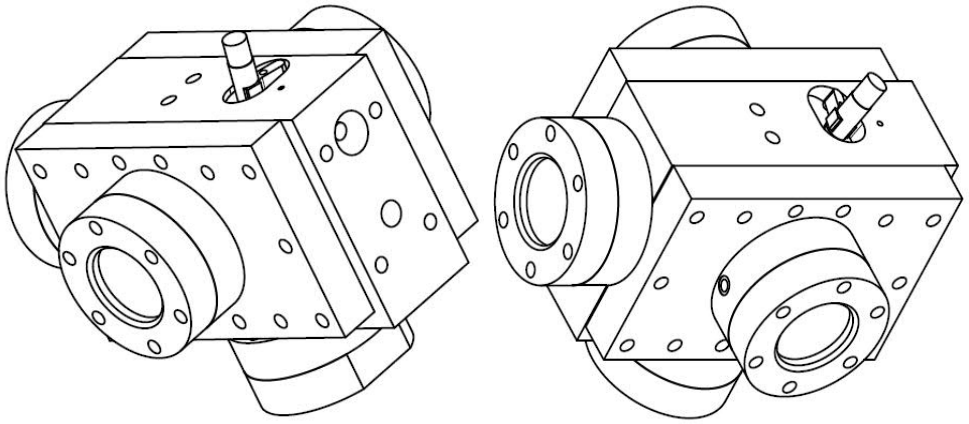

Figure 22 Schematic diagram of chamber (Taken from chamber design data by Teemu Sarjovaara, 2005)

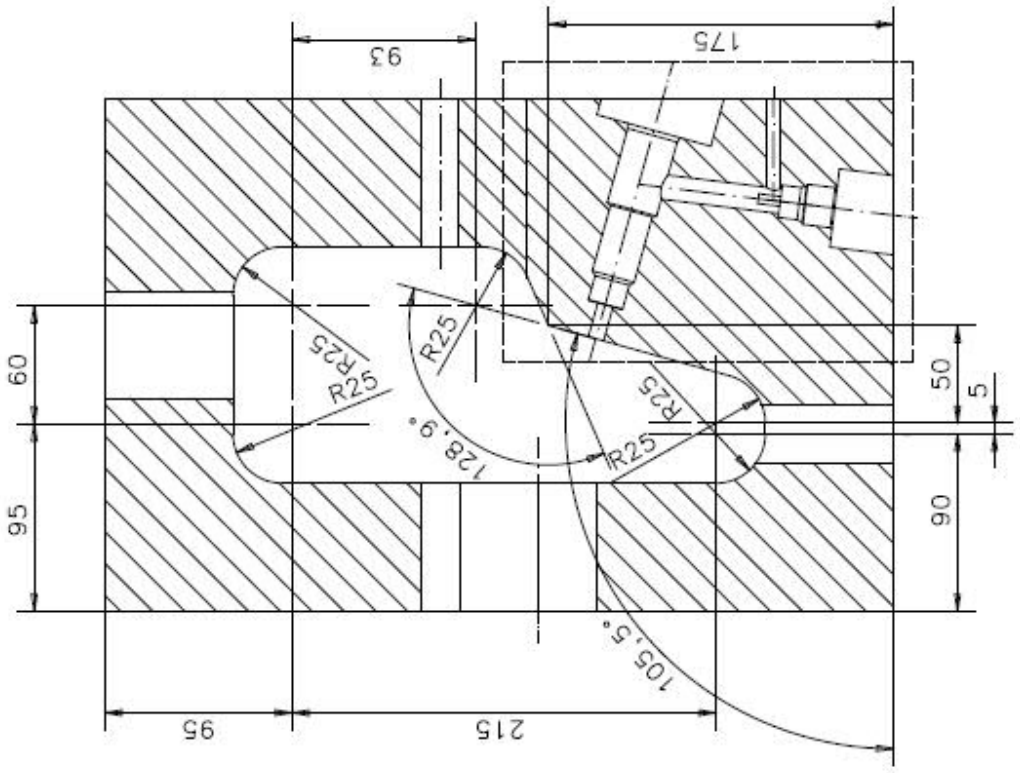

Figure 23 Schematic orientation of injector in the chamber (Taken from chamber design data by Teemu Sarjovaara, 2005)

6.2 Nitrogen gas system

The spray chamber was filled with compressed nitrogen gas in order to have two different chamber densities (i.e. 20 and 40 kg/m^3). As described earlier, nitrogen gas pressure was controlled in order to achieve the required density levels inside the chamber. Certain flow control valves were also equipped with the chamber in order to control the pressure of nitrogen gas. For spray geometry measurements, the nitrogen flow was kept continuous in order to keep the windows clean and to ensure that the coming fuel spray formation will not be affected by the fuel mist and residues already present inside the chamber from the previous spray. However, the nitrogen flow mechanism was not continuous in droplet size measurements, instead, the flow was provided in a periodic manner after each image set. Nitrogen is used specifically due to its resemblance with air along with some other characteristics like inertness and cheapness.

Figure 24 Nitrogen bottles for nitrogen supply to the chamber

6.3 Flow actuators

Nitrogen flow towards the chamber was controlled by a pressure regulator installed right after the nitrogen bottles. However, the needle valve was also attached before the chamber in order to perform minor adjustments for chamber pressure. To maintain a constant nitrogen flow through the chamber, an adjustable spring-loaded pressure control valve was mounted after the chamber. On the other hand, the nitrogen flow procedure was quite different in case of droplet size measurements, where the flow is kept periodic after each image set of 10 injections. The chamber pressure was controlled carefully by suitable adjustments of these actuators in order to achieve the required chamber densities along with suitable nitrogen flow through the chamber.

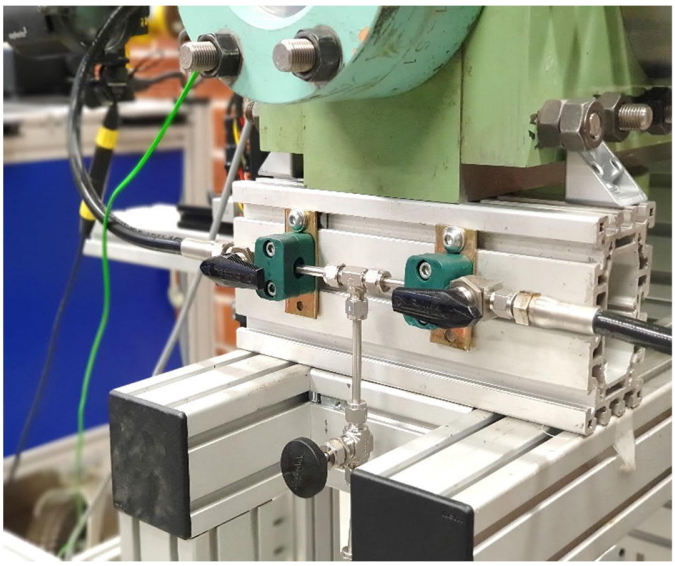

Figure 25 Pressure regulators connected with chamber

6.4 Fuel system

The fuel system includes a fuel tank, fuel pump, fuel filters, a common rail, fuel injector, and fuel cooler (see Fig. 26). The fuel filters were used in order to filter out the impurities coming along with the fuel through the fuel system. To maintain the safe range of fuel temperature in the fuel tank, the system was also equipped with a fuel cooler. The fuel injector was a solenoid driven injector having multiple orifice nozzles. The fuel spray imaging was done for a single spray, therefore, four out of nine nozzle orifices were welded, allowing only one spray coming perpendicular to the camera and backlight axis.

Figure 26 Fuel pump, fuel tank, fuel coolers and common rail (left). Manual pressure control valve to achieve 600 bar (right)

Higher fuel pressures (i.e. 1200 and 2000 bar) in the common rail were controlled by the LabView control program design specifically for the spray measurement system. However, the fuel pressure of 600 bar was achieved by using a manual fuel circulation control valve (see Fig. 26 (right)). Although the pressures were to be kept at the desired values, some variations had to be accepted due to system limitations. The deviations from the desired pressure values were kept in the range of -10 to 10.

Figure 27 shows a schematic flow chart of the complete system including flow actuators, nitrogen gas, and fuel systems.

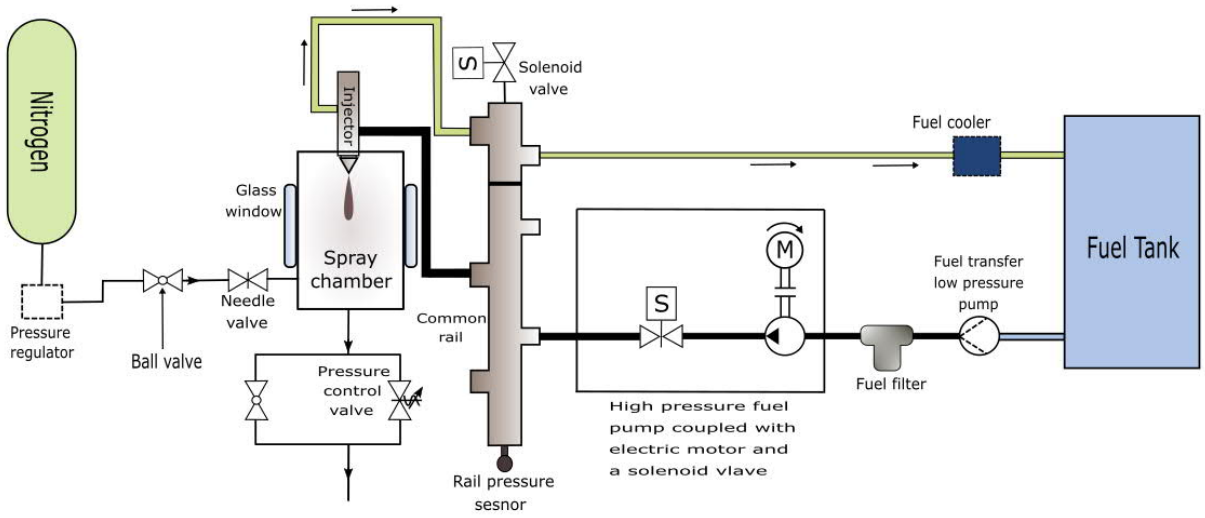

Figure 27 Schematic flow diagram for complete experimental system

6.5 Fuel Injectors

The experiments were conducted by using two solenoid driven injectors. Both injectors were similar to each other except the nozzle and number of orifices. Most of the experiments were performed with injector having smaller nozzle hole diameter, termed as 'Reference nozzle'. However, the other injector with increased nozzle hole size is named as 'Special nozzle'. The purpose of using the special nozzle was to analyze the behavior of nozzle orifice size on fuel geometry and droplet sizes.

The specifications and comparison of both injectors are presented in Table 4.

Specification	**Reference Nozzle**	**Special Nozzle**
Nozzle orifice diameter (mm)	0.138	0.184
Number of holes	9	3
Blocked/Welded orifices	4	N/A
Umbrella angle (deg.)	76.1	76.1

Table 4 Comparison of both injector's specifications

Furthermore, Figure 28 presents the actual images of both fuel injectors used in the experiments. Both injectors differ from each other only by the number of nozzle holes and the orifice diameters.

Figure 28 Actual images of both injectors i.e. with reference nozzle (left) and special nozzle (right)

6.6 Control and logging

The control system for the experimental setup such as data logging, camera and injector triggering, etc. was operated by using LabVIEW software interface. All the information from sensors (i.e. pressure and temperature) installed in the setup along with different variables such as chamber density, fuel rail, and fuel tank temperatures, fuel rail pressure, etc. was displayed on the LabVIEW interface (Figure 30) on the computer screen and the data was logged into a text file. The temperature was measured at the fuel tank, common rail and the chamber, however, the pressure measurement locations were common rail and the chamber. Fuel rail temperatures are also presented in Appendix 4 along with their comparison in Appendix 5. All these values were logged in a single text file for each test point. The normal injection duration in all the test cases was 2.5ms, which was divided into 'lift' and 'hold' phase. Figure 29 shows the time history of a single injection event plotted against the voltage.

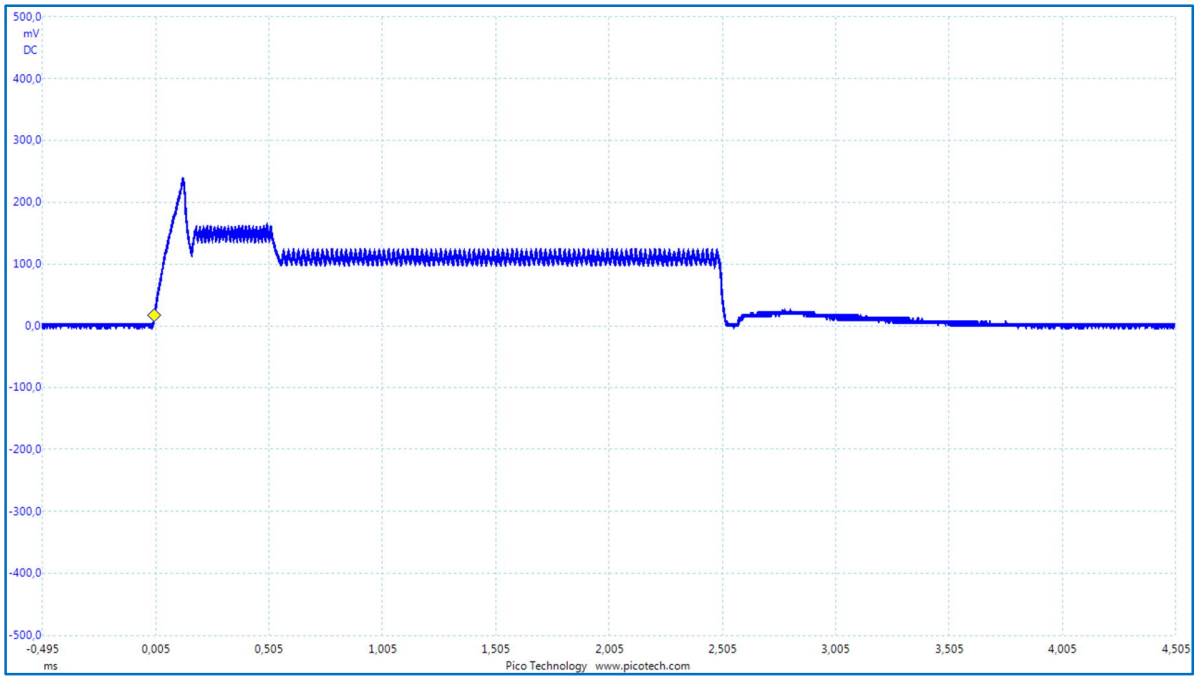

Figure 29 Injection signal profile obtained from Picoscope

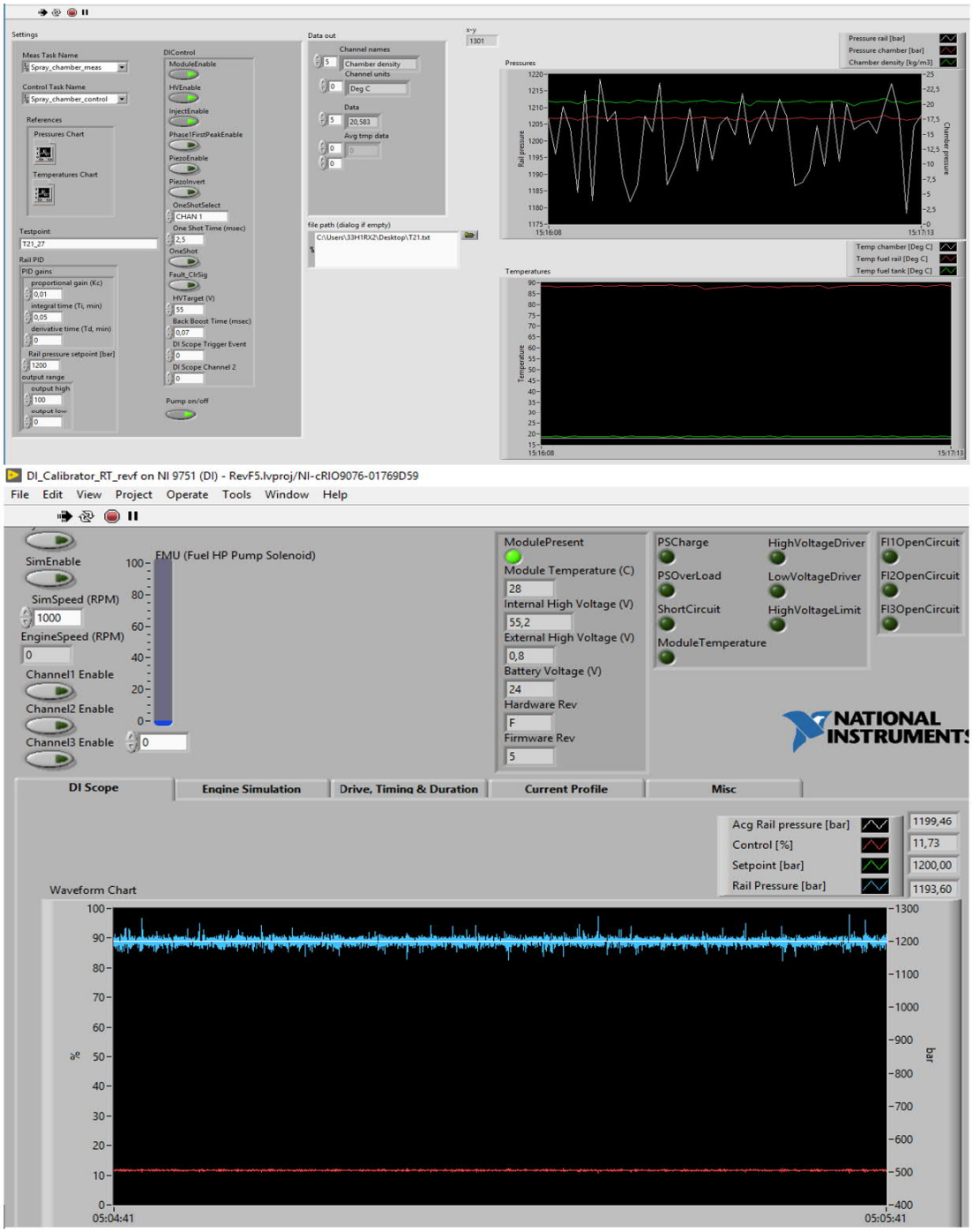

Figure 30 LabView interface for control system

6.7 Imaging system

6.7.1 Spray geometry

The imaging system for the experimental setup of spray geometry comprises a high-speed monochrome camera and backlight. Backlight used for this setup was the combination of a 125 W halogen lamp and RMX140 Ring light (LED), in order to get enough illumination (see Fig. 31). Halogen and LED were used together to get a flicker-free higher intensity light at high frame rates. Halogen lamp was connected to a direct power supply and is turned on throughout the injection phase. However, the LED light was operated with an external trigger, which was synched with the injector and camera trigger.

Figure 31 Light source for backlight

Milk glass was also installed with the glass window to homogenize the light intensity in the image background. The lens used with the high-speed camera possesses a focal length of 105mm with an aperture of f/4. The large aperture setting allowed to get the images with an exposure time of 1/100000 s corresponding to 1µs. An Ethernet connection cable was used to connect the high-speed camera with the PC, which allows the camera software to detect the connected camera. Figure 32 explains the camera and backlight imaging system for the spray geometry experimental setup.

With the above explained backlight setup, the images were taken at a frame rate of 25000 frames per second with the image resolution of 1280 x 720 pixels, corresponding to an image area of 87 mm by 47 mm. In order to analyze the complete spray behavior with an injection duration of 2.5ms, the camera software was set to capture 150 consecutive images after the trigger.

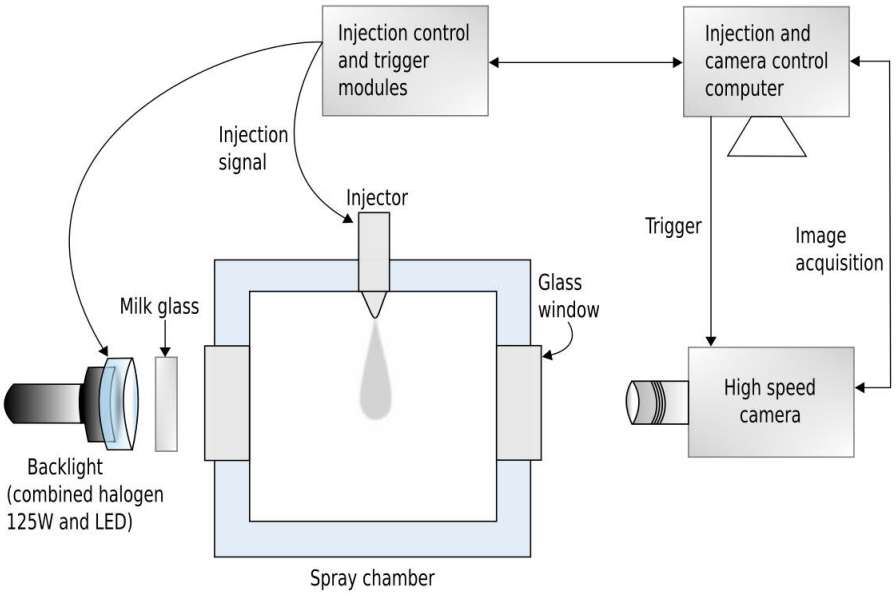

Figure 32 Schematic diagram of imaging system for spray geometry measurements

The working operation of the imaging system starts by giving an injection trigger from the LabVIEW software interface. This triggering leaves a trigger signal from the control system to the camera by using a BNC trigger cable. The same trigger will go to the injector, however, due to the injector inertia, a trigger delay of 600 µs was given to the camera software. This indirectly means that the camera started taking the images 600 µs after the trigger signal reaches the injector. Moreover, the LED light also gets the trigger at the same time with the injection signal. This means that the LED blinks at the same time when the injector injects the fuel spray into the chamber, giving brighter background in the images. The experimental setup was quite close to that of Ainsalo, (2018).

6.7.2 Droplet size measurements

The second phase of the experiments included droplet size measurements that required emendation in the prior system arrangement for spray geometry. The idea behind setting up the new system for droplet size distribution was to focus on a small image area that should sustain the required quantity and quality of the spray droplets. To decrease the image area down to 2.7mm by 2.7mm, a long-distance microscope (Questar QM-1) was attached with a 12-bit greyscale CCD camera, having a resolution of 2048 x 2048 pixels. Moreover, it is to be noted that the exposure time for the camera should be short enough in order to cease the fuel spray motion. The fundamental calculations regarding exposure time to anyhow avoid the motion blur suggested the range to be in nanoseconds. Shorter exposure time requires a high-intensity backlight to provide enough illumination, so an Nd:YAG laser was used as a backlight source. This laser has 200mJ maximum energy per pulse, an output wavelength of 532 nm and pulse duration in the range of 3 to 5 ns. In order to get nearly speckle-free backlight illumination, the laser beam was passed through a diffuser that converted the output wavelength and expanded the beam.

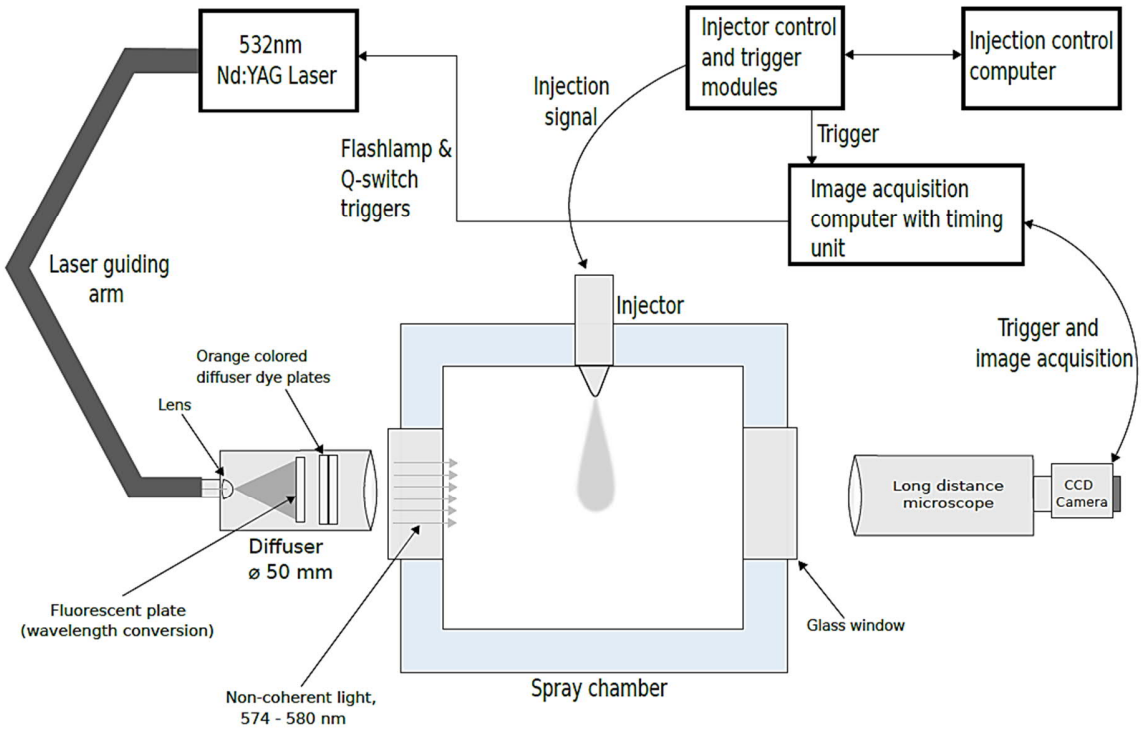

Figure 33 Schematic diagram for droplet size imaging system

The images were taken as one shot per one injection event. This can also be termed as single shot mode. In order to synchronize the trigger with the injector delays and the delay for the spray to reach the measurement location, the reference time was set in the image acquisition computer. The reference trigger location for the spray in every test point was set to be 65mm from the nozzle tip. This means that the trigger activates when the spray has travelled 65mm from the injector nozzle for all the test points. This reference location for the trigger was randomly selected in order to allow the spray to be fully developed before the injection stops. It should be noted, that the reference time could not be kept same because the slower sprays take more time to reach the measurement location and the faster ones comparatively reach the measurement location in lesser time. Therefore, in order to overcome this limitation, the reference time for all the individual test points was calculated manually by image processing of spray geometry images taken in the earlier part of the experimental phase. However, the reference times for special nozzle sprays were kept the same as reference nozzle with same experimental parameters, because the spray geometry images were not available for image processing at that time. The reference times are available in Table 8.

In order to further explain the triggers synchronization and the reference time, let's consider the basic analysis technique for the droplet size measurements. Figure 34 shows the simplest representation of spray coming out of the nozzle orifice. The droplet sizes are calculated at the spray edge when the spray has travelled 35mm from the injector nozzle into the chamber. The

total injection duration was set to be 2ms, however, the camera triggering was synchronized with the reference time explained in the earlier paragraph.

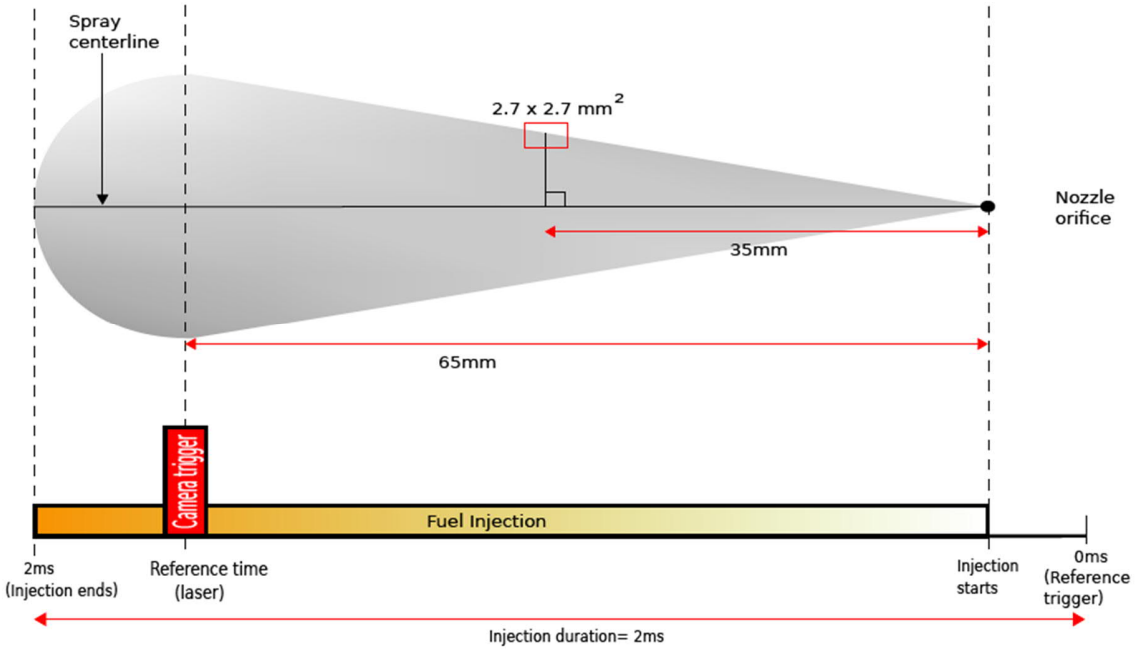

Figure 34 Basic schematic of the imaging technique used for droplet size measurements

The time profile for the above system is explained in the Figure 35 below. It is presented that there is a laser delay of 0.2ms just after the start of injection signal. After 0.2ms, the injection begins and the spray starts to propagate. When the spray reaches at 65mm from the nozzle orifice location, the camera gets the trigger and takes single shot of the spray. This delay was defined manually in the DaVis software as a reference time.

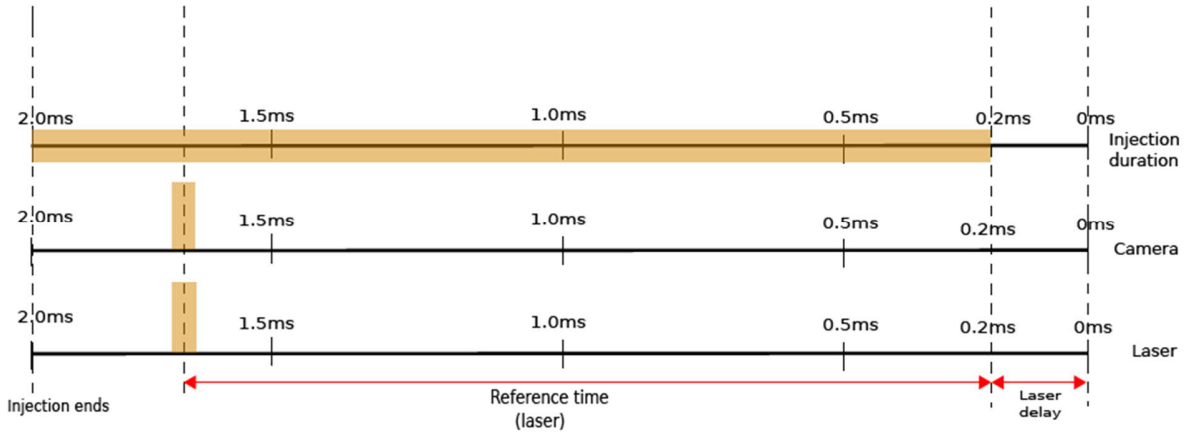

Figure 35 Time profile for the triggers synchronization of droplet size measurement setup

6.8 Image Analysis

6.8.1 Spray geometry

Image analysis of the spray geometry was conducted by using a Matlab script written by R. Sallinen in 2016-2017, followed by Ari Ainsalo in 2018 and modified by the author of this thesis in 2019-20. After the image analysis, results were obtained in the form of numerical data, which were further processed in Matlab to generate graphs and the analyzed images. Matlab considered each monochrome image as a 2-dimensional array having elements that present the corresponding pixel with a specific intensity level.

Spray geometry measurements include the analysis of spray opening angle and spray penetration. During the analysis, spray penetration was defined by a pixel that possesses the longest distance from the nozzle orifice location in the image area (see Fig. 36, green circular marker). On the other hand, opening angles were determined by using triangular markers in the spray image area (see Fig. 36, triangular markers). These markers are defined based on image pixels of the spray area having maximum perpendicular distance from the centerline of the spray (see Fig. 37, x distance). The perpendicular distances from the centerline were calculated at seven different locations having specific distance from the nozzle orifice location (see Fig. 37, y location points). After detecting the pixels on the spray edge, the opening angle was calculated using trigonometric calculations (see Fig. 37, α angle) (Ainsalo, 2018). Opening angles were calculated as α/2 from above and below the centerline and then combining both angles to get the final opening angle values.

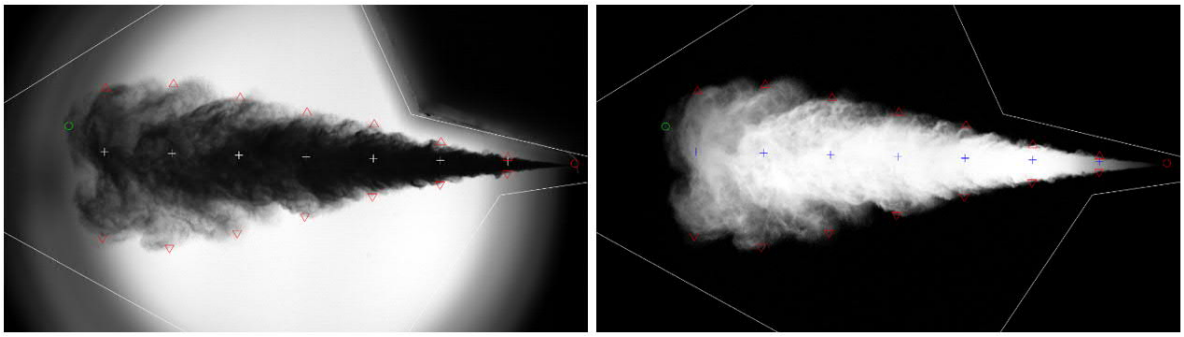

Figure 36 Real experimental images under process. Right image shows the spray area separated from the background for spray geometry determination.

It is to be noted here that the angle of spray centerline (Fig. 36, plus markers) from horizontal axis was calculated manually after taking the dimensions of spray chamber and injector orientation in the chamber. This angle refers to the angle at which spray propagates with the horizontal axis and the value was given to the Matlab script in order to get the proper spray centerline.

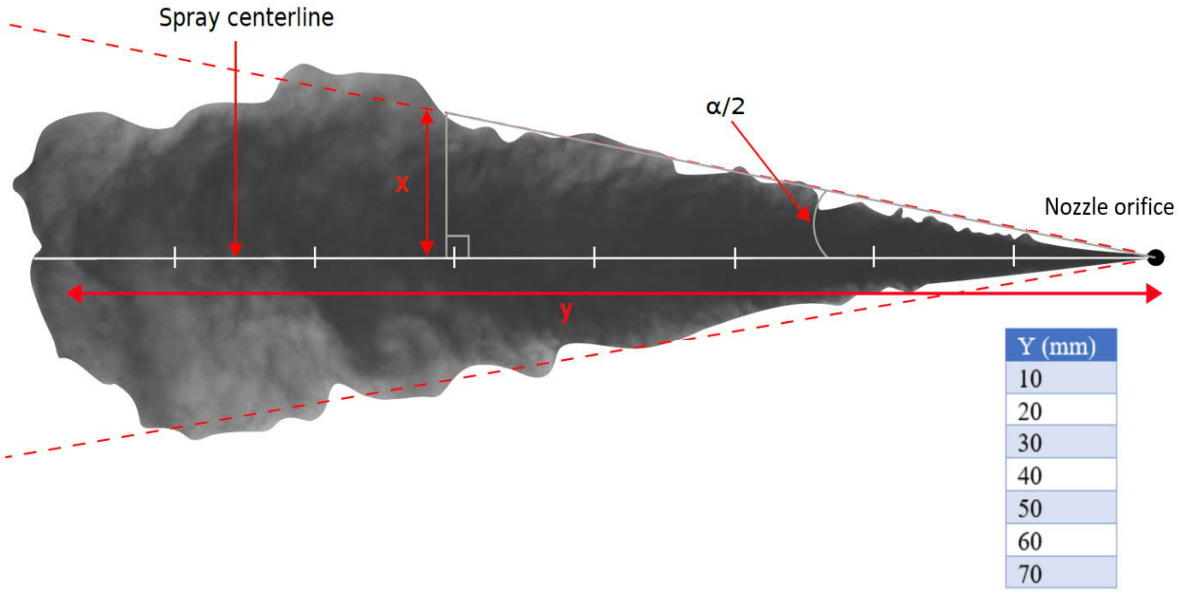

Figure 37 Opening angle (α) determination at different locations from the nozzle orifice (y). 'x' is defined as the vertical distance from centerline and the spray edge.

In Figure 36, there are certain areas in the images marked with white lines. These areas are basically excluded from the image area and are defined in the Matlab script. The purpose of doing so was to avoid any possibility of reflected light from the mechanical parts inside the chamber to appear in the analysis that can lead to false or cumbersome results. The excluded zones are defined by keeping in mind that the exclusion must not affect the spray propagation at all.

6.8.2 Droplet size distribution

For analysis of droplet sizes from the images, DaVis 10 software by LaVision GmbH was used. The software requires some parameter values for image pre-processing and particle detection. After giving these values, the software automatically analyzed the image sets and generated all the required data such as particle lists, droplet size scatter plots, histograms, and some other relevant statistic values. All the images were captured from the same imaging location for all image sets, except some minor adjustments of camera focus and height of the camera in order to capture the spray edge properly. This image location can be explained from the Figure 38:

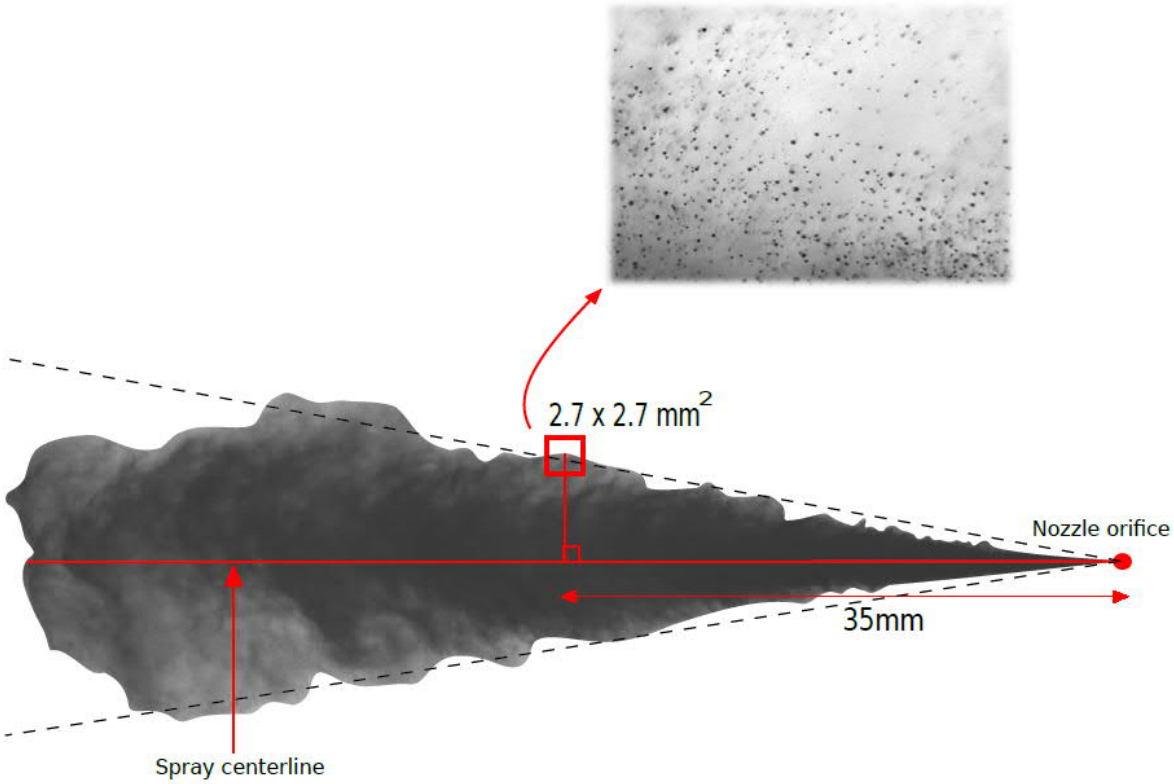

Figure 38 Field of view in droplet size images

The image processing was done based on the defined parameter values. The adjustment of parameters started by normalizing the image intensity levels along with applying denoising filter to smoothen the image background and continues by the detection of droplets based on the detection parameters. Moreover, the detected droplets were sorted by applying minimum and maximum filters in the later stage. Different combination of parameters was tested in order to get the best fit for droplets detection. However, it was observed that minor manipulation of the parameters was needed for individual image sets. Therefore, the parameters were not kept the same for all the test points, however, some minor adjustments have been made. All the pre-processing, detection and other filtering parameters for individual test points are listed in Table 5. Moreover, the test points can be found out from Table 8.

Test point	Normalization radius (px)	Pixel noise reduction	Binarization threshold (%)	Min. shadow area (px)	Min. slope (%)	Max. diameter (µm)	Min. centricity (%)
D1	10	Strong	48	10	12	50	60
D2	20	Strong	28	10	5	50	60
D3	10	Strong	50	12	13	50	60
D4	10	Strong	45	10	10	50	60
D5	12	Strong	51	12	11	50	60
D6	12	Strong	51	12	08	50	60
D7	10	Strong	50	10	06	50	60
D8	10	Strong	48	12	10	50	60
D9	10	Strong	45	10	10	50	60
D10	09	Strong	45	12	10	50	60
D11	10	Strong	45	12	12	50	60
Avg.	**11.18**	**Strong**	**46**	**11.09**	**10**	**50**	**60**

Table 5 Detection parameters chosen for DaVis software

In order to investigate the effect of keeping the same detection parameters for all test points on droplet detection, averages of all detection parameter values (see Table 5, Avg. values) were chosen for all test points. It was observed that the number of detected droplets have increased quite significantly, showing the increased chances of false detections (See Fig. 39 and Table 6). This means that for a similar set of detection parameters, some non-centric droplets and the droplets that are very close to each other may be detected as a single larger sized droplet. These types of situations needed corrective actions. Therefore, the detection parameters had to be manipulated in order to have the best possible particle detection from the software. All the results are based on individually selected droplet detection parameters (see Table 5) for every test point. It is also to be noted that number of detected droplets for D2 was very less (i.e. only 103) when the average detection parameter values were used. The accurate reason for this could not be found. However, it was seen that by using the average parameter values, there is no or very less droplet detection in the images, probably because of the variation in the intensity levels.

The difference in the number of detected droplets by changing the detection parameters is presented in Table 6.

Test point	No. of detected droplets (individual set of parameters)	No. of detected droplets (same set of avg. parameters)
D1	12776	17059
D2	8727	103
D3	12154	19373
D4	12702	12315
D5	9558	13649
D6	7747	8839
D7	11471	12717
D8	8621	9746
D9	12287	11749
D10	12394	12207
D11	11395	13114

Table 6 Number of detected droplets for every test point

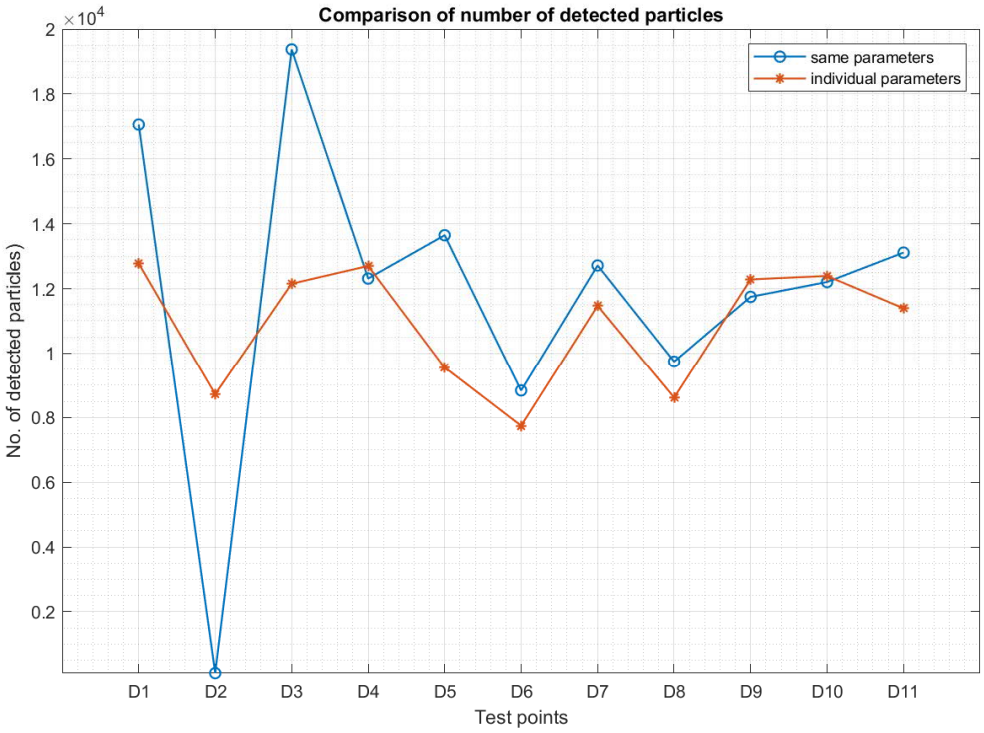

Figure 39 Comparison of number of detected particles for individual and same set of detection parameters for all test points

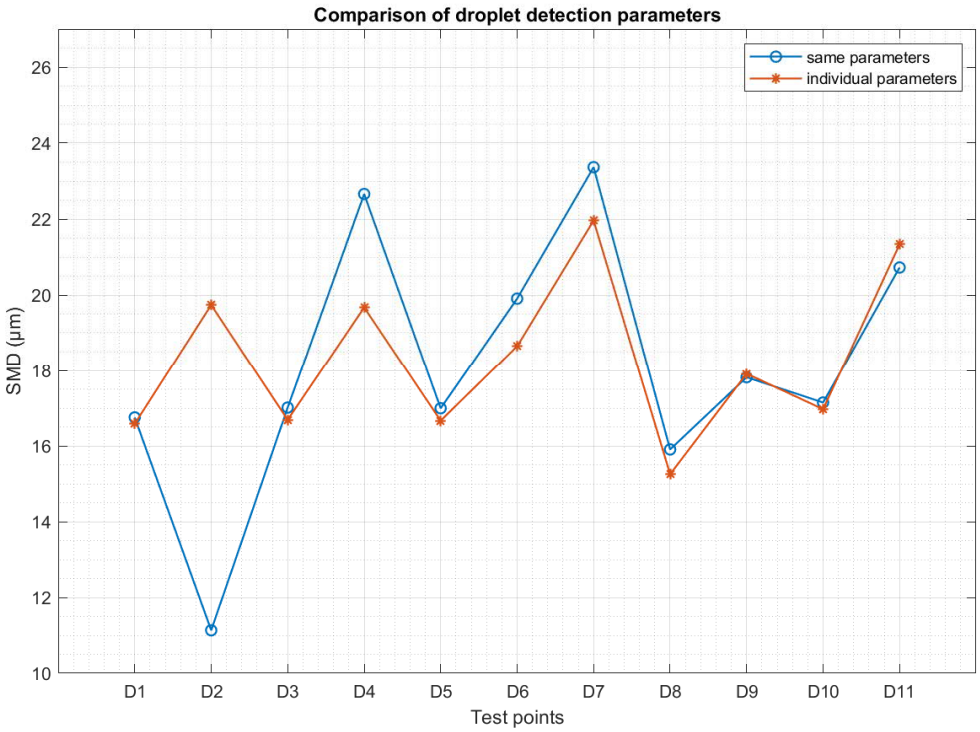

Figure 40 Comparison of SMD's detected by individual and same set of detection parameters for all test points

For particle recognition, the normalized images were processed by setting the percentage level of binarization threshold in order to set the black and white separation. The next step was to decide which particles to be added to the particle list. This was done by using two other filters: minimum shadow area and minimum slope. Defining the minimum shadow area restricts too small particles to appear in the particle list while the minimum slope corresponds to the droplet's sharpness. Setting the higher value of minimum slope relates to the droplets sharper edges and lower values will accept the droplets that are far away from the focal plane (i.e. not sharp enough). However, the lower values of the minimum slope may lead to false detections. The detected droplet areas were highlighted with ellipses that fit the droplet areas. The centricity was defined as the ratio between the short and long axes of the ellipse. Moreover, the droplet diameters were calculated corresponding to the diameter of the highlighted circle/ellipse, considering that circles/ellipses have the same area as the droplet area. Figure 41 elaborates the detected particles along with their diameters.

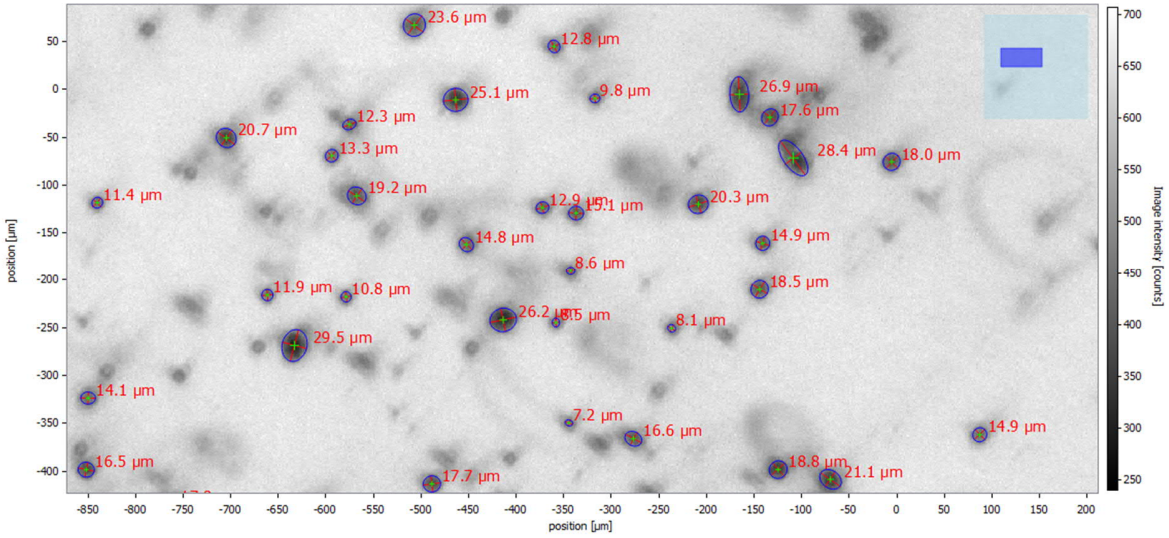

Figure 41 A screenshot of detected droplets in an image

During the droplet detection phase of analysis, clear false detections were observed. Mostly, the droplets having the smallest and the largest detected areas having unexpected diameter values proved to be false detections. Similarly, detection areas having lower centricity values also correspond to uncertain and false detections. In order to overcome these uncertainties in the droplet detection, minimum and maximum filters were applied. A maximum diameter filter of 50µm was applied to reduce the false detections of larger detected areas. Similarly, a minimum centricity filter of 60% was applied to avoid the lower centricity detection areas. By applying these filters, it was expected that some real droplets might have been excluded. However, this exclusion of real droplets is acceptably compromised because of the necessary exclusion of falsely detected droplets.

It is to be noted that the DaVis software version lacks in applying the minimum and maximum filters to the exported results. Therefore, a Matlab script was used to arrange the exported droplet lists based on required minimum and maximum filters.

Furthermore, Figure 42 shows the actual images captured during the droplet sizes measurements for all three fuels at same conditions of injection pressures and chamber density.

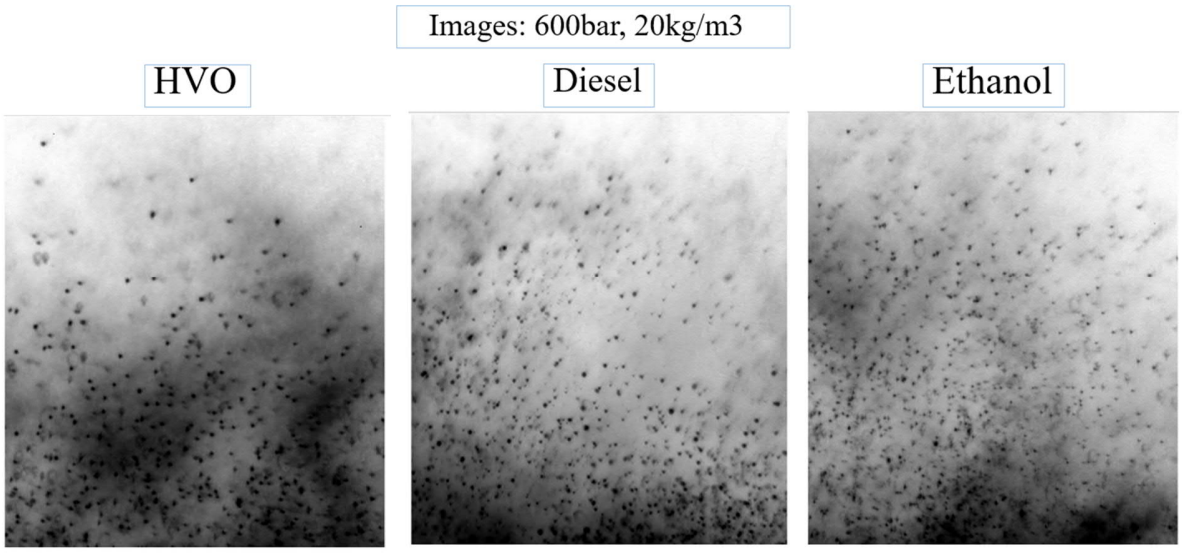

Figure 42 Actual images captured from spray edges for droplet size measurements

7 Test matrix

7.1 Spray geometry

The first part of the experimental phase was based on the spray geometry measurements divided into 14 test points that are presented in the test matrix (Table 7). Every test point was performed with 50 consecutive injections each and then taking the arithmetic average of the numerical data to get the results. This method helped to reduce the impact of spray-to-spray variations amongst consecutive injections on the results. The test matrix for spray geometry tests was created based on following experimental parameters:

- Fuels: Ethanol, Diesel EN590, Hydrotreated Vegetable Oil (HVO).
- Injection pressures: 600, 1200 and 2000bar.
- Chamber gas densities: 20 and 40 kg/m^3.
- Injector nozzles: Reference, Special nozzle (increased diameter)

On the other hand, some parameters defined for the imaging system were as follows:

- Camera frame rates per second: 25000
- Image resolution: 1280 x 720
- Camera lens aperture: f/4
- Exposure time: 1 µs

Furthermore, the spray geometry tests were also performed with special nozzle having increased nozzle hole size. The experimental parameters for special nozzle tests were:

- Fuel: Diesel EN590

- Injection pressures: 600, 1200
- Chamber gas density: 20 kg/m^3

Sr. No.	ρ_N2 (kg/m^3)	P_rail (bar)	Fuel	Inj. time (ms)	Nozzle	camera_fps	Res. (x*y)
T1	20	1200	HVO	2.5	Ref.	25000	1280*720
T2	20	600	HVO	2.5	Ref.	25000	1280*720
T3	40	1200	HVO	2.5	Ref.	25000	1280*720
T4	40	600	HVO	2.5	Ref.	25000	1280*720
T5	20	1200	EN590	2.5	Ref.	25000	1280*720
T6	20	600	EN590	2.5	Ref.	25000	1280*720
T7	40	1200	EN590	2.5	Ref.	25000	1280*720
T8	40	2000	EN590	2.5	Ref.	25000	1280*720
T9	20	1200	Ethanol	2.5	Ref.	25000	1280*720
T10	20	600	Ethanol	2.5	Ref.	25000	1280*720
T11	40	1200	Ethanol	2.5	Ref.	25000	1280*720
T12	40	600	Ethanol	2.5	Ref.	25000	1280*720
T13	20	1200	EN590	2.5	Special	25000	1280*720
T14	20	600	EN590	2.5	Special	25000	1280*720

Table 7 Test matrix for spray geometry (spray penetration and opening angles)

7.2 Droplet size measurements

The tests matrix for droplet size distribution (Table 8) was divided into 11 test points with following experimental parameters:

- Fuels: Ethanol, Diesel EN590, Hydrotreated Vegetable Oil (HVO).
- Injection pressures: 600, 1200 and 2000bar.
- Chamber gas densities: 20 and 40 kg/m^3.
- Injector nozzles: Reference, Special nozzle (increased diameter)

Furthermore, two test points were performed for droplet size distribution with special nozzle having increased nozzle orifice size. The experimental parameters for special nozzle tests were:

- Fuel: Diesel EN590
- Injection pressures: 600, 1200
- Chamber gas density: 20 kg/m^3

Sr. No.	ρ_N2 (kg/m^3)	P_rail (bar)	Fuel	Inj. Time (ms)	Nozzle	Reference time
D1	20	1200	HVO	2.0	Ref.	1.2
D2	20	600	HVO	2.0	Ref.	1.65
D3	20	1200	EN590	2.0	Ref.	1.2
D4	20	600	EN590	2.0	Ref.	1.65
D5	40	2000	EN590	2.0	Ref.	1.45
D6	40	1200	EN590	2.0	Ref.	1.8
D7	40	600	EN590	2.0	Ref.	2.6
D8	20	1200	Ethanol	2.0	Ref.	1.3
D9	20	600	Ethanol	2.0	Ref.	1.83
D10	20	1200	EN590	2.0	Special	1.2
D11	20	600	EN590	2.0	Special	1.65

Table 8 Test matrix for droplet size measurements

8 Uncertainties and errors analysis

8.1 General discussions

During the experiments and analysis, several errors have been observed. For a better explanation, these errors can be explained by dividing them into experimental and analysis or post-processing errors. The experimental errors can be explained further as imaging or optical system errors and spray formation errors. Moreover, it should be noted that these errors and observations are based on the experiments performed and not from the literature.

Imaging or optical system:

Thick glass windows used in the experimental setup may have contributed to some optical distortions during the experiments. Light enters and leaves the spray chamber by passing through thick glass windows, so there are possibilities of light reflections. For the droplet imaging system, glass windows were covered with a non-reflecting sheet of paper, which helped in avoiding reflection of light due to the glass windows. Moreover, nitrogen flow through the chamber was set in order to take out all the fuel droplets from the chamber. However, it was observed that there were some droplets, sticked to the inner glass surfaces, which may cause some optical falsifications. Nevertheless, the inner glass surfaces were cleaned many times during the experiments when the droplets seemed to be covering the windows.

The fuel spray penetrates with remarkably high velocities, so the motion blur had to be accepted in the images. High spray velocities might affect the fuel spray penetration but the effect on opening angles should not be that much. For droplet size imaging, high spray velocities gave rise to small droplets having small tails and distorted shapes. However, as the spray velocities

decelerate quite quickly, the motion blur effect also decreases. Based on this, the droplet analysis location was selected, and due to short applied exposure time, it was assumed that the effect of motion blur would be smaller at the selected spray droplet analysis location. The high spray velocities due to higher injection pressures give the reason that the images for the test points for droplet size distributions with lower injection pressure were comparatively of better quality than those with higher injection pressures.

In order to observe the effect of window surface quality on the droplets imaging, different set of images were captured with different rotations of the glass window. In doing so, four different points were marked (perpendicular to each other) on the window surface and it was rotated on all four points for 4 different sets of images. It was observed that while rotating the window at 90 degrees, the tails in the droplets seemed to be changing their directions almost to 90 degrees. Moreover, rotation of the window at point 3 seemed to be giving the best image set amongst all. This explains that the quality of glass window has a significant effect on droplet imaging.

Spray formation:

Minor fuel rail and chamber pressure variations had to be accepted during the experiments. However, by performing different actions, the pressure variation was kept less than 10% of the target values. From the equations (2-5) explained earlier in Section 3.2.3 for spray penetration, it can be inferred that minor fuel rail and chamber pressure variations do not have any significant effect on the spray formation.

Moreover, fuel mist and fuel impurities left inside the chamber during fuel injections may have some effect on the spray formation. Nevertheless, for spray geometry tests, a reasonable delay was kept during fuel injections and a continuous nitrogen flow was kept through the chamber, in order to clean up the entire chamber from fuel residues and mist. The chamber was continuously observed visually before every injection, to ensure that the chamber is clean and nearly all the fuel mist has been taken away. However, there are possibilities that there was still some left-over fuel mist that can affect the spray formation.

Image analysis or post-processing:

The errors and uncertainties regarding image analysis and post-processing of the images differ for spray geometry and droplet size measurements. However, the accurate detection of edges between the dark and bright pixels of the fuel spray and the individual droplets was the common uncertainty cause between the two analysis systems. Spray-to-spray variations in spray geometry measurements caused some false detections of spray edges that affected the analysis for spray opening angles. Moreover, the chamber design did not allow the light to reach properly near the injector nozzle. Therefore, the area near the injector nozzle was not comparatively that bright, leading to difficulties regarding the real injection starting and ending time detections. Regarding the droplet distribution measurements, errors in detections of the smallest droplets may appear due to the limitation of image resolution.

8.2 Spray geometry measurements

As explained earlier that false detections of spray edges were observed because of the spray-to-spray variations between different injections. Similarly, variations in the injection delays

between consecutive injections were observed by manually checking the images. Moreover, the spray tip penetration and opening angles also showed some variations between different shots for the same test points. However, these variations and uncertainties were reduced to minimum by averaging the results over 50 injections per every test point.

The backlight intensity seemed to be a very important factor while considering the image analysis. As explained in the experimental setup that two different light sources are combined to use as a single light source in order to increase the backlight intensity. The idea is to sharply separate the spray from the background for proper spray edge detection. This was done later by using background subtraction in Matlab. Considering the area close to the injector nozzle, the backlight intensity is even lower, causing uncertainties in the nozzle orifice location and actual injection starting and ending time. To get better results for the actual start and end time of injection with short injection durations, the camera location was moved in a way that it will capture the images with a comparatively brighter background. However, the orifice location and centerline angle were manually detected from the images.

There were possibilities of error while determining the orifice location and centerline angle manually. From the images, it was observed lately that the nozzle orifice location had some variation between different image sets. The possible reasons behind this source of error are the vibrations/motion in the system caused by running high-pressure fuel pump. Moreover, the setup on which the camera was mounted was not rigid enough to bear those vibrations during the injections. Therefore, the nozzle orifice location was determined for every test point manually. This helped in reducing the false detection of centerline angle and nozzle orifice location. However, by averaging the image results over 50 injections for each test point, it can be safe to say that the effects caused by these errors can be compensated and somehow overlooked.

Injection delay between consecutive injections was determined by visually seeing the chamber. After every injection, nitrogen flow is used to take out the fuel mist and residues out of the chamber. The time delay from the previous injection to the next one is determined by visually observing the chamber when it looked free from previous injection's fuel mist. This might have some effects on the spray formation if some fuel mist still stays in the chamber from the previous injection.

8.3 Droplet size measurements

While performing the droplet size measurements, one of the major constraints is the light penetration and scattering through the spray droplets. The image area under observation was set to be at the edge of spray and at 35mm distance from the injector nozzle tip. The reason behind choosing this specific location for droplet size analysis is the reduced effects of light scattering and penetration from the droplets at this location. Moreover, the high velocity fuel spray decelerates quite quickly after it starts penetration in the chamber. Therefore, the possibility of getting better fuel droplets at this location is increased. The shallow depth of field also reduces the effects of these errors and allows detecting droplets with sharp edges.

The quality of images for different image sets varies quite significantly from each other. The images with lower injection pressure possesses better image quality than the images with higher

injection pressures. The underlying reason is again the higher spray velocities with higher injection pressures. Fuel sprays injected at higher injection pressure possesses higher spray velocities that might result in some turbulence in the droplets, which in turn affects the detection of droplets with proper centricity. Due to the limitation of exposure time/pulse duration of laser, this constraint had to be accepted. However, certain modifications have made in order to minimize the effects.

The images are captured at a specific location in the spray and the image area is very small. This implies to the information of droplet size distribution for that specific point in the spray, and not for the complete spray. It is possible that for ethanol, diesel and HVO, the variations in droplet size distributions will be different at different spray locations.

Thick glass windows of the chamber can contribute to the light reflection. As the light enters and leaves the chamber by passing through the glass windows, there are certain possibilities of light reflection from the surfaces of the windows. However, in order to avoid this, major part of windows was covered with black non-reflecting sheet of paper. To avoid the motion blur, pin hole setup was manually arranged on the glass windows. Moreover, the complete experimental setup was covered with a tent to avoid the influence of external light and keep the surroundings safe from the laser.

Spray-to-spray variations between different set of images showed that sometimes there were images with no or very small number of droplets and in some image sets, the whole image area was covered with mist of fuel without any separated droplets. This indicated that either the location of camera is above the spray edge or the camera is capturing close to the centerline of the spray. To overcome this, the height of the camera was adjusted several times vertically, in order to get the proper location on the spray where the possibility of capturing droplets appearance was maximum.

It was observed during the image acquisition phase of the experiments that there exist certain factors causing uncertainties, because there were considerable number of low-quality images. Although, they were not included in the analysis but they showed the existence of uncertainties. Moreover, the quality of images varied quite significantly between different sets of images. This variation in image quality was mainly based on the injection pressures and chamber densities. After these observations, it can be concluded that certain factors such as light reflection from the windows and refraction might have given rise to those low-quality images. To improve the reliability of results, only good quality images for every set of images were selected for analysis.

During the image analysis for droplet size measurements, droplet detection was one of the challenging part. The user manual of the software says that the droplets detection depends on the droplets sizes. The software does not detect the smaller and larger particles with the same probability, even if their distribution is homogeneous in the image. Therefore, the software has a bias, based on droplet sizes. Mainly, two factors are responsible for this bias called as Boerder effect and depth of field effect. The effective depth of field becomes broader with the increase in droplet sizes, making the larger droplets appear to be in focus. This causes the bias in droplet size analysis. This phenomenon can be compensated with the effect that the field or area of view is smaller for larger droplets. In order to compensate both the phenomena, the software introduces a parameter called statistical weight for every droplet, which compensates the

detection probability bias related to the droplets sizes. Therefore, the results should be bias free considering the impact of statistical weight.

Furthermore, droplet detection can also be affected by small resolution limitations. As explained earlier that the image area is very small (i.e. 1.32 µm × 1.32 µm in focal plane), there is a possibility that some smaller droplets with size of few micrometers cannot be detected properly by the software. Another effect can be the background noise that makes it hard for the software to detect the smaller particles completely. In order to reduce the background noise, pixel noise reduction was implied in the software, which can also affect the smaller droplets detection. However, the effect of this constraint was minimized by using background subtraction in order to compensate for the backlight intensity variations. Background subtraction also helped to exclude the small impurities appearing in the optics.

9 Results

9.1 Spray geometry

9.1.1 Visual Observations

This section focuses on some qualitative observations made on the basis of visually analyzing the images captured during the experiments. Considering the general spray behavior, the creation of eddies in the spray edges is visible in the spray images presented in Figure 43. In the images, the eddies seem to be created more frequently downstream the injector nozzle, justifying the common flow theory. Moreover, sprays seem to have significantly dynamic spray edges, showing that the spray flow is unstable and turbulent. Due to the turbulency in the spray edges, the bahavior of the spray boundary is very difficult to analyze. However, the averaging of image sets has helped to investigate the visual differences in the spray geometry between different fuels and with changing chamber densities.

In Figure 43, spray propagation of HVO, diesel EN590, and ethanol sprays is presented to get a visual comparison of the behavior of different fuel sprays. Some clear differences can be seen from the images regarding the spray geometry. The figure explains that HVO and diesel sprays possess quite a similar spray geometry. However, ethanol sprays have slight differences from the other two on the basis of spray tip penetration and opening angles.

Figure 44 shows the significant effect of chamber densities on the spray geometry. HVO and diesel sprays showed slight differences in the spray geometry with varying chamber density. However, ethanol spray seems to be affected quite significantly by varying the chamber density from 20 to 40 $\mathrm{kg/m^3}$. In general, it can be seen visually from the images presented in Figure 44, that the spray penetration seems to reduce by increasing the chamber density. Moreover, the increasing trend of opening angles can also be observed with increased chamber density.

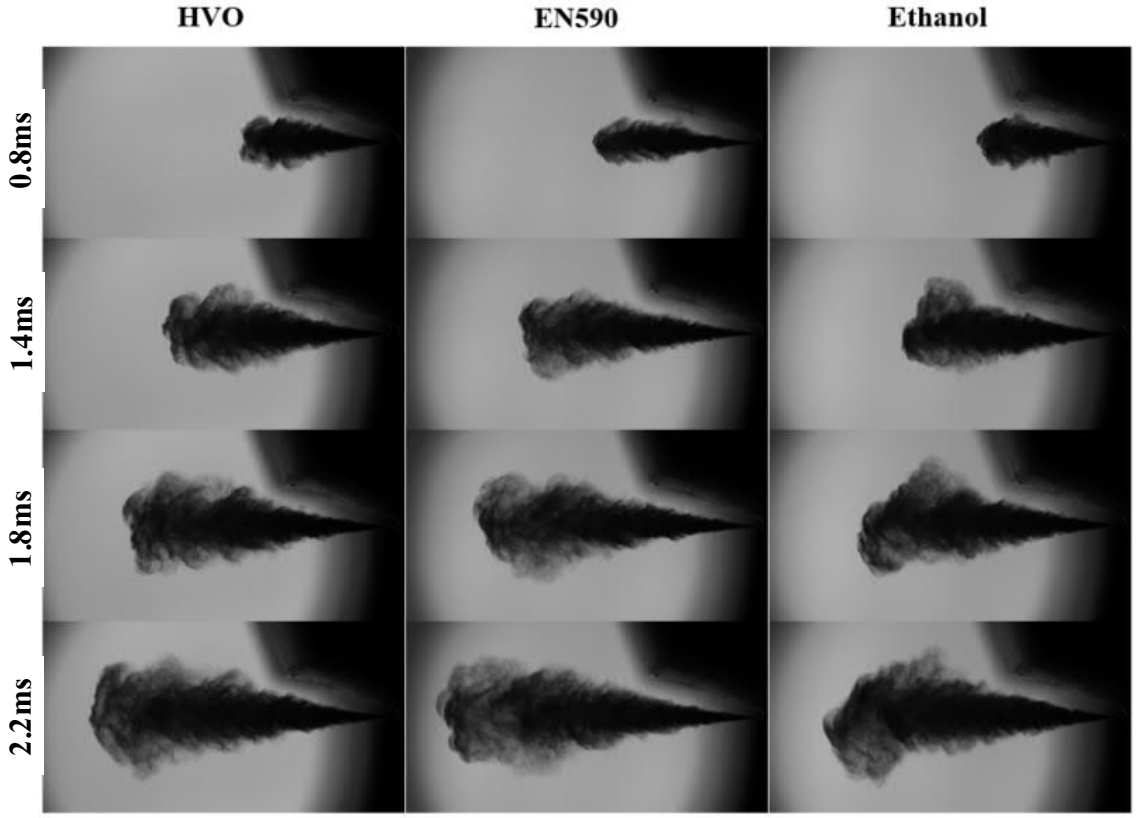

Figure 43 Comparison of spray evolution for HVO, Diesel EN590 and Ethanol. Injection pressure 1200 bar, Chamber density 40 kg/m^3. Shot 10/50

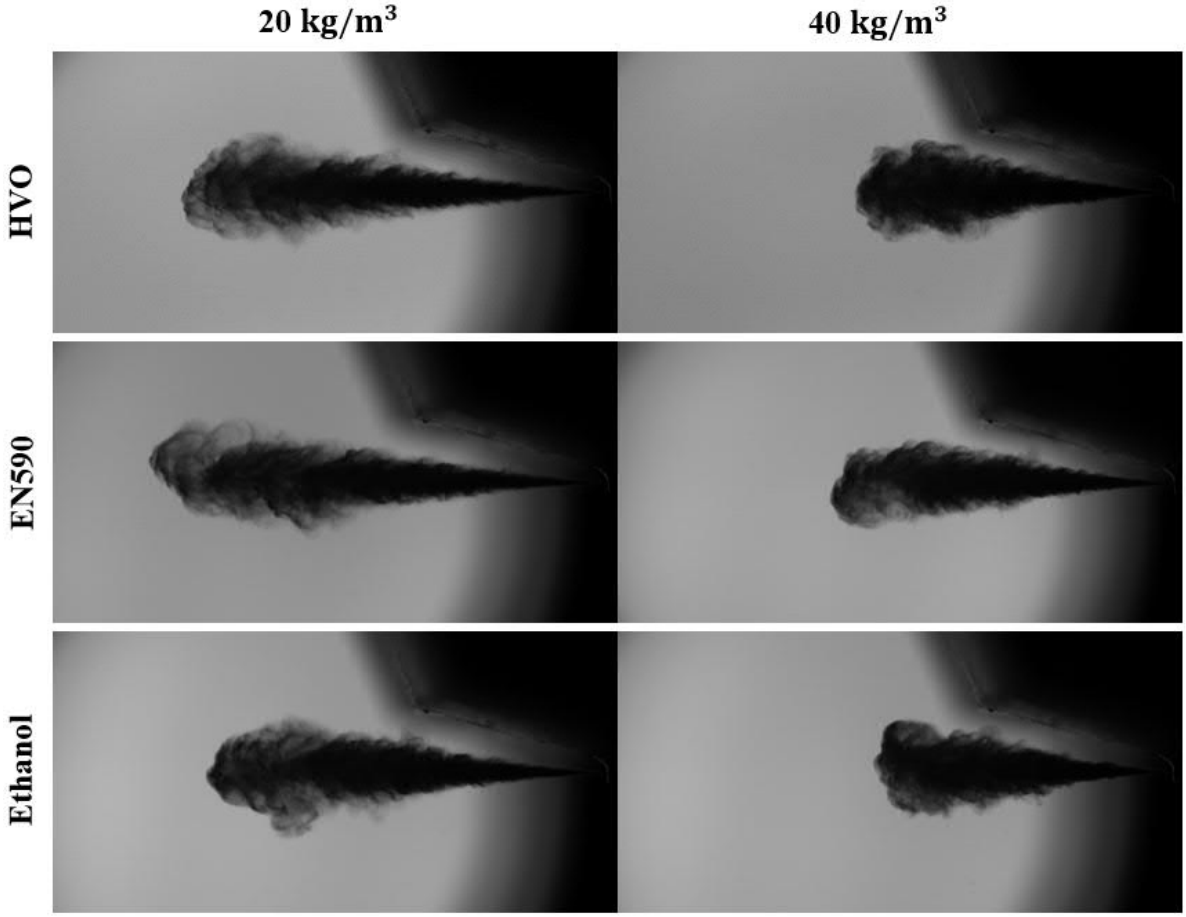

Figure 44 Effect of chamber density on spray evolution of HVO, EN590 and Ethanol sprays. Injection pressure 1200bar. Images are taken at the same time with respect to the injection signal. Shot 10/50

Although the information regarding the spray behavior at spray boundary is very difficult to observe, averaging the image sets proved to be a feasible solution in order to analyze the repetitive visual variations in the overall spray geometry between different fuels at different chamber densities. Figure 45 reveals very slight differences between HVO and EN590 Diesel sprays at 20 and 40 kg/m^3 chamber densities. First image set in Fig. 45 was taken approximately 0.12 - 0.16ms after the start of injection and the second image set was taken after 0.12ms from the spray propagation shown in the first image set. Ethanol spray seems to have quite a similar spray geometry with HVO and diesel at the beginning (first image set in Fig. 45). However, as the spray propagates at approx. 0.25ms from the start of injection (second image set in Fig. 45), the difference of overall spray geometry of ethanol with HVO and diesel is quite significant.

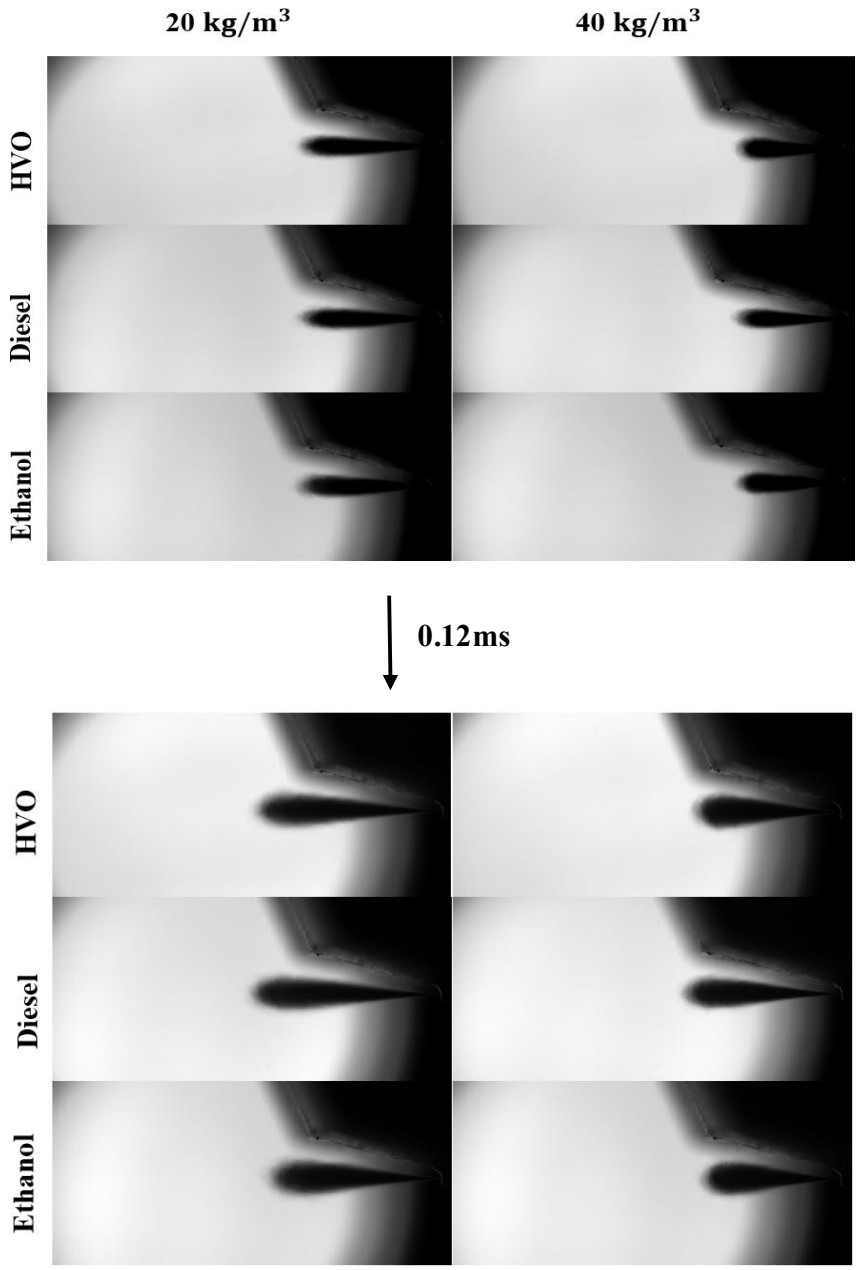

Figure 45 Evolution and shape of average sprays at different chamber densities. Images averaged over 50 shots. Injection pressure 1200 bar. Start of injection approximately 0.12 - 0.16ms before the upper image series.

9.1.1.1 Special Nozzle:

At the same experimental parameters, the spray geometry tests were also performed for another injector having special nozzle with increased nozzle hole diameter, to analyze the effect of nozzle orifice size on spray geometry. Figure 46 shows the comparison of diesel EN590 spray evolution with reference and special nozzle. Significant differences in spray geometry can be observed with different injector nozzles. Other than spray geometry, it can also be seen that the spray injected with special nozzle seems to be denser than the spray injected from the reference nozzle. This probably relates to the fact that more amount of fuel is injected with an increased diameter nozzle at the same injection duration.

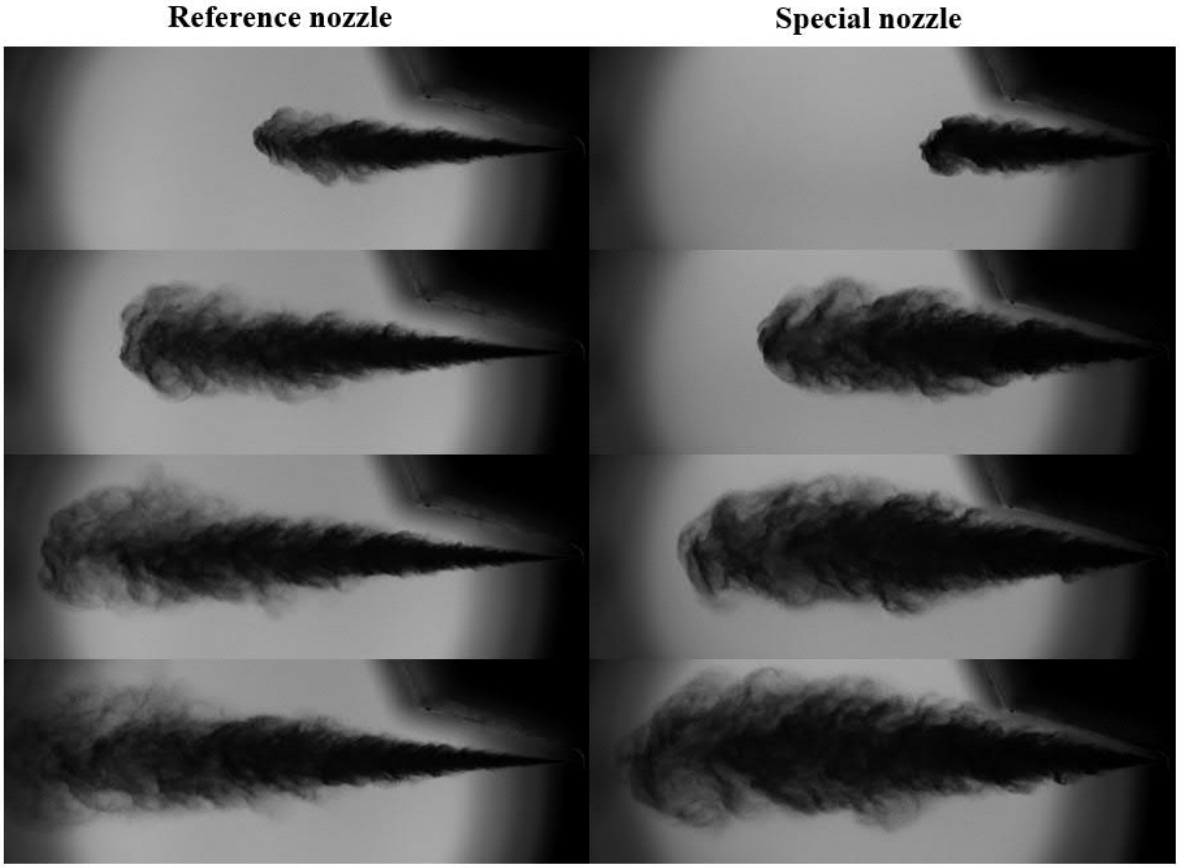

Figure 46 Comparison of spray evolution for diesel EN590 sprays injected with reference and special nozzle. Injection pressure 1200 bar, Chamber density 20 kg/m^3. Shot 10/50

9.1.2 Spray-to-spray variations

Spray-to-spray variations refer to the differences in the spray behaviors coming out in consecutive spray injections. Although the experimental parameters were kept as constant as possible, significant variations have been observed in the consecutive sprays. In Figure 47, the

images are taken at the same time with respect to the injection signal for four consecutive HVO spray injections at 1200 bar injection pressure and chamber density of 40 kg/m^3. From the images, the spray-to-spray variations can be observed quite clearly with respect to the opening angles and penetration. However, analyzing the images closely shows that the variations in spray width are more than the spray penetration variations.

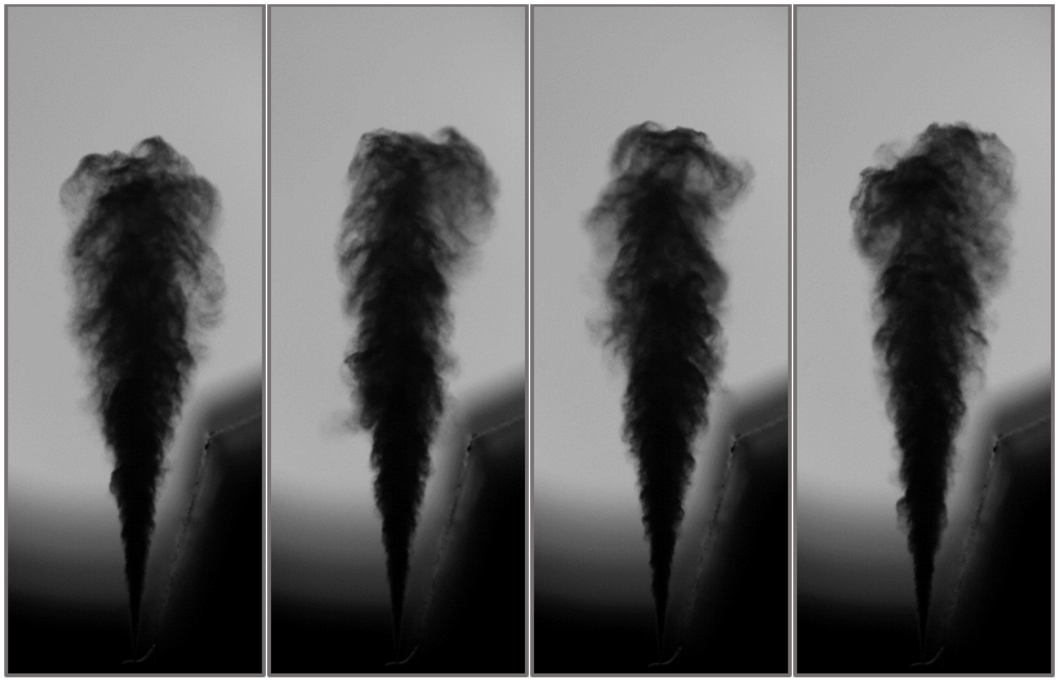

Figure 47 Example of spray-to-spray variation of HVO sprays captured from consecutive injections. Injection pressure 1200 bar, Chamber density 40kg/m^3. Shot 10/50

Furthermore, Figure 48 explains the spray-to-spray variations of diesel spray injected with special nozzle (inc. diameter) at 1200 bar injection pressure and chamber density of 20 kg/m^3. The experimental parameters were kept as constant as possible and the images are taken at the same time with respect to the injection signal for four consecutive injections. The spray-to-spray variations, in this case, are relatively more noticeable with respect to penetration and spray angles. The extreme right image in Figure 48 suggests a significant difference in the spray penetration from others. Moreover, the plotted results in the previous section regarding the opening angles for special nozzle tests can also be justified quite clearly from Figure 48, where the variations in spray angles can be observed quite evidently. Furthermore, the larger opening angles also affected the spray propagation by making the spray to propagate very close to the chamber walls. However, this does not have any effect on the analysis, because the portion of the chamber wall close to the spray seen in the images was excluded from the image area in the Matlab script for analysis (see Fig. 36).

Figure 48 Example of spray-to-spray variation of diesel EN590 sprays injected from special nozzle. Images are captured from consecutive injections. Injection pressure 1200 bar, Chamber density 20 kg/m^3. Shot 10/50

9.1.3 Spray tip penetration

The differences in average spray tip penetration among HVO, EN590 Diesel, and Ethanol can be seen from Figure 49. The first two plots in Figure 49 include the data for two injection pressures (i.e. 600 and 1200 bar). However, the results with 2000bar injection pressure are available in last plot of the figure. Only diesel fuel was tested at a higher injection pressure of 2000bar with 40 kg/m^3 chamber density.

Average penetration trends for HVO and Diesel EN590 are quite close to each other, however, small differences can be seen between them. The general trend for all three fuels is quite similar for both injection pressure values of 600 and 1200 bar. HVO and Diesel sprays are ahead of Ethanol in both cases of varying injection pressures. However, this difference is minor or non-existent in the early stages of fuel spray propagation, where ethanol sprays are almost matching the trend of the other two fuels.

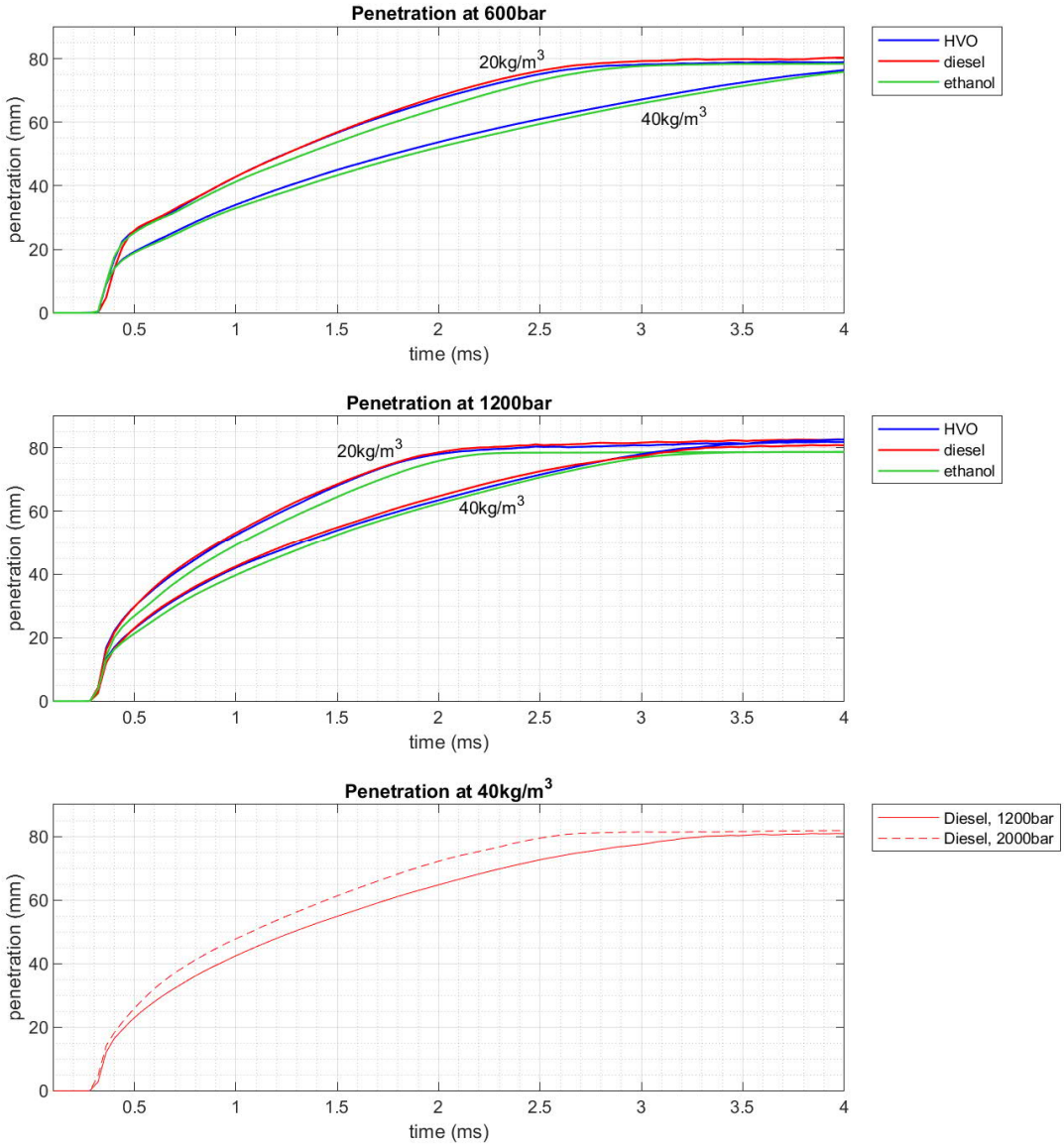

Figure 49 Average spray tip penetration at 600, 1200 & 2000 bar injection pressure with 20 & 40 kg/m^3 chamber densities.

By changing the chamber densities from 20 kg/m^3 to 40 kg/m^3, the average penetration trends shifted towards relatively lower penetration values. At chamber density of 40 kg/m^3, diesel fuel spray injected at 2000bar (presented in Figure 49) is ahead of same fuel spray injected at 1200bar. This is justified from the actual images of the sprays presented in Figure 50. By seeing from the actual images taken for diesel spray at 40 kg/m^3 and at injection pressures of 1200 and 2000bar, it is quite noticeable that the spray penetrated more with 2000bar injection pressure than 1200bar. It is to be noted that the images are captured at the same time from the injection signal.

Figure 50 Images captured for diesel spray at 40 kg/m^3 chamber density to show the penetration comparison at 1200 and 2000bar injection pressure.

Furthermore, at 600bar and 20 kg/m^3, a special shape of the plot could be observed quite evidently at the beginning of injection (Figure 49, first plot). In order to justify this special penetration trend, the respective images were carefully observed and it was concluded that spray from reference nozzle propagates quite fast in the first few milliseconds of the injection as compared to the spray from the special nozzle, where the spray is propagating gradually. This rapid spray penetration from reference nozzle at the beginning of injection gave the special shape to the penetration curve in the graph for the first few milliseconds, after which, the spray penetration curve gets smoother and spray penetrates gradually.

9.1.3.1 Special nozzle

The idea was to compare the diesel spray geometry results for both nozzles with different nozzle hole diameters. The average spray penetration for reference nozzle is ahead of special nozzle (inc. dia.) for both injection pressures. Moreover, the average penetration trends for special nozzle shifted towards relatively lower penetration values, by reducing the injection pressure values from 1200 to 600bar.

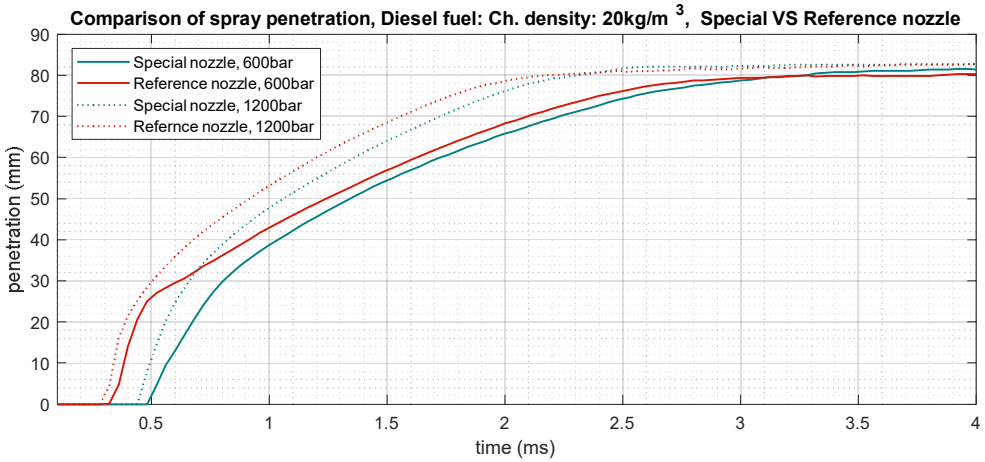

Figure 51 Comparison of average spray tip penetration of EN590 diesel fuel injected with special and reference nozzle. Chamber density: 20 kg/m^3

The penetration comparison results presented in Figure 51 above are justified by the experimental images shown in the Figure 52 below. The images were captured at the same time from the injection signal for diesel spray at 600 bar injection pressure and 20 kg/m^3 gas density. It is evident from the images that increased nozzle hole diameter (special nozzle) possesses decreased spray penetration as compared to the reference nozzle.

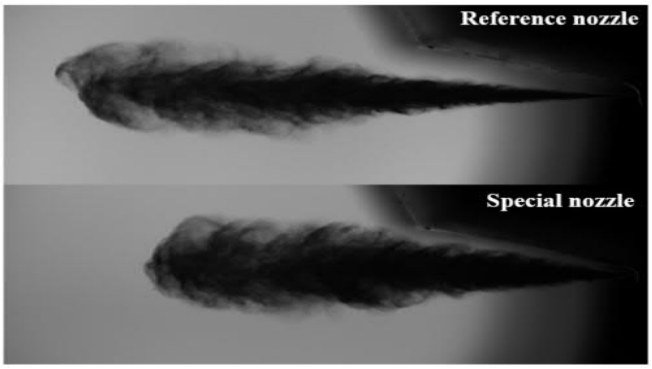

Figure 52 Images captured for diesel spray injected at 600 bar injection pressure with 20 kg/m^3 gas chamber density to show the penetration comparison of special and reference nozzle.

9.1.4 Spray opening angles

The trends for characteristic opening angles with varying injection pressures and chamber densities are presented in Figure 53 below. The characteristic opening angles were determined from the lowest average opening angle values after the spray has well passed the transient phase at the beginning of injection. Spray experience a similar transient phase at the end of injection as well. The transient phases can be clearly seen from Appendix 2. Figure 53 shows the effects of varying injection pressures and chamber densities on opening angles calculated at 40mm distance from the nozzle orifice of the injector.

Figure 53 suggests that opening angles for ethanol sprays are ahead from HVO and diesel for both injection pressures of 600 and 1200 bar. Similarly, ethanol sprays also possess higher opening angles than the other two fuels in both cases of varying chamber densities from 20kg/m^3 to 40 kg/m^3. In Figure 53, opening angles for HVO sprays are ahead of diesel sprays at 600bar injection pressure. However, this trend reversed at a higher injection pressure of 1200 bar. Moreover, at the maximum condition of 2000bar injection pressure and 40 kg/m^3 chamber density, opening angles for diesel sprays shows an increasing trend with increased injection pressure from 1200 to 2000bars.

Figure 53 (right) presents that the overall trend for opening angles shifted towards increased values by increasing the chamber density from 20 kg/m^3 to 40 kg/m^3. Opening angles for ethanol sprays show a similar trend with increased chamber densities, by leading the other fuel sprays in both cases of chamber densities.

Figure 53 also suggests that the overall behavior of all three fuels is quite similar to the increase in injection pressure, but the trends could be completely opposite at other distances from the

nozzle orifice. Therefore, it is hard to come up with a patent conclusion regarding the opening angles due to inconsistent results at different distances from the nozzle orifice.

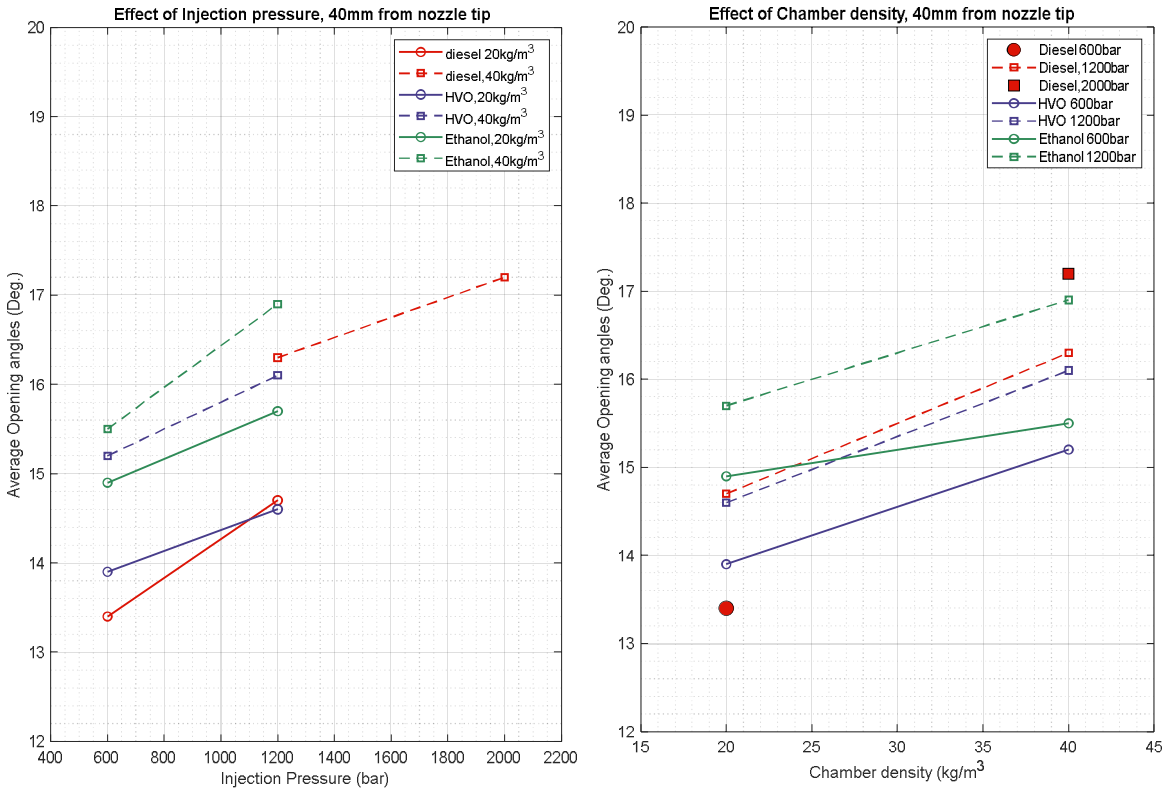

Figure 53 Characteristic opening angles plotted as a function of chamber density (right) and injection pressure (left). Distance from the injector nozzle: 40mm

9.1.4.1 Special nozzle

The comparison of the effect of varying injection pressures on opening angles calculated at 40mm distance from the injector nozzle, for both nozzles of different hole diameters can be seen from Figure 54.

The figure suggests that the opening angle trend for special nozzle sprays is way ahead than the sprays coming out of the reference nozzle. The trend is the same for increased injection pressure of 1200 bar with special nozzle having greater opening angles than the reference nozzle. This refers to the fact that increasing the nozzle orifice size increases the opening angles of the spray.

The increased average value of diesel spray opening angle for special nozzle injector compared to the reference nozzle can also be observed evidently from Figure 55. The images are captured at the same time from the injection signal of diesel spray injected at 600 bar and gas density of 20 kg/m^3.

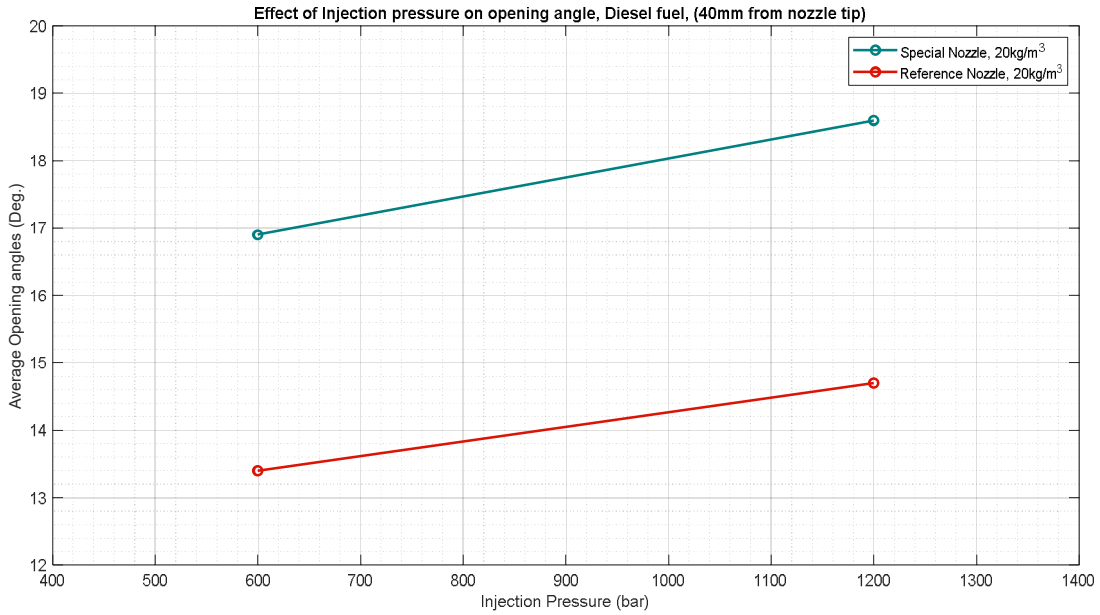

Figure 54 Comparison of average opening angles for EN590 diesel spray injected with special and reference nozzle and plotted as a function of injection pressures.

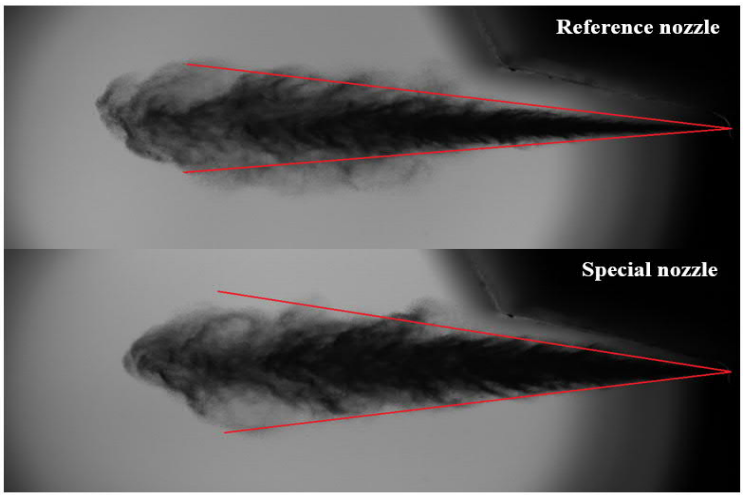

Figure 55 Images captured for diesel spray injected at 600 bar injection pressure with 20 kg/m^3gas density to show the opening angle comparison for special and reference nozzle.

9.2 Droplet size distributions

9.2.1 Mean diameter

In Figure 56 and 57, Sauter Mean Diameters (or D32) have been plotted against varying injection pressures and chamber densities. The figures present the effect of changing injection pressures and chamber densities on SMD's of fuel droplets. It is clear from the plots that ethanol sprays possess least SMD's in comparison with other fuels. HVO and diesel sprays are characterized with almost similar SMD's at both injection pressures of 600 and 1200 bar. Moreover, the trend shifts towards smaller SMD values when the injection pressure was increased. However, the general trend is quite similar for all three fuels at lower and higher injection pressures, with minor or non-existent variation in HVO and diesel spray's SMD values. Increasing the chamber density from 20 to 40 kg/m^3, the SMD trend for diesel spray has moved towards higher SMD's. This trend is quite opposite to Ainsalo, (2018) results. Increasing injection pressure at increased chamber density (i.e. 40 kg/m^3), shows a similar trend of SMD as shown for lower chamber density (i.e. 20 kg/m^3).

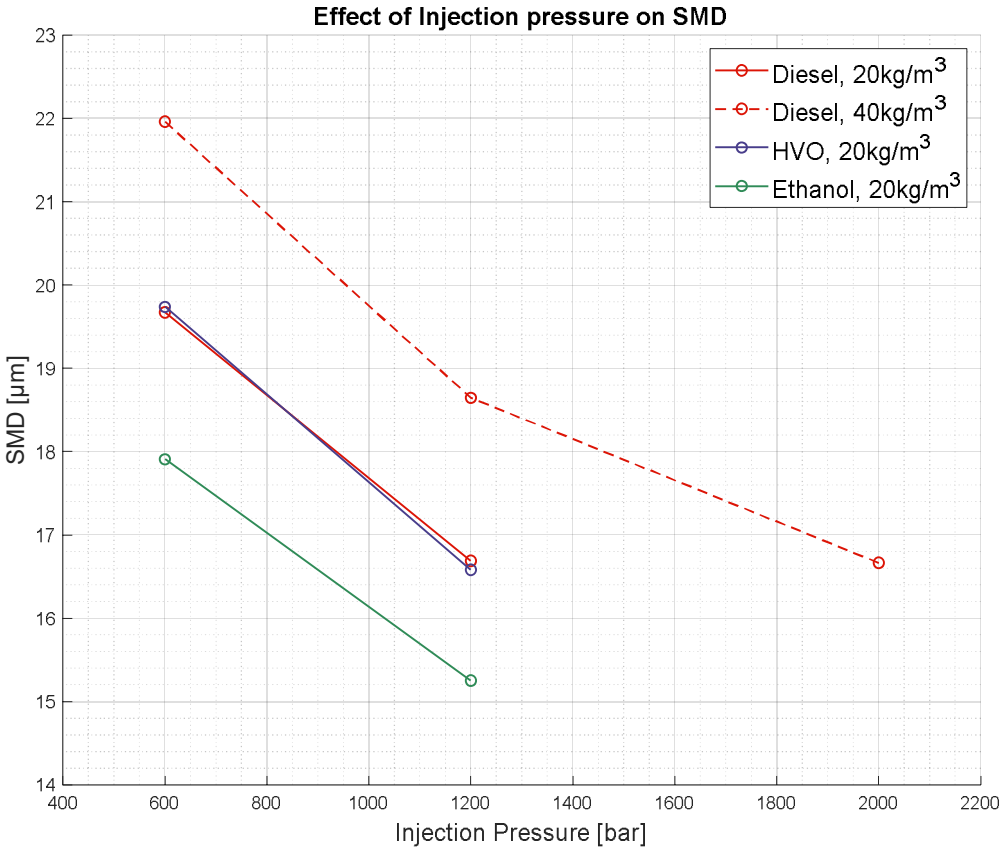

Figure 56 Effect of injection pressure on Sauter Mean Diameter

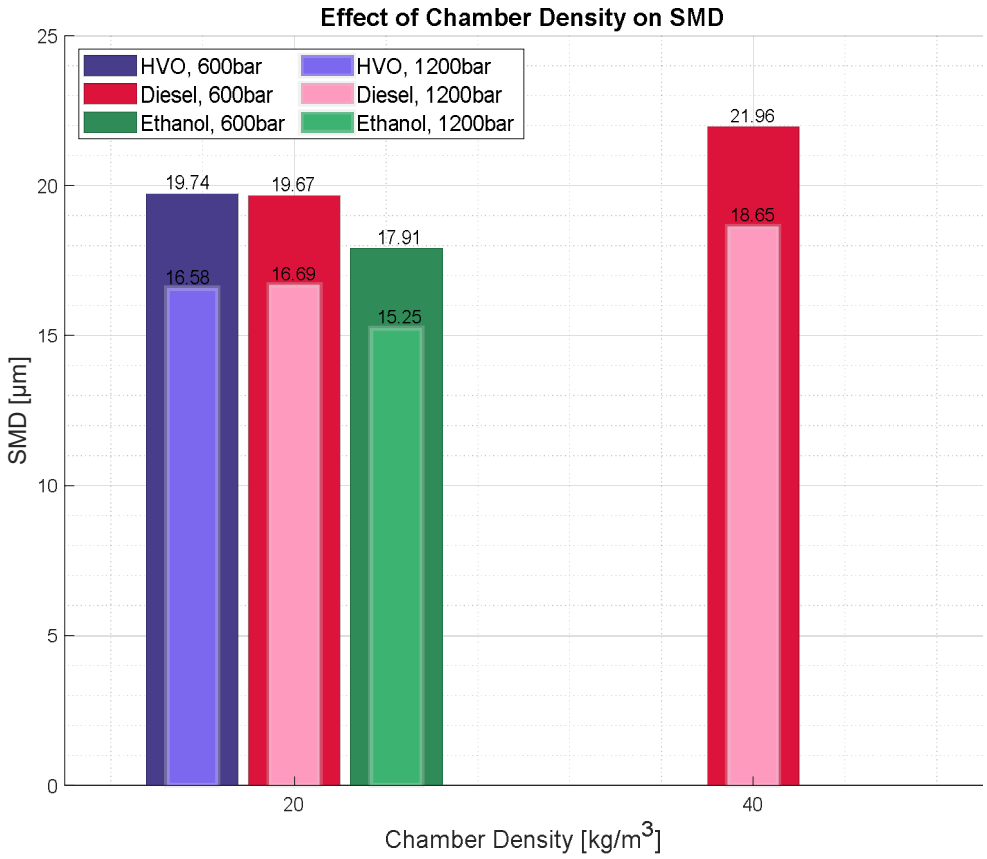

Figure 57 Effect of chamber densities on Sauter Mean Diameter

9.2.2 Special nozzle:

Considering the SMD's for diesel sprays injected from special and reference nozzle, it can be observed from Figure 58 that Sauter Mean Diameters for special nozzle sprays are larger than that of the reference nozzle. However, the difference in SMD is more at lower injection pressure (i.e. 600 bar) and the SMD for both nozzles are quite close to each other at a higher injection pressure of 1200 bar.

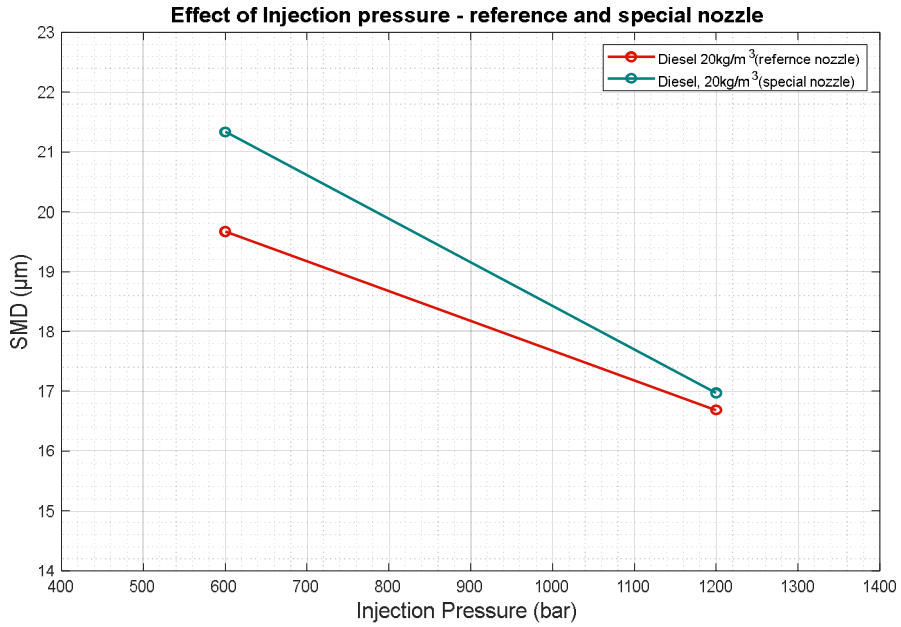

Figure 58 Comparison of effect of injection pressure on SMD's of diesel sprays injected with special and reference nozzle.

9.2.3 Size distributions

9.2.3.1 Size distributions – Number Based

Figure 59 – 62 presents the droplet size distributions based on droplets number. The size class interval for each droplet class presented in the graphs is 1µm. In the graphs, the statistical weight for every droplet is taken as it was explained in the image analysis section. The figures show that ethanol sprays possess smallest SMD's than HVO and diesel sprays.

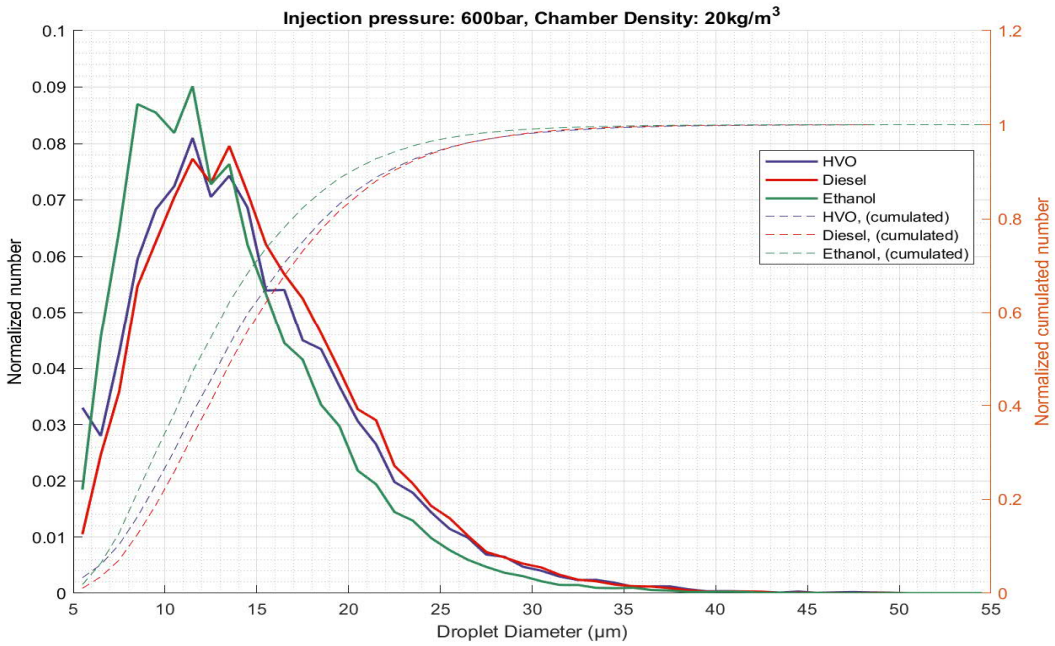

Figure 59 Droplet distribution with 20 kg/m^3 chamber density and 600bar injection pressure

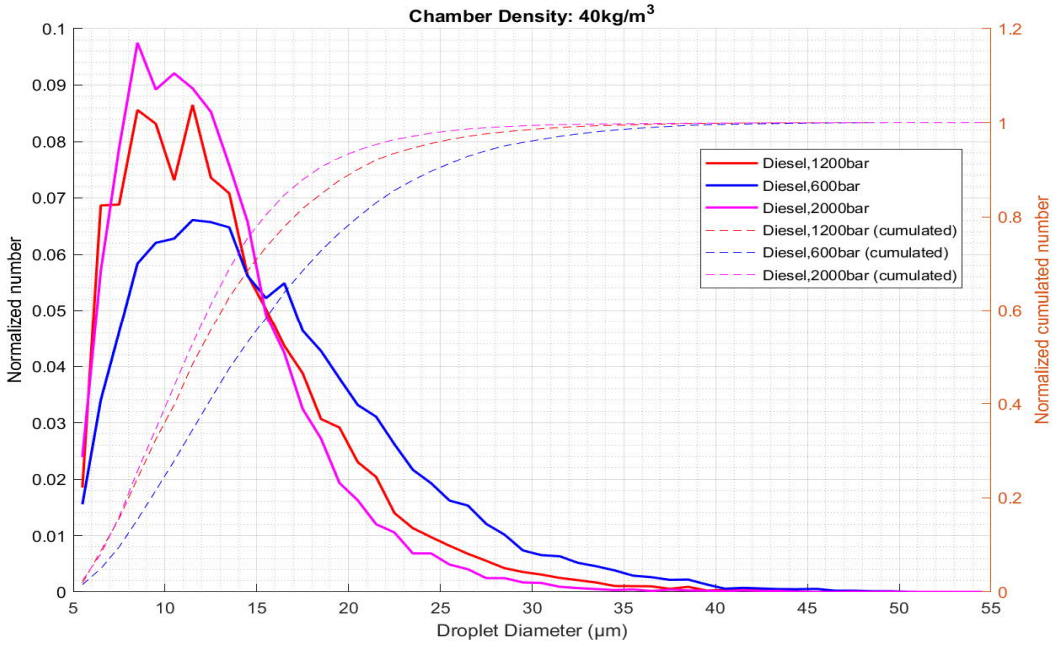

Figure 60 Droplet distribution with 40 kg/m^3 chamber density and 600, 1200 & 2000bar injection pressures

- **Special nozzle**

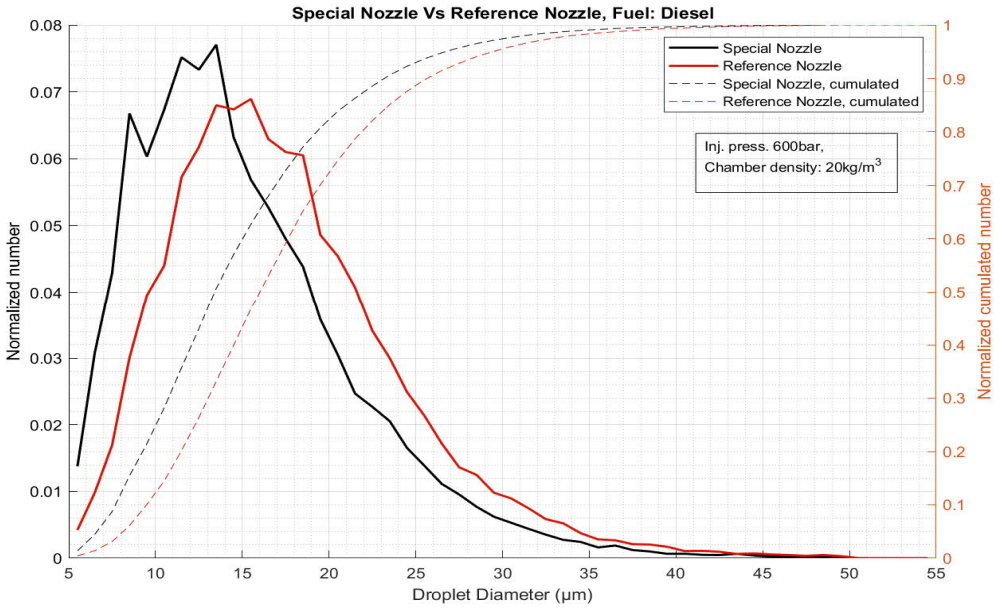

Figure 61 Comparison of droplet distribution from special and reference nozzle with 20 kg/m^3 chamber density and 600 bar injection pressures. Fuel: EN590 diesel

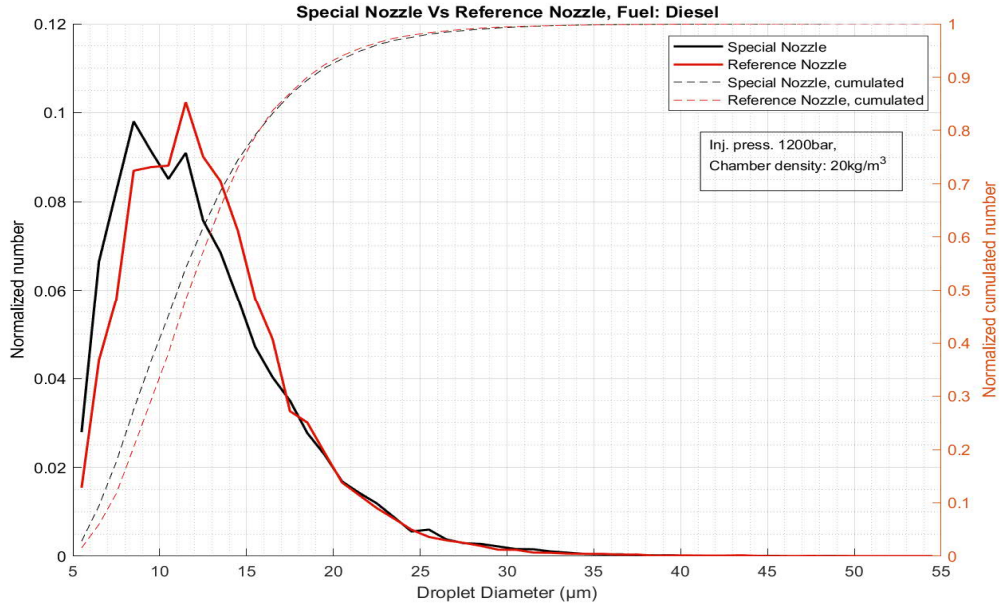

Figure 62 Comparison of droplet distribution from special and reference nozzle with 20 kg/m^3 chamber density and 1200 bar injection pressures. Fuel: EN590 diesel

9.2.3.2Size distributions – Volume Based

Figure 63 – 67 presents the droplet size distributions based on droplets volume. The graphs for normalized volume-based results have been plotted from the data where statistical weight of each droplet is further multiplies by the cube of droplet diameter.

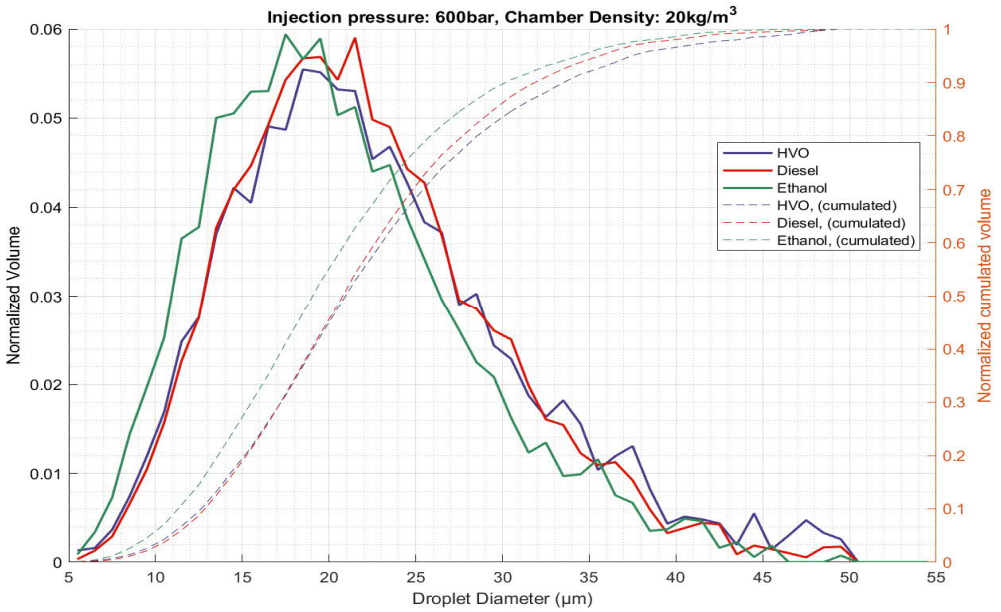

Figure 63 Volume based droplet distribution with 20 kg/m^3 chamber density and 600bar injection pressure.

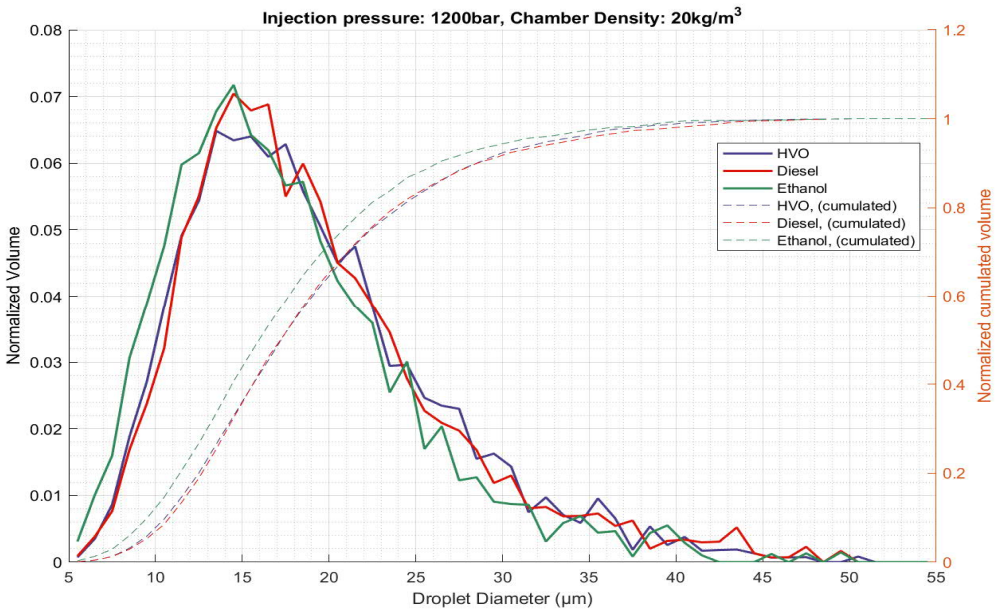

Figure 64 Volume based droplet distribution with 20 kg/m^3 chamber density and 1200bar injection pressure.

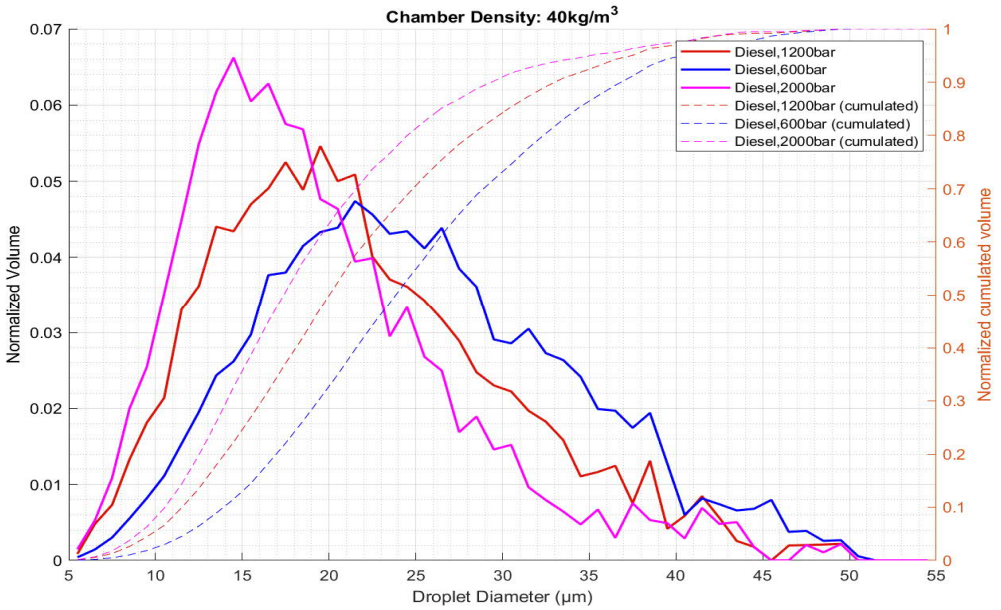

Figure 65 Volume based droplet distribution with 40 kg/m^3chamber density and 600, 1200 & 2000bar injection pressures

- **Special nozzle**

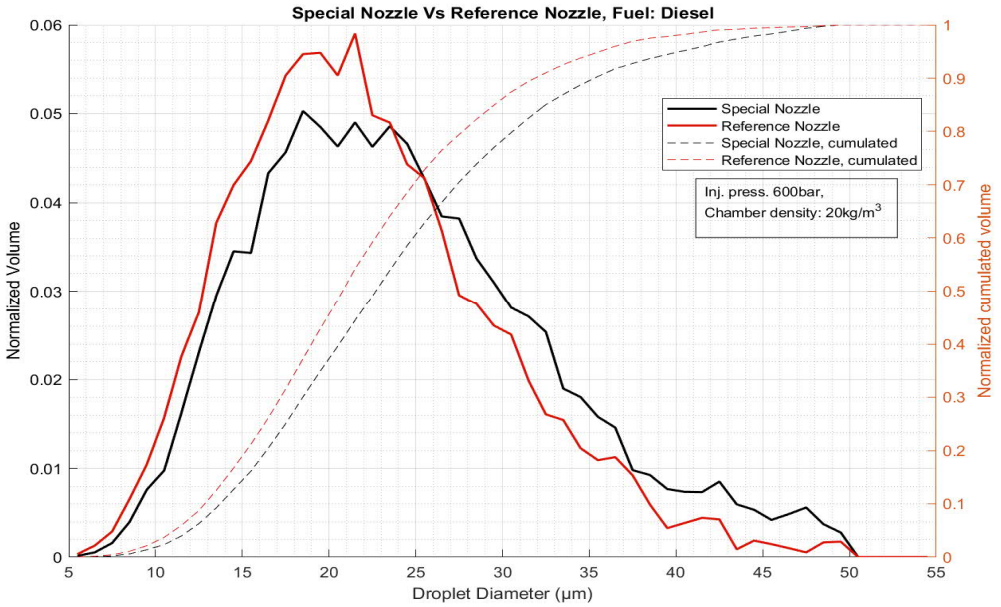

Figure 66 Comparison of volume based droplet distribution from special and reference nozzle with 20 kg/m^3 chamber density and 600 bar injection pressures. Fuel: EN590 diesel

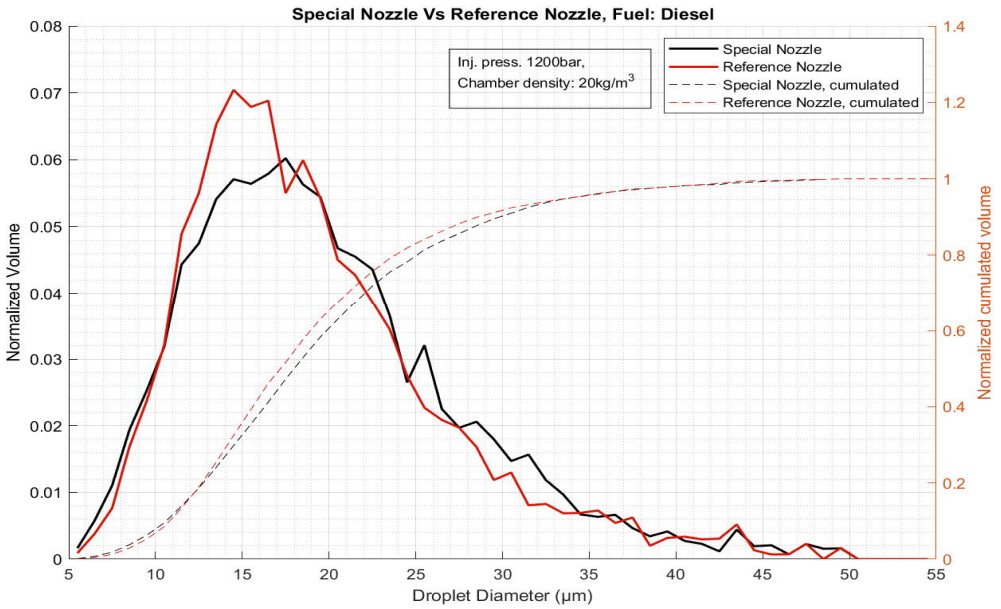

Figure 67 Comparison of volume based droplet distribution from special and reference nozzle with 20 kg/m^3 chamber density and 1200 bar injection pressures. Fuel: EN590 diesel

10 Conclusion

The aim of this thesis was to analyze and compare Hydrotreated Vegetable Oil (HVO), EN590 Diesel and ethanol fuel sprays by using the image analysis technique. Furthermore, the analysis of fuel spray characteristics based on nozzle orifice sizes of the fuel injector was also one of the objectives of this thesis. The complete analysis was divided into two parts in which the first part focused on the analysis of overall fuel spray geometry that included spray penetration and opening angles. The later part of the thesis was based on the droplet size analysis of the fuel sprays. The common objective behind the spray geometry and droplet size analysis was to study the characteristic features fuel spray that has a significant impact on the air and fuel mixing in the combustion chamber, thus affecting the combustion efficiency and the emissions. In addition to this, essential fuel spray parameters, fuel spray theory, and the optical measurement techniques, comparison of fuel properties and their impact on the spray characteristics have also been discussed in the theoretical section of this thesis.

Fuel spray characterization was carried out with two different gas densities (i.e. 20 and 40 kg/m^3), three injection pressures (i.e. 600, 1200 and 2000 bar) and three different fuels mentioned in the previous paragraph. The image analysis for spray penetration and opening angle was performed completely with Matlab script. However, droplet size analysis required a separate software (DaVis 10 by LaVision) for droplet detections in the greyscale images. Moreover, two injectors with different nozzle hole diameters were used to investigate the effect of orifice size on the fuel sprays.

All the required objectives (i.e. experiments and analysis) for this thesis were fulfilled with good success along with few challenges in building up the system as accurately as possible. For instance, experiments for spray geometry measurements were performed without facing unexpected challenges. However, few arrangements were done to make the system precise for the measurements. In order to get enough bright background of the images captured at 25000fps, two different light sources (Halogen and LED ring light) were used in a combined arrangement (see section 6.7.1).

On the other hand, few challenges (mostly related to the optics and imaging system) have been experienced while performing the experiments for droplet size distributions. The main reasons behind the constraints in the imaging system were the small image area, shallow depth of field, light reflections and refractions from the glass windows of the chamber and large spray-to-spray variations. Moreover, various test images were captured with small modifications in the imaging system (i.e. covering most part of the glass window surface with black sheet to avoid light refractions) to improve the image quality. In order to minimize the chances of error, large image sets with a large number of images were captured and then choosing the best images amongst those for the next phase of the analysis. Adjusting the detection parameters in DaVis software was also challenging in the analysis phase of droplet size measurements. In order to overcome this, the analysis was performed for all the test points first with the same detection parameters and then comparing them with the results obtained by setting an individual set of parameters for each test points. It was observed that keeping the individual set of parameters (although quite close to each other) for every test point, gives better droplets detection.

Regarding the analysis results, HVO and EN590 diesel fuel sprays showed quite similar behavior regarding the spray penetration, opening angles and droplet sizes. However, significant differences have been observed in the results for ethanol sprays. The spray penetration for ethanol was lagging from HVO and EN590, however, the opening angles for ethanol sprays were larger than the other two fuel sprays. Smaller droplet sizes for ethanol than HVO and EN590 were also observed quite significantly. Furthermore, the effect of chamber densities and injection pressures on fuel sprays has also been witnessed quite remarkably. Increasing the injection pressures, the spray penetration for all three fuels was increased. Furthermore, increase in injection pressures from 600 to 1200 and 2000bar, the mean diameters and droplet size distributions were significantly decreased. Significant effects on opening angles have also been observed by increasing chamber densities and changing the distances form the nozzle at which the spray opening angles were calculated. The results also provided significant information regarding the spray-to-spray variations for consecutive fuel injections. Regarding the droplet size distributions, notable effects of droplet detection parameters on the resulting droplet size distributions have also been viewed.

Moreover, the comparison of results for special (increased nozzle dia.) and reference injector nozzle have also revealed remarkable information regarding the effect of increasing nozzle hole diameter on spray geometry and droplet size distributions. The results have shown a decreasing trend for penetration and increasing trend of opening angles for larger diameter nozzle. The Sauter Mean Diameters (SMD's) for the special nozzle with increased orifice diameter have seen to be larger than the reference nozzle. The difference in SMD's is more significant at a lower injection pressure of 600bar.

References

Aatola, H. *et al.* (2009) 'Hydrotreated Vegetable Oil (HVO) as a Renewable Diesel Fuel: Trade-off between NO?, Particulate Emission, and Fuel Consumption of a Heavy Duty Engine', *SAE International Journal of Engines*. JSTOR, 1(1), pp. 1251–1262.

Agarwal, A. K. (2007) 'Biofuels (alcohols and biodiesel) applications as fuels for internal combustion engines', *Progress in energy and combustion science*. Elsevier, 33(3), pp. 233–271.

Ainsalo, A. (2018) 'Optical characterization of high-pressure methanol sprays'.

Arai, M. (2012) 'Physics behind Diesel Sprays. In: Proceedings of ICLASS, 12th Triennial International Conference on Liquid Atomization and Spray Systems. Heidelberg, Germany. 2 – 6 September 2012.' Available at: http://www.ilasseurope.org/ICLASS/iclass2012_Heidelberg/Contributions/Paper-pdfs/Contribution1419_b.pdf.

Arai, M. (2016) *Physics behind Diesel Spray and its combustion.* Saarbrücken, Germany: Lap Lambert Academic Publishing. 342 p. ISBN 978-3-659-97160-0.

Van Basshuysen, Richard, and F. S. (2004) *Internal Combustion Engine Handbook - Basics, Components, Systems, and Perspectives*. Warrendale: PA: SAE international.

Bechtold, R. L. (1997) 'Alternative fuels guidebook properties, storage, dispensing, and vehicle facility modifications'. Warrendale, Pennsylvania, USA: SAE International. ISBN 978-0-7680-0052-8 (print). ISBN 978-0-7680-3357-1 (online)., p. 204.

Bezergianni, S. and Dimitriadis, A. (2013) 'Comparison between different types of renewable diesel', *Renewable and Sustainable Energy Reviews*. Elsevier, 21, pp. 110–116.

Brink, A. *et al.* (1986) 'Carburettor corrosion: the effect of alcohol petrol blends', in *Symposium international sur les carburants alcoolisés. 7*, pp. 172–177.

Cardona, C. A. and Sánchez, Ó. J. (2007) 'Fuel ethanol production: process design trends and integration opportunities', *Bioresource technology*. Elsevier, 98(12), pp. 2415–2457.

Coghe, A. and Cossali, G. E. (2012) 'Quantitative optical techniques for dense sprays investigation: A survey', *Optics and Lasers in Engineering*. Elsevier, 50(1), pp. 46–56.

Crepeau, G. *et al.* (2009) *Engine impacts and opportunities of various fuels, including GTL and FAME: Toward specific engine calibration?*

Dietsche, K.-H. and Reif, K. (2011) *Automotive Handbook. 8th Edition*. Plochingen, Germany: Robert Bosch GmbH, 2011. p. 1265. ISBN: 978-0-7680-4851-3.

F. payri, V. Bermúdez, R. Payri, F. J. S. (2003) 'The influence of cavitation on the internal flow and the spray characteristics in diesel injection nozzles', (CMT-Motores Te ´rmicos, Universidad Polite ´cnica de Valencia, Camino de Vera s/n, E-46022 Spain).

Greenhalgh, D. A. and Jermy, M. (2002) 'Laser diagnostics for droplet measurements for the study of fuel injection and mixing in gas turbines and IC engines', *Applied combustion diagnostics*. CRC Press, pp. 408–428.

H. Chaves, M. Knapp, A. K. (1995) 'Experimental Study of Cavitation in the Nozzle Hole of Diesel Injectors Using Transparent Nozzles.', (SAE Paper 950290; 1995. Reprinted from: Engine and Multidimensional Engine Modeling (SP-1101)).

Hartikka, T., Kuronen, M. and Kiiski, U. (2012) *Technical performance of HVO (hydrotreated vegetable oil) in diesel engines*.

Heisler, H. (1995) *Advanced Engine Technology.* Reprinted in Great Britain by Butterworth-Heinemann at the Bath Press, 2003. ISBN:0-340-56822-4.

Hillamo, H. *et al.* (2010) 'Diesel spray visualization and shockwaves', *Atomization and sprays*. Begel House Inc., 20(3).

Hillamo, H. (2011) *Optical fuel spray measurements*. Doctoral Dissertations. Aalto University, Department of Energy Technology. 79p. ISBN: 879-952-60-4378-4.

Hiroyasu, H. and Arai, M. (1990) 'Structures of Fuel Sprays in Diesel Engines. SAE Technical Paper 900475.', (DOI: 10.4271/900475).

Hulkkonen, T. *et al.* (2011) *Experimental study of spray characteristics between hydrotreated vegetable oil (HVO) and crude oil based EN 590 diesel fuel.*

Itani, L. (2016) 'Development and application of optical diagnostic techniques for assessing the effects of preferential evaporation of multi-component fuels under engine-relevant conditions', *Thesis*, (Electric power. Université Paris-Saclay; Universität Duisburg-Essen, 2015).

John B. Heywood (1988) *Internal combustion engine fundamentals*. Edited by A. Duffy and M. M. John. International edition. Singapore: McGraw-Hill. 930p. ISBN: 0-07-100499-8.

Karimi, E. R. (1989) 'High-speed photography of fuel spray and combustion events in a production diesel engine and combustion bomb', *Proceedings of the Institution of Mechanical Engineers, Part A: Journal of Power and Energy*, 203(4), pp. 269–281. doi: 10.1243/PIME_PROC_1989_203_037_02.

Lapuerta, M. *et al.* (2011) 'Key properties and blending strategies of hydrotreated vegetable oil as biofuel for diesel engines', *Fuel processing technology*. Elsevier, 92(12), pp. 2406–2411.

Larmi, M. *et al.* (2002) *Simulation of non-evaporating diesel sprays and verification with experimental data*.

Lefebvre, A. H. (1989) *Atomization and Sprays*. Edited by N. Chigier. The USA: Taylor & Francis. 421 p. Combustion: An International Series.

Lequien, G. (2015) *Investigations of Diesel Sprays in Optical Engines-Liquid Fuel Penetration and Lift-Off Length*. Lund University.

Linne, M. (2013) 'Imaging in the optically dense regions of a spray: A review of developing techniques', *Progress in Energy and Combustion Science*. Elsevier, 39(5), pp. 403–440.

Mofijur, M. *et al.* (2016) 'Role of biofuel and their binary (diesel--biodiesel) and ternary (ethanol--biodiesel--diesel) blends on internal combustion engines emission reduction', *Renewable and Sustainable Energy Reviews*. Elsevier, 53, pp. 265–278.

Mollenhauer, K. and Tschoeke, H. (2010) *Handbook of Diesel Engines*. Edited by Prof. Dr.-Ing. Klaus Mollenhauer and Prof. Dr.-Ing. Helmut Tschoeke. p. 636. ISBN 978-3-540-89082-9.

Naber, J. and Siebers, D. L. (1996) 'Effects of Gas Density and Vaporization on Penetration and Dispersion of Diesel Sprays', *SAE Technical Paper Series 960034. DOI: 10.427/960034*.

Nakata, K. *et al.* (2006) *The effect of ethanol fuel on a spark ignition engine*.

Ning, Wei & Reitz, R. D. and Lippert, R. D. & A. M. (2008) 'A Numerical Investigation of Nozzle Geometry and Injection Condition Effects on Diesel Fuel Injector Flow Physics', *SAE Technical Paper Series 2008-01-0936*, p. 25.

Rantanen, P., Paloposki, T. and Kankkunen, A. (1993) *Kuva-analyysin käyttö pisarakoon mittaukseen*. Otaniemi: Teknillinen korkeakoulu. Available at: https://aalto.finna.fi/Record/alli.168419.

Robert Bosch (1994) *Diesel Fuel Injection*. Edited by H. Bauer and A. Beer. 1st Edition printed in Germany by Robert Bosch GmbH. p. 199. ISBN: 1-56091-542-0.

Sayin, C. (2010) 'Engine performance and exhaust gas emissions of methanol and ethanol--diesel blends', *Fuel*. Elsevier, 89(11), pp. 3410–3415.

Sirignano, W. A. and Tryggvason, G. (2000) *Fluid Dynamics and Transport of Droplets and Sprays*, *Journal of Fluids Engineering*. Cambridge, United Kingdom: Cambridge University Press. p.311 ISBN: 0-521-63036-3.

Stein, R. A., Anderson, J. E. and Wallington, T. J. (2013) 'An overview of the effects of ethanol-gasoline blends on SI engine performance, fuel efficiency, and emissions', *SAE International Journal of Engines*. JSTOR, 6(1), pp. 470–487.

Stiesch, G. (2003) *Modelling Engine Spray and Combustion*. Springer-Verlag Berlin Heidelberg 2003. p.282.

Sugiyama, K. *et al.* (2012) 'Effects of hydrotreated vegetable oil (HVO) as renewable diesel fuel on combustion and exhaust emissions in diesel engine', *SAE International Journal of Fuels and Lubricants*. JSTOR, 5(1), pp. 205–217.

Taylor, A. B. *et al.* (1996) *Gasoline/alcohol blends: exhaust emissions, performance and burn-rate in a multi-valve production engine.*

Ueki, H., Ishida, M. and Sakaguchi, D. (2005) *Investigation of droplet disintegration in diesel spray core by Advanced Laser 2-Focus velocimeter*.

Wyman, C. E. and Hinman, N. D. (1990) 'Ethanol', *Applied Biochemistry and Biotechnology*. Springer, 24(1), pp. 735–753.

Zhao, H. (2012) 'Laser Diagnostics and Optical Measurement Techniques', *Internal Combustion Engines*.

Appendix 1 Variations in spray tip penetration

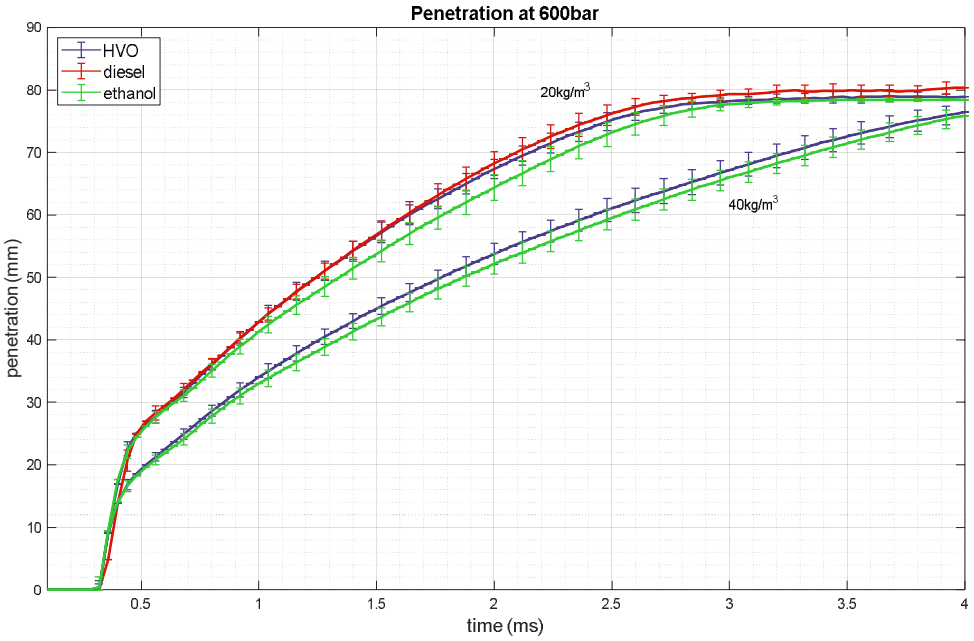

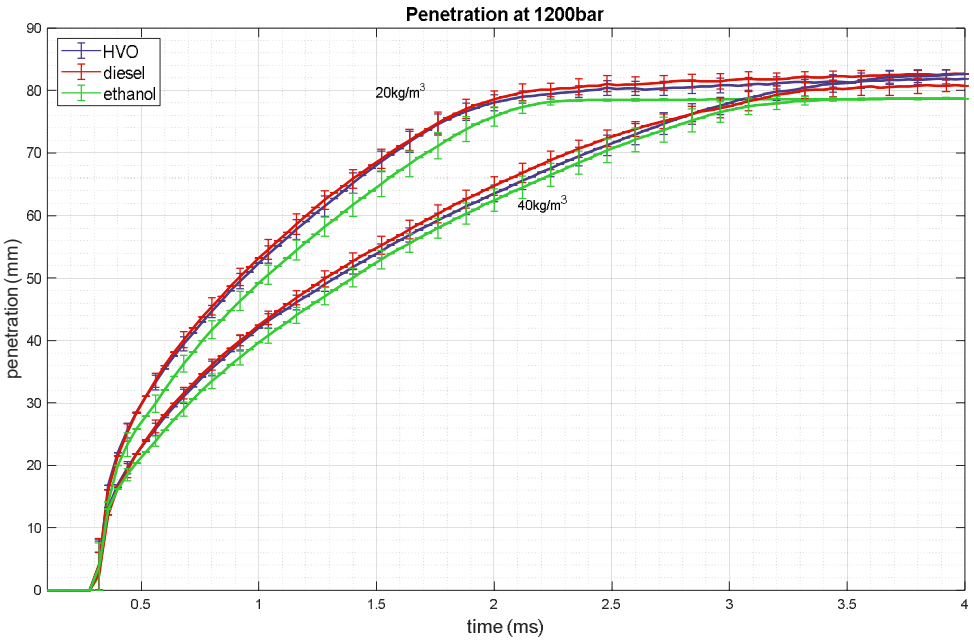

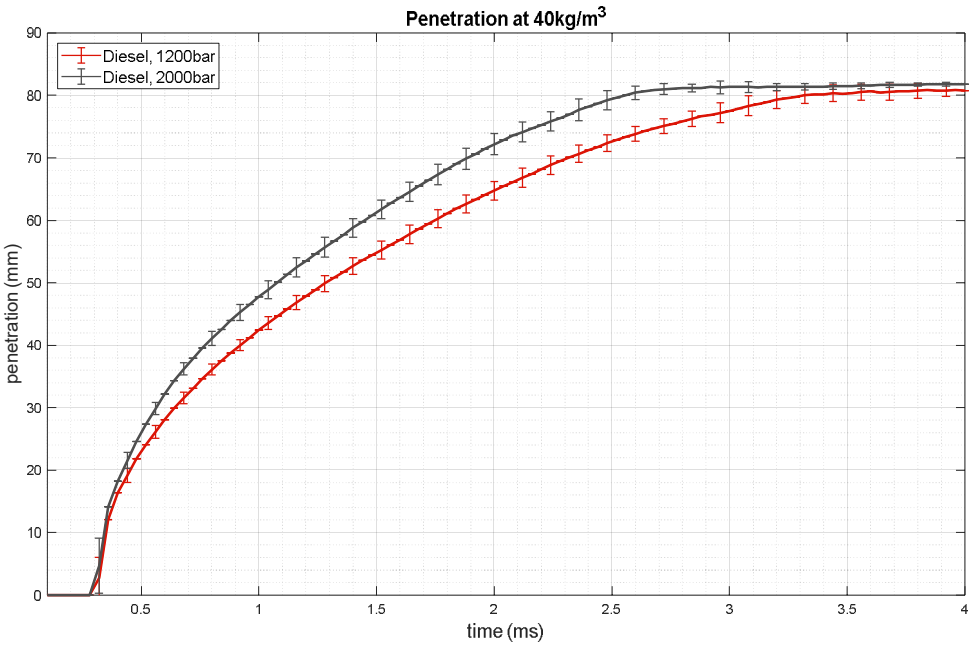

Comparison of spray penetration variation: Special Vs Reference nozzle

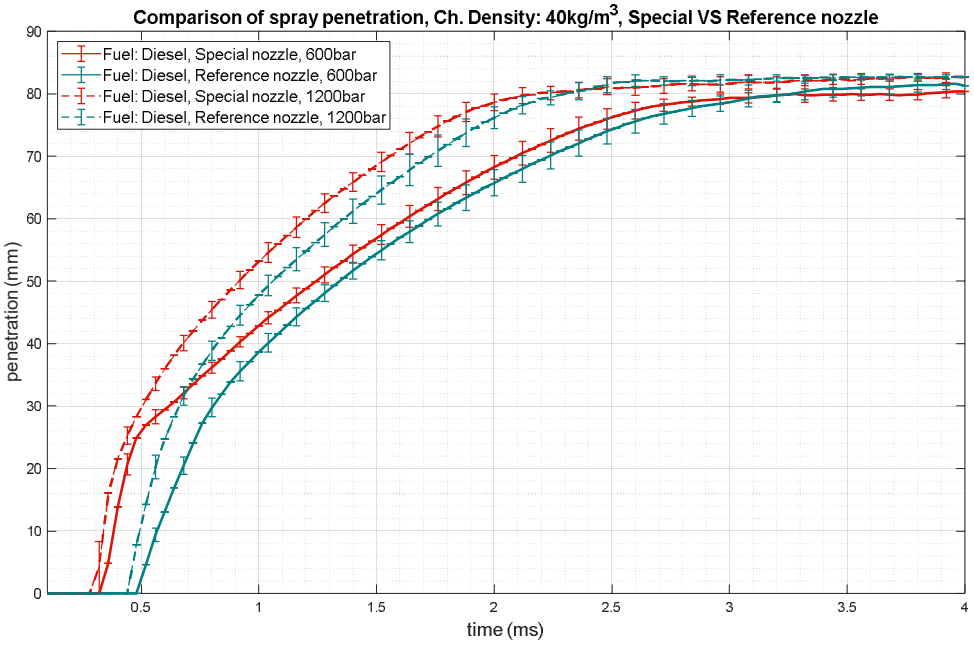

Appendix 2 Time histories of opening angles

Injection pressure: 600 bar, Chamber density = 20 kg/m^3

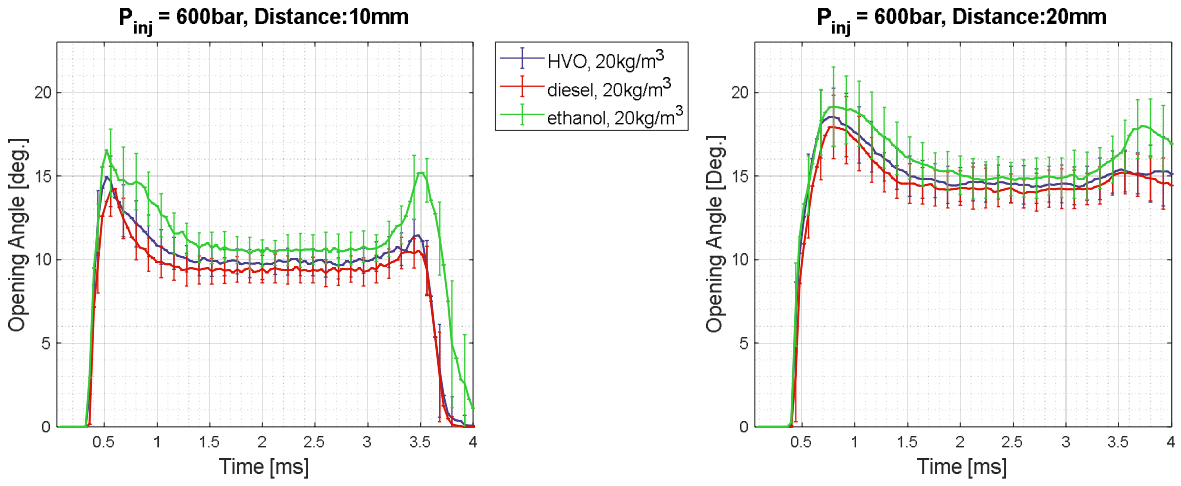

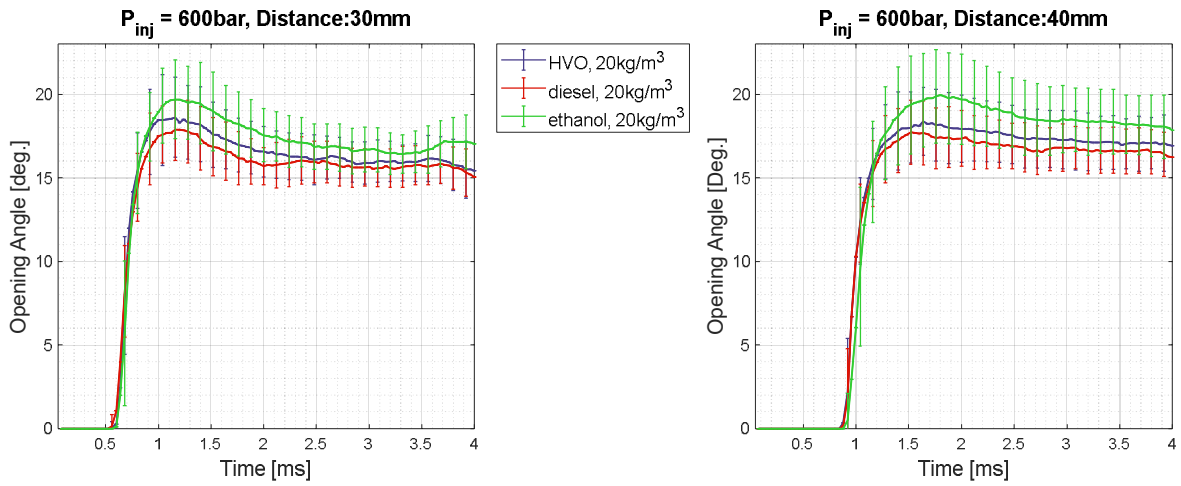

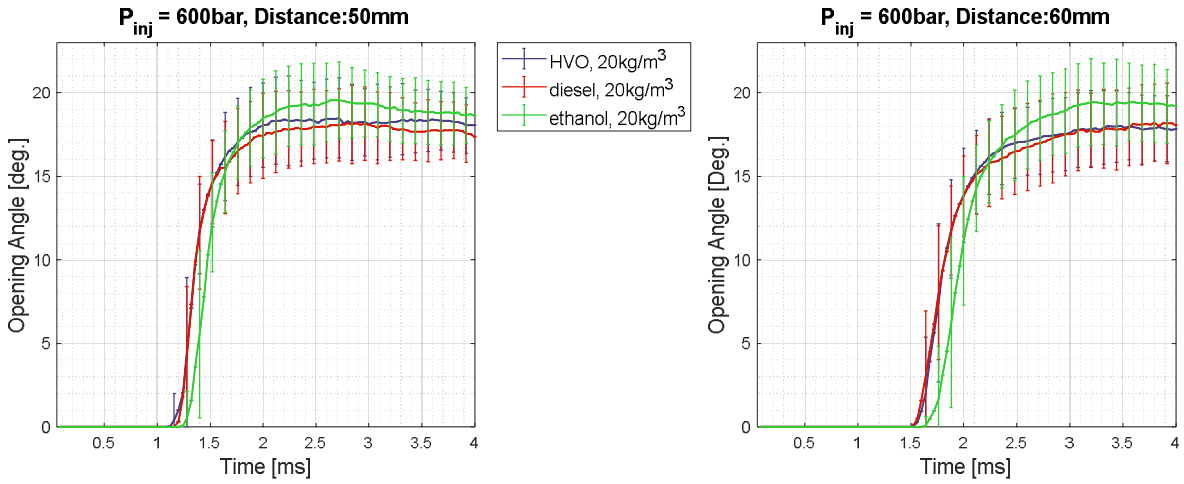

Injection pressure: 1200 bar, Chamber density = 20 kg/m^3

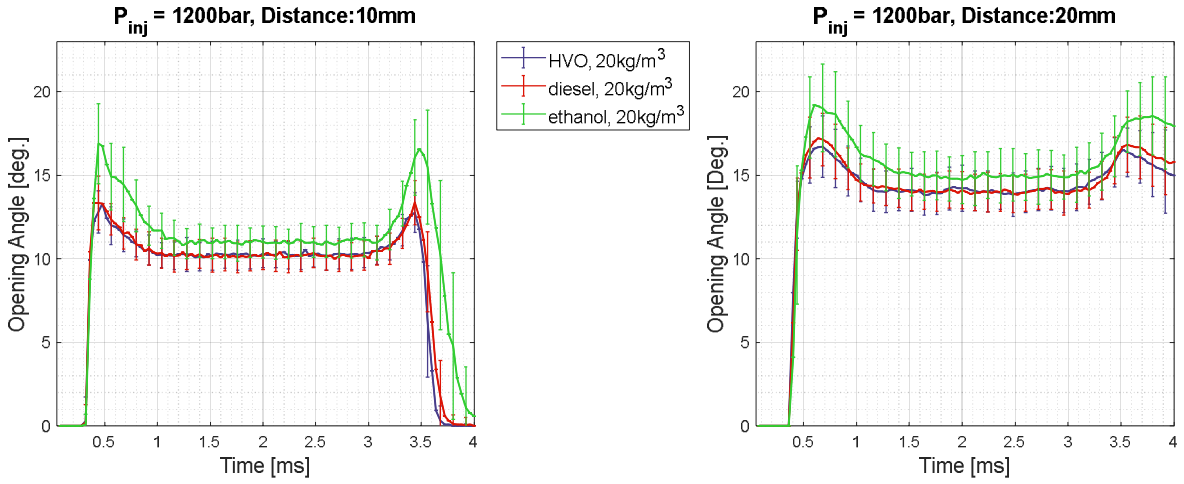

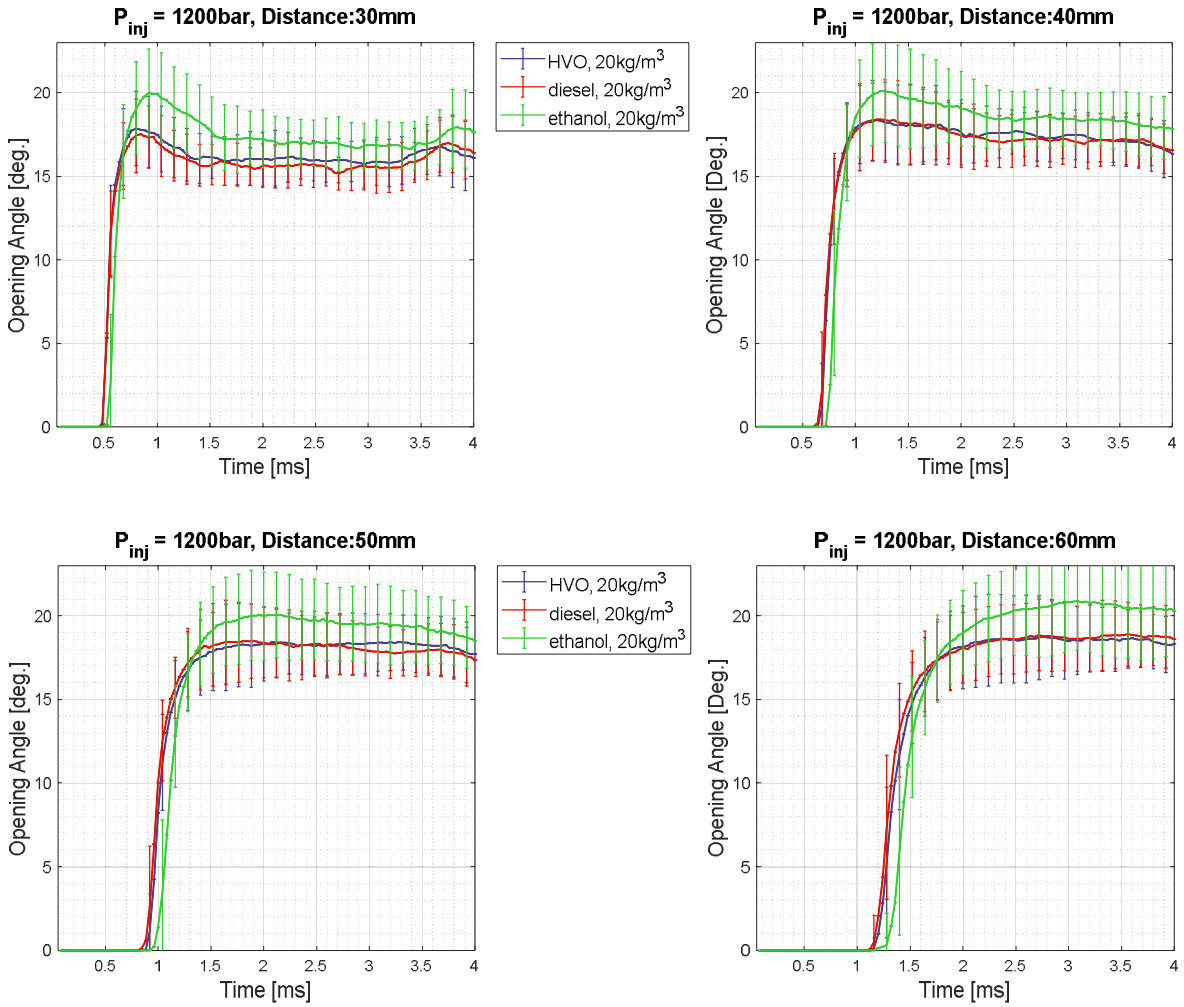

Injection pressure: 1200 bar, Chamber density: 40 kg/m^3

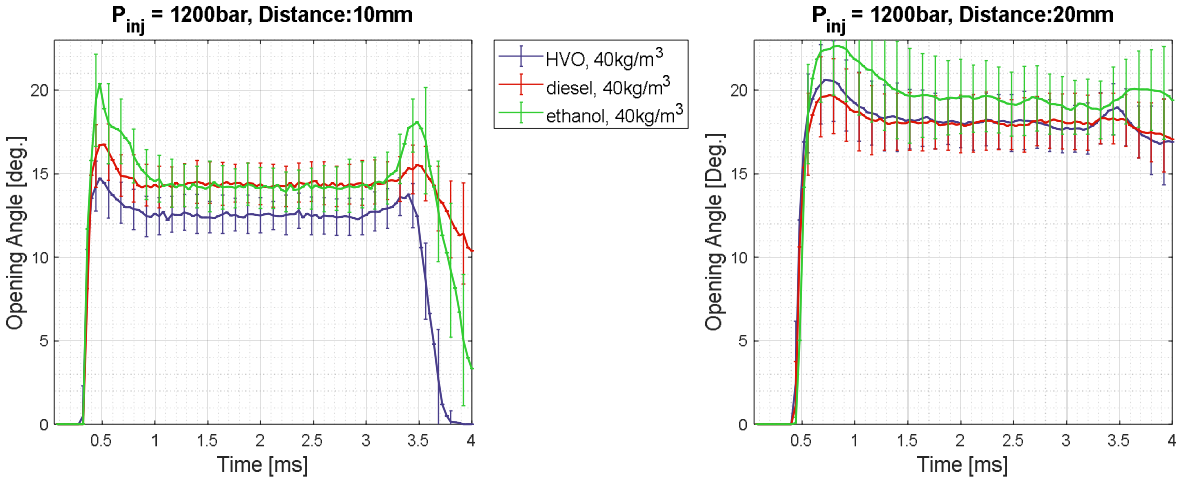

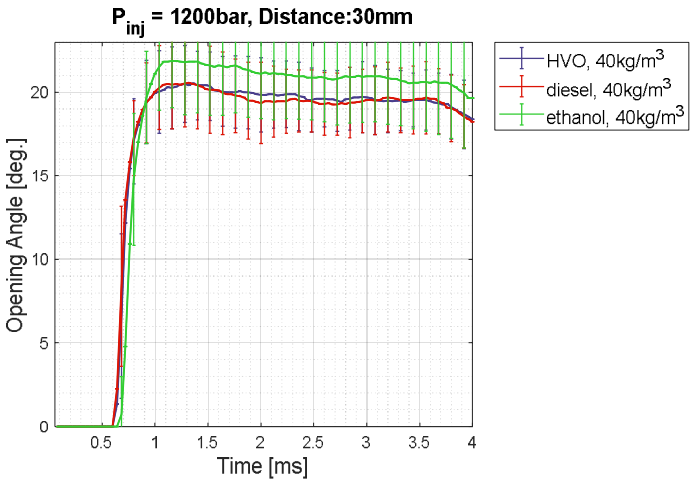
P inj = 1200bar, Distance:30mm
Opening Angle [deg.]
Time [ms]
HVO, 40kg/m3
diesel, 40kg/m3
ethanol, 40kg/m3

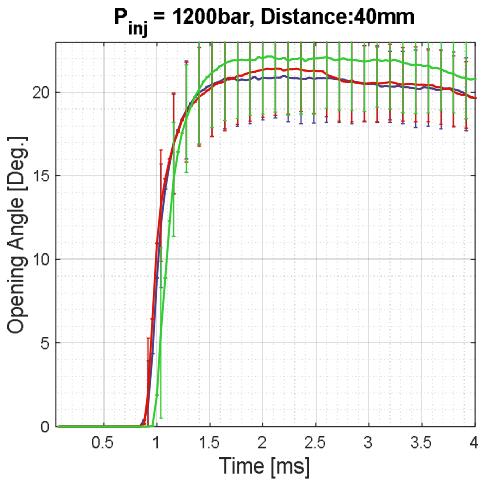
P inj = 1200bar, Distance:40mm
Opening Angle [Deg.]
Time [ms]

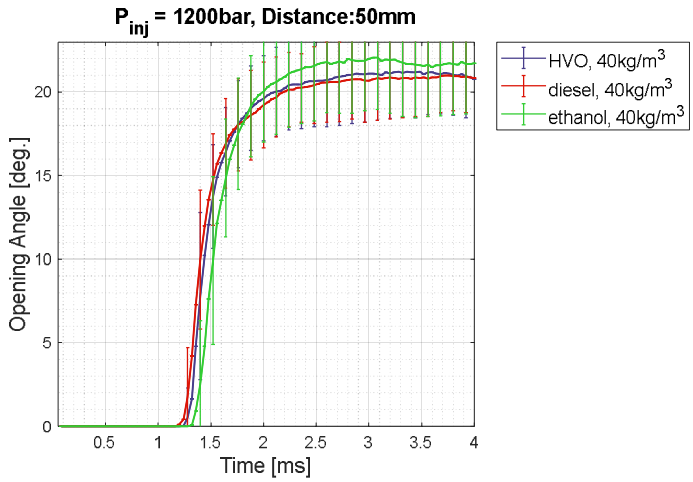
P inj = 1200bar, Distance:50mm
Opening Angle [deg.]
Time [ms]
HVO, 40kg/m3
diesel, 40kg/m3
ethanol, 40kg/m3

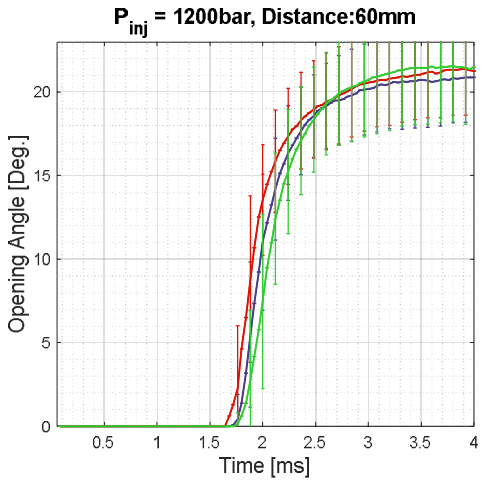
P inj = 1200bar, Distance:60mm
Opening Angle [Deg.]
Time [ms]

Comparison of opening angles at different chamber densities:

Injection pressure: 600bar

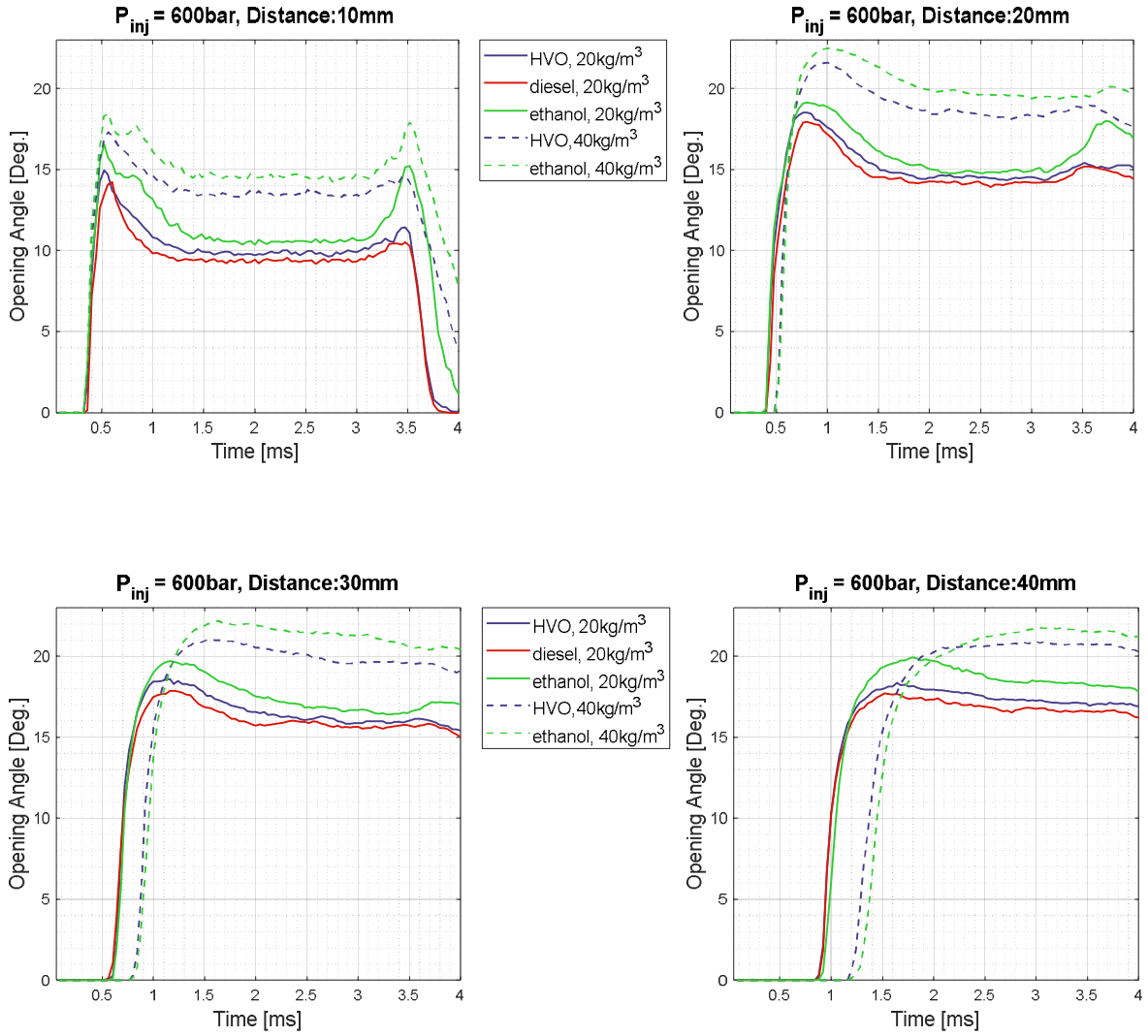

Injection pressure: 1200bar

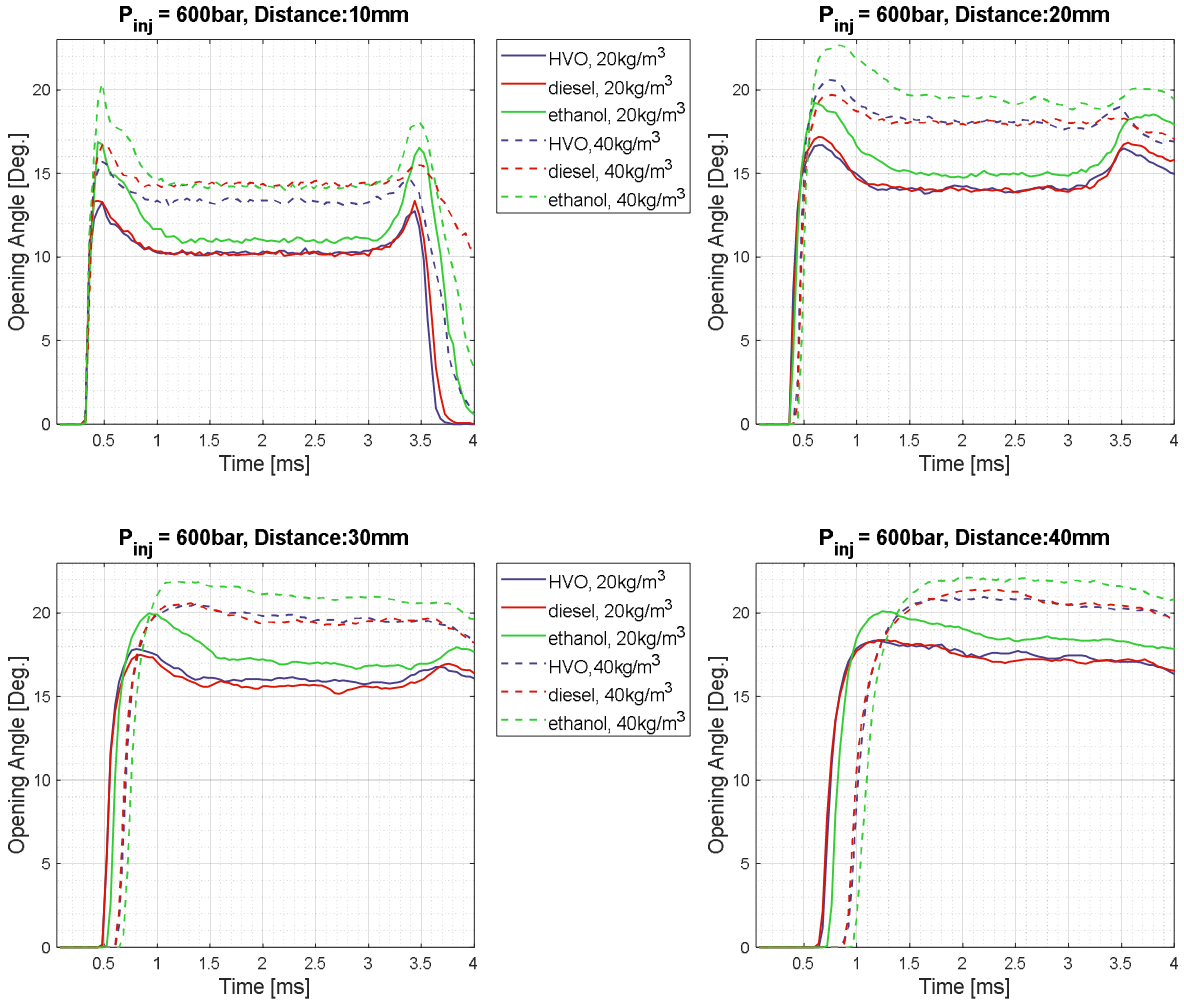

Comparison of opening angles at 1200 & 2000bar

Fuel: Diesel, Chamber density: 40 kg/m^3

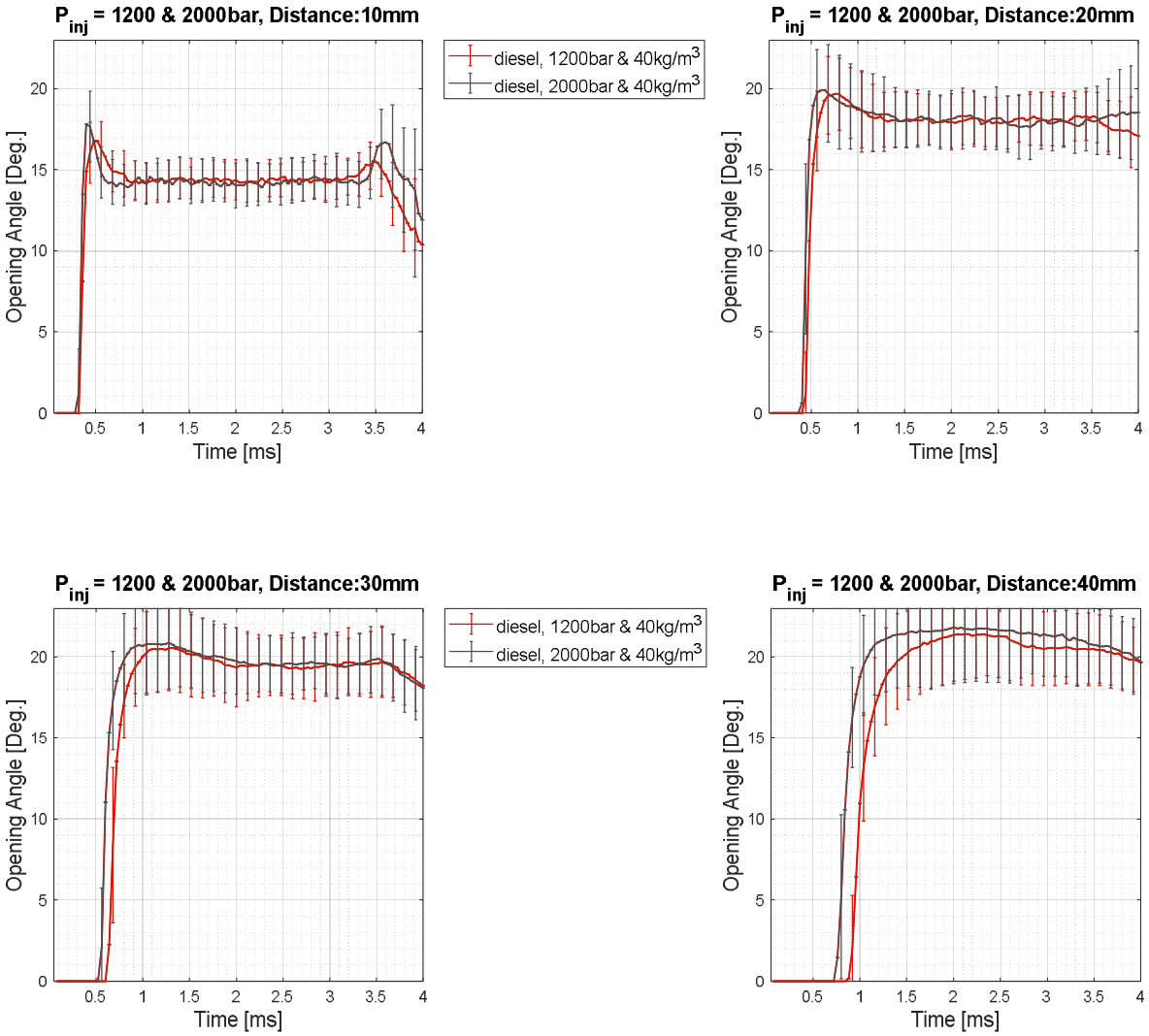

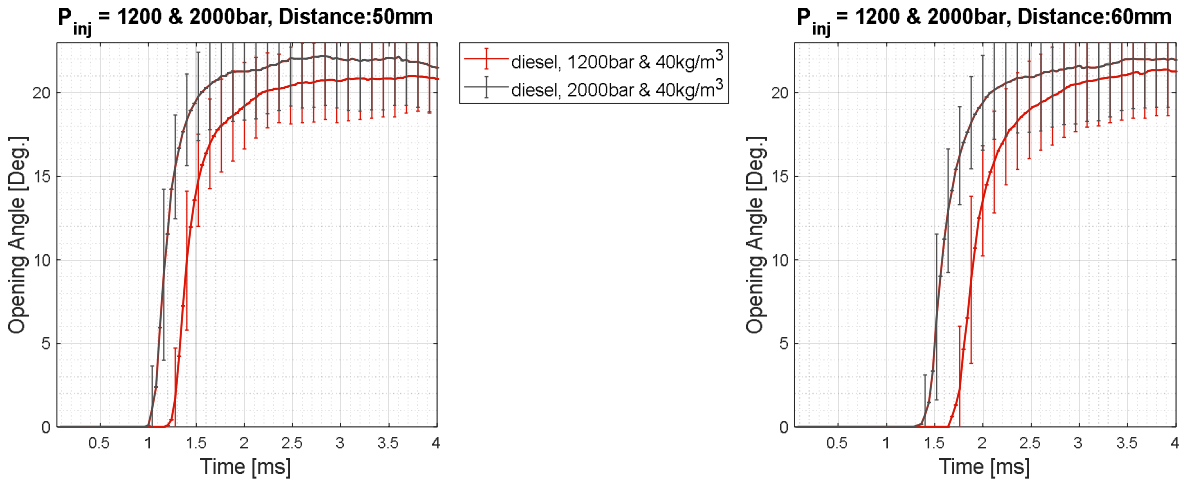
P inj = 1200 & 2000bar, Distance:50mm
Opening Angle [Deg.]
Time [ms]
diesel, 1200bar & 40kg/m3
diesel, 2000bar & 40kg/m3
P inj = 1200 & 2000bar, Distance:60mm
Opening Angle [Deg.]
Time [ms]

Appendix 3 Comparison of opening angles: Special Vs Reference nozzle

Injection pressure: 600 bar

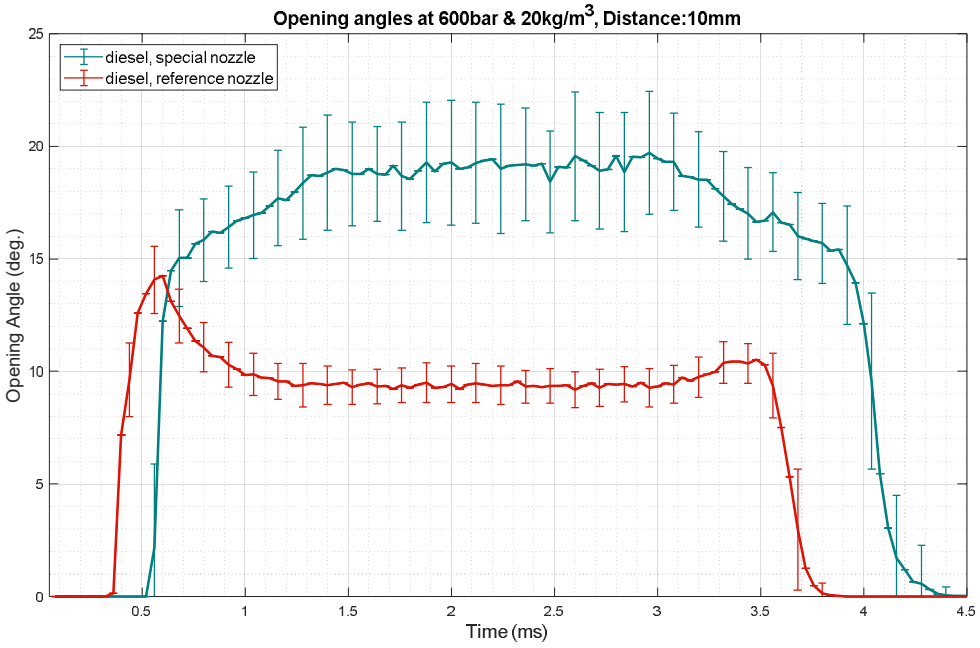

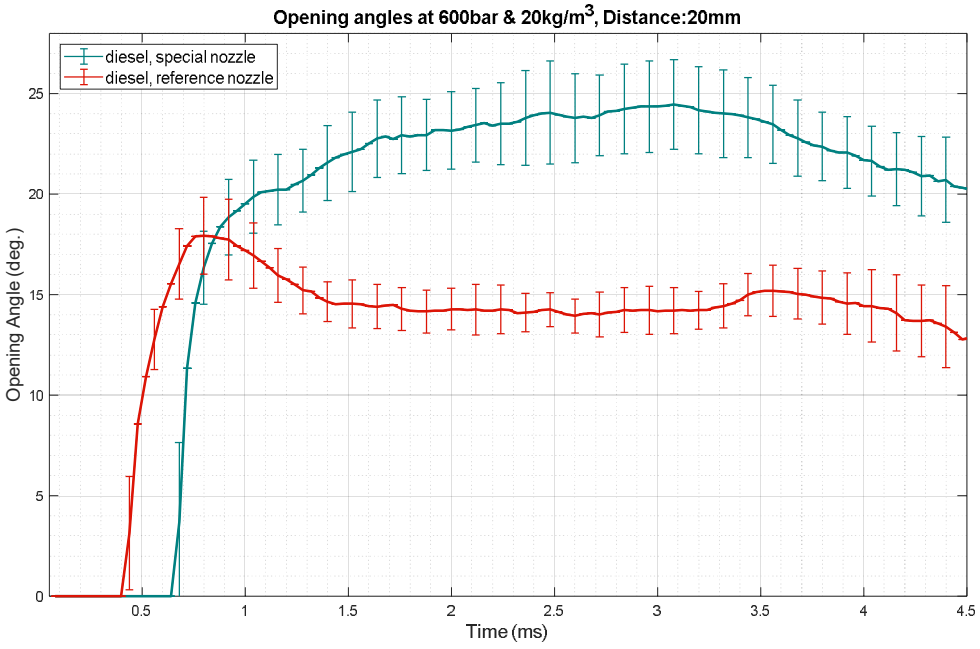

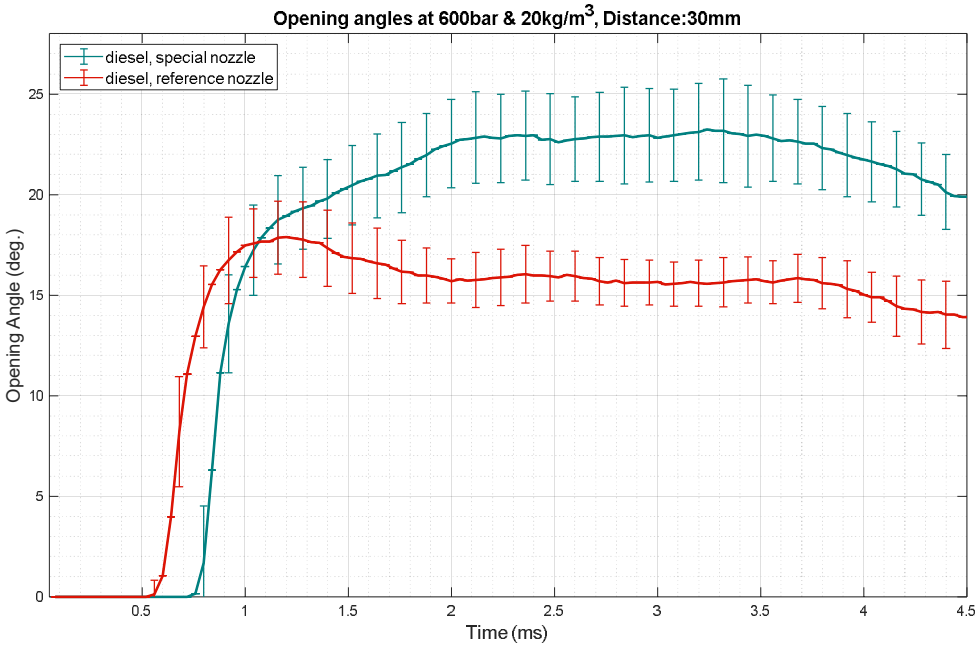
Opening angles at 600bar & 20kg/m3, Distance:30mm
diesel, special nozzle
diesel, reference nozzle
Opening Angle (deg.)
Time (ms)
0
5
10
15
20
25
0.5
1
1.5
2
2.5
3
3.5
4
4.5

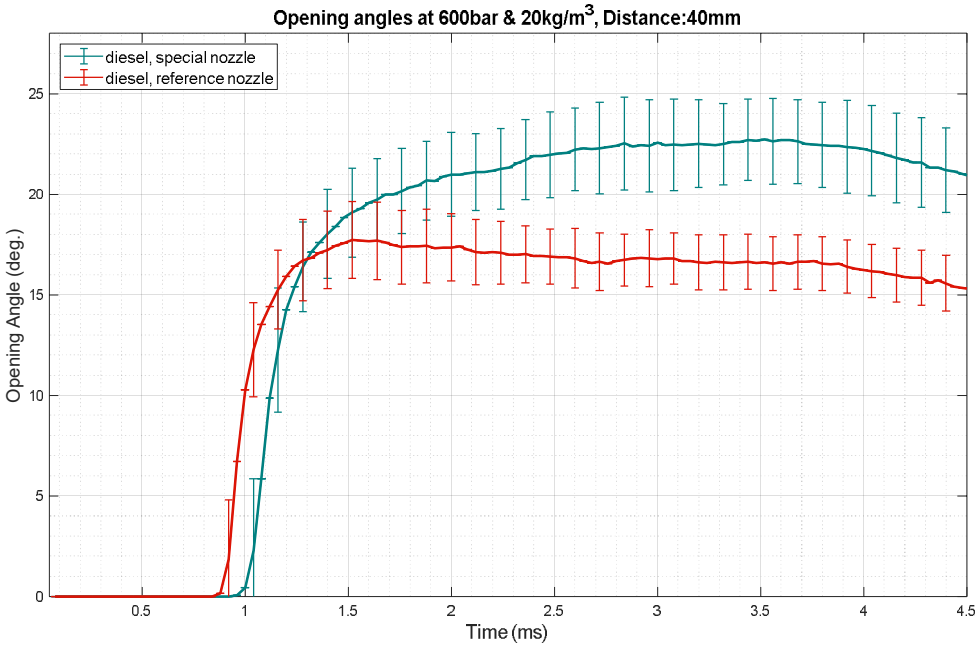
Opening angles at 600bar & 20kg/m3, Distance:40mm
diesel, special nozzle
diesel, reference nozzle
Opening Angle (deg.)
Time (ms)
0
5
10
15
20
25
0.5
1
1.5
2
2.5
3
3.5
4
4.5

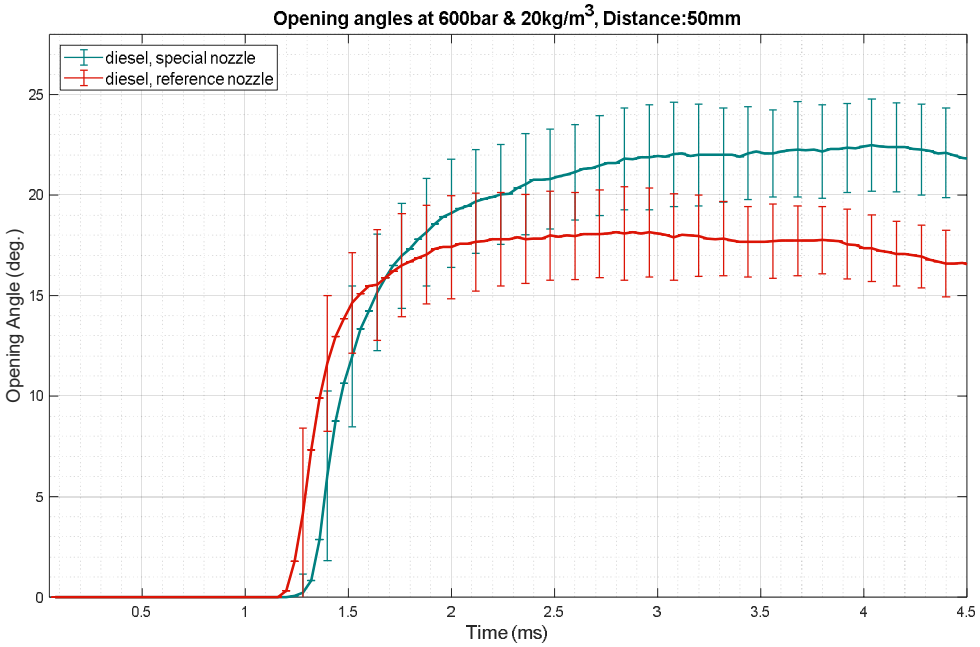

Injection pressure: 1200 bar

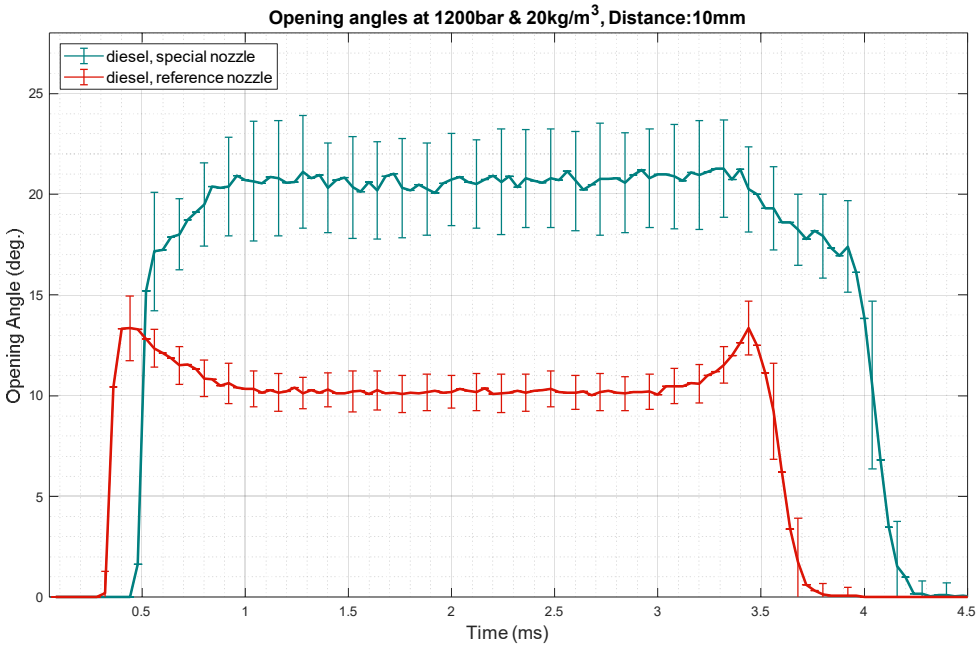

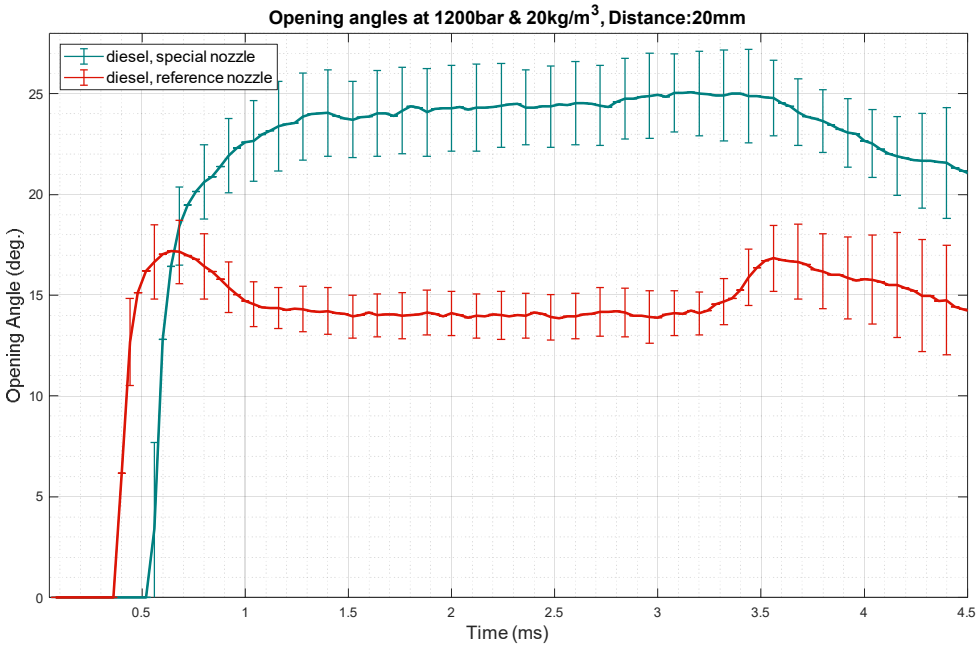
Opening angles at 1200bar & 20kg/m3, Distance:20mm
diesel, special nozzle
diesel, reference nozzle
Opening Angle (deg.)
Time (ms)
0
5
10
15
20
25
0.5
1
1.5
2
2.5
3
3.5
4
4.5

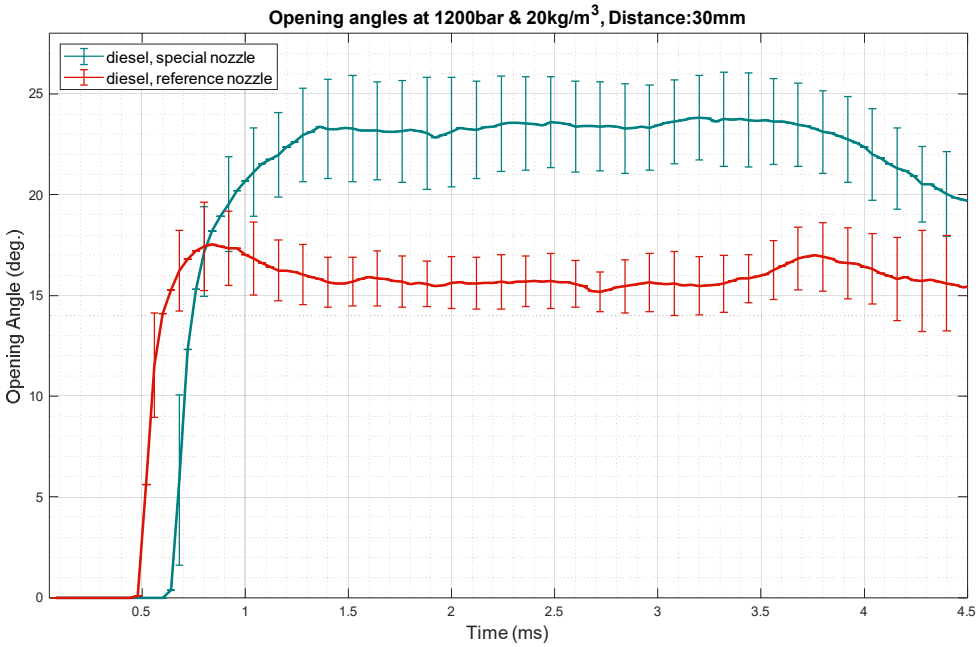
Opening angles at 1200bar & 20kg/m3, Distance:30mm
diesel, special nozzle
diesel, reference nozzle
Opening Angle (deg.)
Time (ms)
0
5
10
15
20
25
0.5
1
1.5
2
2.5
3
3.5
4
4.5

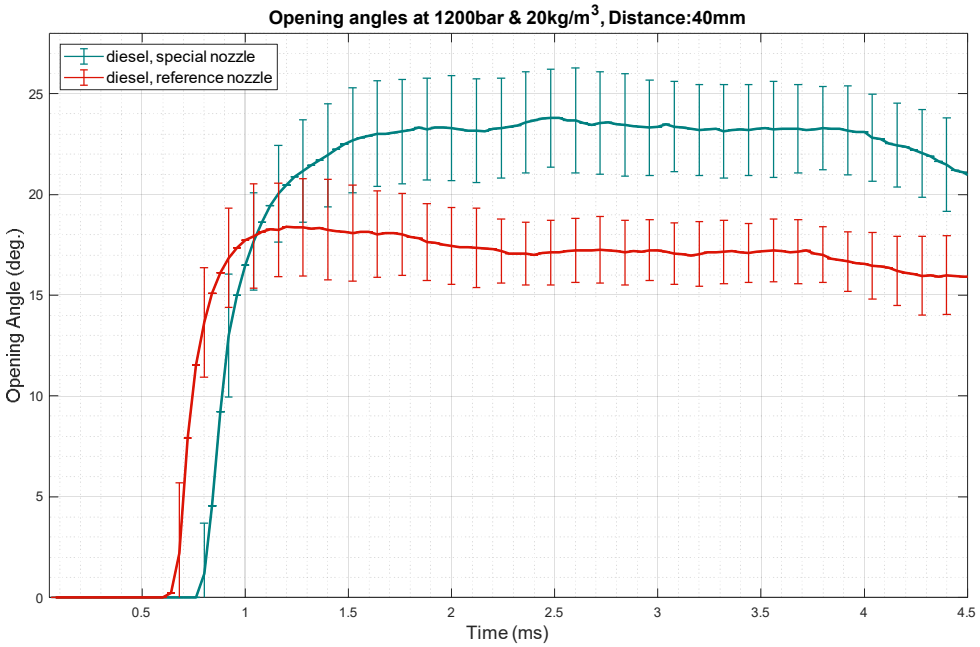
Opening angles at 1200bar & 20kg/m3, Distance:40mm
diesel, special nozzle
diesel, reference nozzle
Opening Angle (deg.)
Time (ms)
0
5
10
15
20
25
0.5
1
1.5
2
2.5
3
3.5
4
4.5

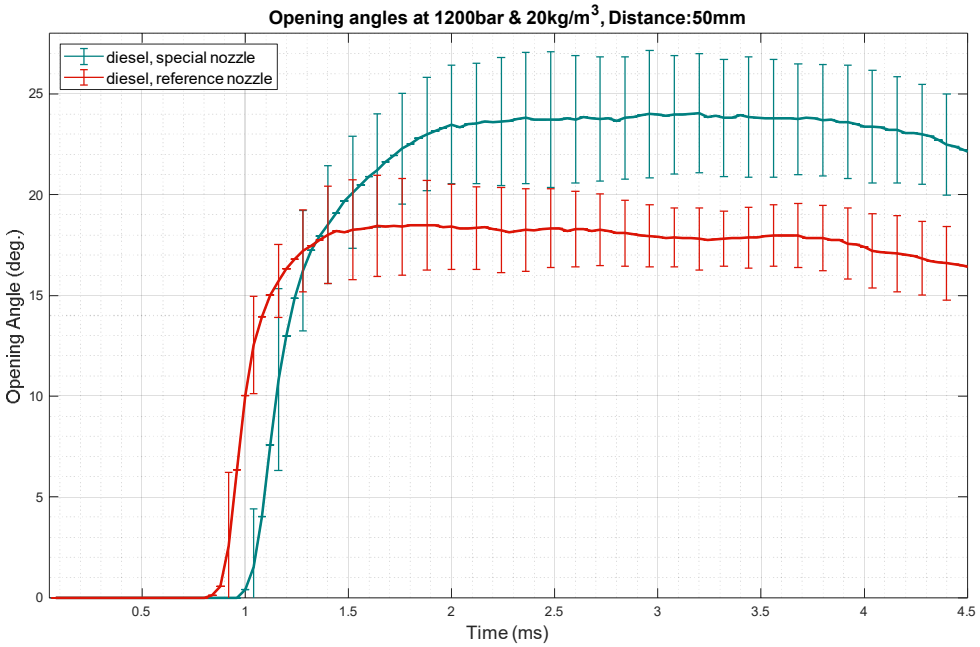
Opening angles at 1200bar & 20kg/m3, Distance:50mm
diesel, special nozzle
diesel, reference nozzle
Opening Angle (deg.)
Time (ms)
0
5
10
15
20
25
0.5
1
1.5
2
2.5
3
3.5
4
4.5

Appendix 4 Average fuel temperatures

For Spray geometry tests

Test Point #	Avg. Fuel rail Temp. (°C)	Avg. Fuel tank Temp. (°C)
T01	76.26	26.24
T02	50.26	22.31
T03	74.31	23.85
T04	48.29	19.68
T05	77.77	25.91
T06	49.27	20.21
T07	76.63	23.36
T08	87.35	24.14
T09	51.05	14.48
T10	43.40	13.11
T11	51.39	17.02
T12	42.42	12.54
T13	88.16	18.70
T14	51.98	18.05

Table 9 Average temperatures for Spray geometry tests

For droplet size measurement tests

Test Point #	Avg. Fuel rail Temp. (°C)	Avg. Fuel tank Temp. (°C)
D1	71.57	19.53
D2	47.04	18.57
D3	63.59	18.25
D4	42.00	17.04
D5	97.10	18.56
D6	65.35	22.76
D7	41.69	16.10
D8	41.33	21.37
D9	42.32	20.12
D10	63.30	17.53
D11	44.75	18.26

Table 10 Average temperatures for Droplet size measurement tests

Appendix 5 Comparison of average fuel rail temperatures

For Spray geometry tests

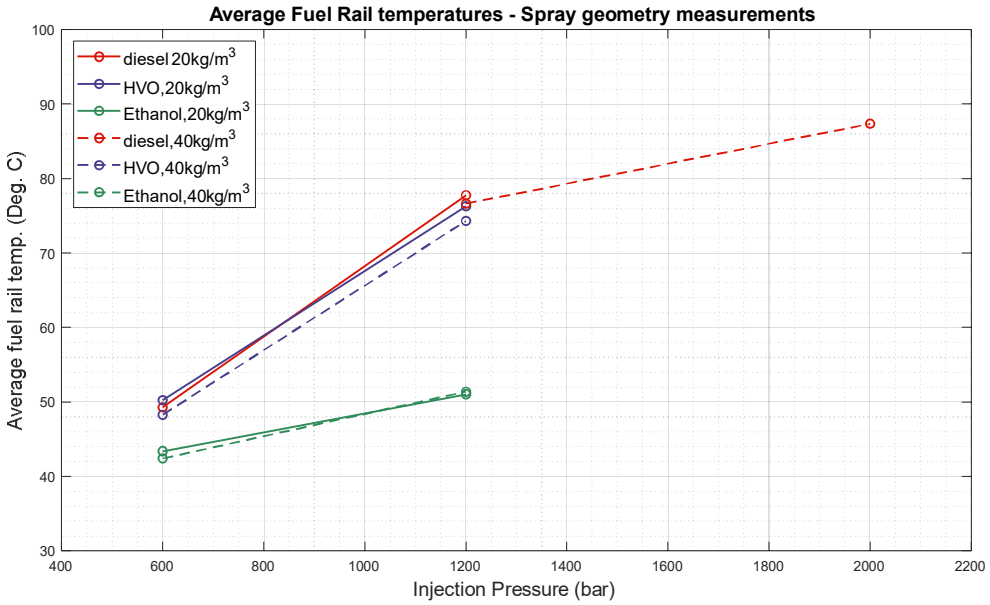

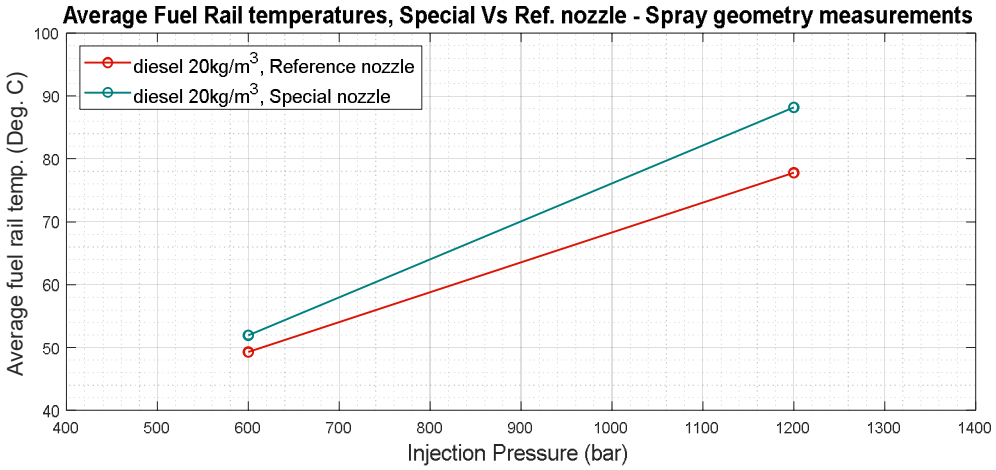

For droplet size measurement tests

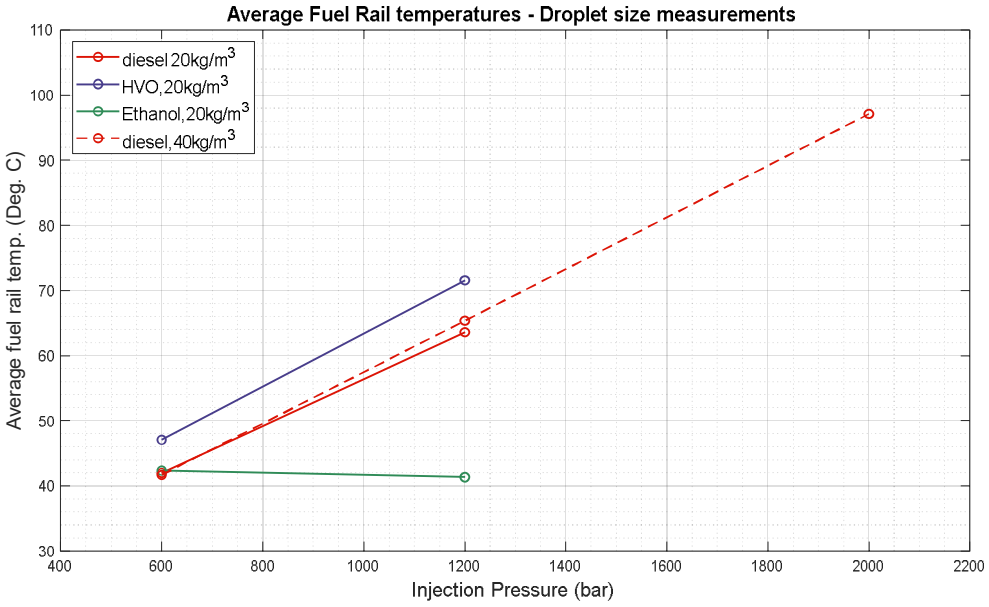

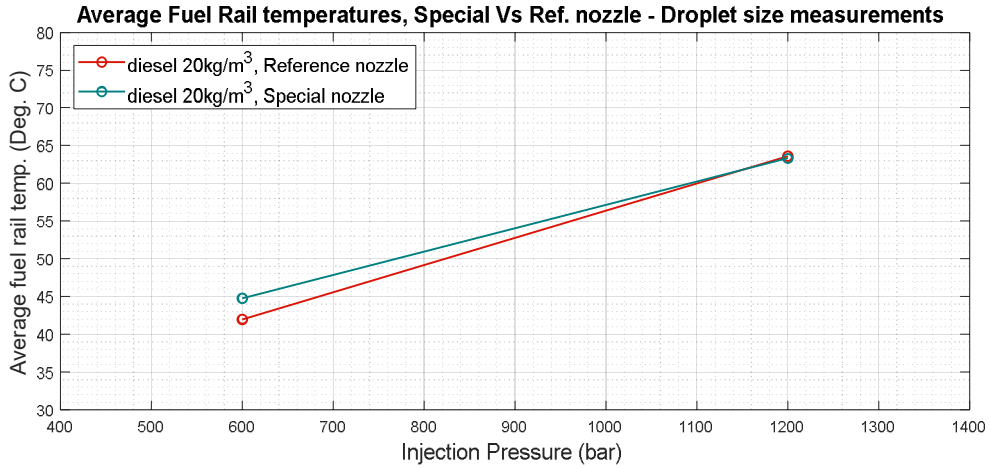

Appendix 6 Certificate of analysis for HVO

NESTE OIL

Certificate of Analysis

TT-15-000229

21.1.2015

Distribution

Ari Engman
Kuronen Markku

Subject

NExBTL 395/14

Samples

		Collectiondt	Sampleid
1.	NExBTL 395/14	29.12.2014	03534382

Results

Physical property	Method	Unit	Sample 1.
Density at 15°C	ENISO12185	kg/m3	779,8
Cloud point, not rounded	ASTMD7689	°C	-36,9
Cold filter plugging point	EN116	°C	-40
Viscosity at 40 °C	ENISO3104	mm2/s	2,919
Sulphur, UV	ENISO20846	mg/kg	<1
Water coloumetric	ENISO12937	mg/kg	17
Flash point, Pensky Martens	ENISO2719	°C	79,5
Copper Corrosion 3 h 50 °C	ENISO2160	no	1a
Water Reaction Interface Rating	ASTMD1094		2
Water Reaction Separation Rating	ASTMD1094		3
Contamination	EN12662	mg/kg	3
Ash, 775°C	ENISO6245	wt-%	<0,001
Micro Carbon Residue 10% bottom	ENISO10370	wt-%	<0,01
Acidity Total (TAN)	ASTMD3242	mg KOH/g	0,001
Monoaromatics	EN12916	wt-%	<0,2
Diaromatics	EN12916	wt-%	<0,1
Tri+-aromatics	EN12916	wt-%	<0,02
Polyaromatics	EN12916	wt-%	<0,1
Aromatics	EN12916	wt-%	<0,2
Gross heat of comb. calor.	ASTMD4809	MJ/kg	47,045
Conductivity Measuring Temp.	ISO6297	°C	22
Hydrogen	ASTMD5291	wt-%	15,2
Electrical Conductivity	ISO6297	pS/m	146
High Frequency Reciprocating Rig	ENISO12156-1	µm/60°C	260
Cetane Number by IQT-analyser	ASTMD6890		78,9
Distillation IBP	ENISO3405	°C	209,9
Distillation 5 vol-%	ENISO3405	°C	251,0
Distillation 10 vol-%	ENISO3405	°C	261,1
Distillation 20 vol-%	ENISO3405	°C	269,6
Distillation 30 vol-%	ENISO3405	°C	272,9
Distillation 40 vol-%	ENISO3405	°C	275,4
Distillation 50 vol-%	ENISO3405	°C	277,4
Distillation 60 vol-%	ENISO3405	°C	279,4
Distillation 70 vol-%	ENISO3405	°C	281,7
Distillation 80 vol-%	ENISO3405	°C	284,8
Distillation 90 vol-%	ENISO3405	°C	289,0

Certificate of Analysis

TT-15-000229

Physical property	Method	Unit	Sample 1.
Distillation 95 vol-%	ENISO3405	°C	293,2
Distillation FBP	ENISO3405	°C	301,9
Distillation Recovery	ENISO3405	vol-%	98,0
Distillation Residue	ENISO3405	vol-%	2,0
Distillation 180°C (E180)	ENISO3405	vol-%	<0,1
Distillation 250°C (E250)	ENISO3405	vol-%	4,7
Filter blocking tendency	IP387		1,01
Freezing point	IP529	°C	-32,4
Net heat of combustion	ASTMD4809	MJ/kg	43,824
Net heat of combustion	ASTMD4809	MJ/l	34,170

Electronical approval

Authored by

Sari Väisänen
Laboratory Technician
sari.vaisanen@nesteoil.com

Approved by

Ari Engman
Group Manager
ari.engman@nesteoil.com

Laboratory

Neste Oil Oyj, Physical Analyses
Neste Oil Oyj, Research and Technology, Central Laboratory, P.O. Box 310, 06101 Porvoo, FINLAND

Appendix 7 Certificate of analysis for EN590 Diesel

NESTE

Certificate of Analysis

TT-19-003558

2.10.2019

Distribution

Kuronen Markku

Subject

Analysis results

Samples

Item	Samplesource	Samplingpoint	Sampleid
1. DIESEL DIR-0/7	MOOTTORIL erät	216/19	14724722

Results

Physical property	Method	Unit	Sample 1.
Density at 15°C	ENISO12185	kg/m3	839,2
Cloud point, not rounded	ASTMD7689	°C	-3,4
Cold Filter Plugging Point	EN116	°C	-14
Viscosity at 40 °C	ENISO3104	mm2/s	3,545
Sulphur, UV	ENISO20846	mg/kg	4,5
Water coulometric	ENISO12937	mg/kg	43
Flash point, Pensky Martens	ENISO2719	°C	62,0
Contamination in middle distillates	EN12662	mg/kg	<1
Monoaromatics	EN12916	wt-%	17,3
Diaromatics	EN12916	wt-%	1,5
Tri+-aromatics	EN12916	wt-%	0,12
Polyaromatics	EN12916	wt-%	1,6
Aromatics	EN12916	wt-%	18,9
High Frequency Reciprocating Rig	ENISO12156-1	µm/60°C	319
Cetane index	ENISO4264		>56,5
Cetane Number by IQT-analyser	ASTMD6890		54,6
Distillation IBP	ENISO3405	°C	177,3
Distillation 5 vol-%	ENISO3405	°C	214,9
Distillation 10 vol-%	ENISO3405	°C	231,3
Distillation 20 vol-%	ENISO3405	°C	249,8
Distillation 30 vol-%	ENISO3405	°C	265,0
Distillation 40 vol-%	ENISO3405	°C	278,1
Distillation 50 vol-%	ENISO3405	°C	290,1
Distillation 60 vol-%	ENISO3405	°C	301,8
Distillation 70 vol-%	ENISO3405	°C	313,3
Distillation 80 vol-%	ENISO3405	°C	325,3
Distillation 90 vol-%	ENISO3405	°C	340,0
Distillation 95 vol-%	ENISO3405	°C	350,4
Distillation FBP	ENISO3405	°C	357,9
Distillation Recovery	ENISO3405	vol-%	98,2
Distillation Residue	ENISO3405	vol-%	1,4
Distillation Loss	ENISO3405	vol-%	0,4
Distillation 180°C (E180)	ENISO3405	vol-%	0,6
Distillation 340°C (E340)	ENISO3405	vol-%	90,0

Electronical approval

Authored by
Jenni Nortio
Associate, Diesel / +358504582239
jenni.nortio@neste.com

Laboratory

Neste Oyj, Water and Oil laboratory
Neste Oyj, Research and Development, Central Laboratory, P.O. Box 310, 06101 Porvoo, FINLAND